LAWRENCE
LIVERMORE
NATIONAL
LABORATORY

UCRL-SR-228092

Integrated Seismic Event Detection and Location by Advanced Array Processing

T. Kvaerna, S. J. Gibbons, F. Ringdal, D. B. Harris

February 15, 2007

This work was performed under the auspices of the U.S. Department of Energy by University of California, Lawrence Livermore National Laboratory under Contract W-7405-Eng-48.

Final Scientific Report

Contract No. DE-FC52-03NA99517/A000

Integrated Seismic Event Detection and Location by Advanced Array Processing

submitted by

NORSAR
Kjeller, Norway

30 January 2007

Principal Investigator:

Dr. Tormod Kværna
NORSAR, P.O. Box 53
N-2027 Kjeller, Norway

Contributors

Tormod Kværna, NORSAR
Steven J. Gibbons, NORSAR
Frode Ringdal, NORSAR
David B. Harris, LLNL

Page left intentionally blank

Executive Summary

In the field of nuclear explosion monitoring, it has become a priority to detect, locate, and identify seismic events down to increasingly small magnitudes. The consideration of smaller seismic events has many implications for an exhaustive and reliable monitoring regime. Firstly, the number of events which have to be considered increases greatly; an exponential increase in naturally occurring seismicity is compounded by the addition of large numbers of seismic signals generated by human activity. Secondly, the signals from smaller events become more difficult to detect above the background noise and estimates of parameters required for locating the events may be subject to greater errors. Thirdly, events are likely to be observed by a far smaller number of seismic stations, and the reliability of event detection and location using a very limited set of observations needs to be quantified.

For many key seismic stations, detection lists may be dominated by signals from routine industrial explosions which should ideally be ascribed, fully-automatically and with a high level of confidence, to a known source. This means that expensive analyst time is not spent on locating routine events from repeating seismic sources and that events from unknown sources, which could be of concern in an explosion monitoring context, are more easily identified and can be examined with due care. We have obtained extensive lists of confirmed seismic events from mining and other artificial sources which have provided an excellent opportunity to assess the quality of existing fully-automatic event bulletins and to guide the development of new techniques for online seismic processing.

Comparing the times and locations of confirmed (Ground Truth) events from several sources in Fennoscandia and NW Russia with the corresponding origin time and location estimates reported in the existing automatic bulletins has revealed substantial mislocation errors which preclude a confident association of the detected signals with known industrial sources. The causes of the errors are well understood and are primarily the result of

- spurious identification or association of phases. This problem is often exacerbated by complicated events with multiple sources and ripple-firing techniques. This often results in extended and noisy wavetrains which can obscure secondary phase arrivals that are of paramount importance in event location at regional distances.
- excessive variability in estimates for the velocity and direction of incoming seismic phases. This is often the result of the selection of different frequency bands in which to make these measurements, which can demonstrably be subject to different uncertainties and biases at different frequencies.

The mitigation of these causes has led to the development of two complimentary techniques for classifying seismic sources by testing detected signals under mutually exclusive event hypotheses. Both of these techniques require appropriate calibration data from the region to be monitored, and are therefore ideally suited to mining areas or other sites with recurring seismicity.

The first such technique is a classification and location algorithm where a template is designed for each site being monitored which defines which phases should be observed,

and at which times, for all available regional array stations. For each phase, the variability of measurements (primarily the azimuth and apparent velocity) from previous events is examined and it is determined which processing parameters (array configuration, data window length, frequency band etc.) provide the most stable results. This allows us to define optimal diagnostic tests for subsequent occurrences of the phase in question. The calibration of templates for this project revealed significant results with major implications for seismic processing in both automatic and analyst reviewed contexts:

- one or more fixed frequency bands should be chosen for each phase tested for.
- the frequency band providing the most stable parameter estimates varies from site to site and a frequency band which provides optimal measurements for one site may give substantially worse measurements for a nearby site.
- slowness corrections applied depend strongly on the frequency band chosen.
- the frequency band providing the most stable estimates is often neither the band providing the greatest SNR nor the band providing the best array gain. For this reason, the automatic template location estimates provided here are frequently far better than those obtained by analysts.

The second technique is that of matched field processing whereby spatial covariance matrices calculated from large numbers of confirmed events from a single site can be used to generate calibrated narrow-band steering vectors which can replace the theoretical plane-wave steering vectors of traditional f-k analysis. This provides a kind of fingerprint which is specific to a given source region and is effective to higher frequencies than traditional beamforming since deviations from the theoretical planewave model are compensated for in the calibrations. The narrow-band nature of the technique makes the source identification most sensitive to the spatial nature of the recorded wavefield and less sensitive to the temporal nature. This may make the method far more suitable for events with very complicated seismic sources than full waveform-correlation methods.

1. Introduction

1.1 Objective

The principal objective of this two-year study is to develop and test a new advanced, automatic approach to seismic detection/location using array processing. We address a strategy to obtain significantly improved precision in the location of low-magnitude events compared with current fully-automatic approaches, combined with a low false alarm rate. We have developed and evaluated a prototype automatic system which uses as a basis regional array processing with fixed, carefully calibrated, site-specific parameters in conjuction with improved automatic phase onset time estimation.

We have in parallel developed tools for Matched Field Processing for optimized detection and source-region identification of seismic signals. This narrow-band procedure aims to mitigate some of the causes of difficulty encountered using the standard array processing system, specifically complicated source-time histories of seismic events and shortcomings in the plane-wave approximation for seismic phase arrivals at regional arrays.

1.2 Motivation

One of the current priorities within the field of nuclear explosion monitoring is a reduction of the magnitude above which seismic events can, with a high level of confidence, be detected, located, and classified. Such a reduction in magnitude is inevitably associated with a vast increase in the number of events needing to be processed which, given limited analyst resources, leads to a greater reliance upon robust and accurate, fully-automatic, event bulletins. A majority of the low-magnitude events detected by many seismic stations are routine industrial explosions which, ideally, should be associated confidently with a known source such that they can be eliminated from the lists of events of unknown origin which need to be scrutinized for potential clandestine nuclear tests. Low-magnitude seismic events are recorded by fewer stations than larger events and we must also be able to evaluate and optimize the ability to detect and locate events using a minimal number of observations. In particular, the International Monitoring System (IMS) of seismic stations installed to verify compliance with a comprehensive nuclear-test-ban treaty (CTBT) is such that many significant events may only be detected by a single array station.

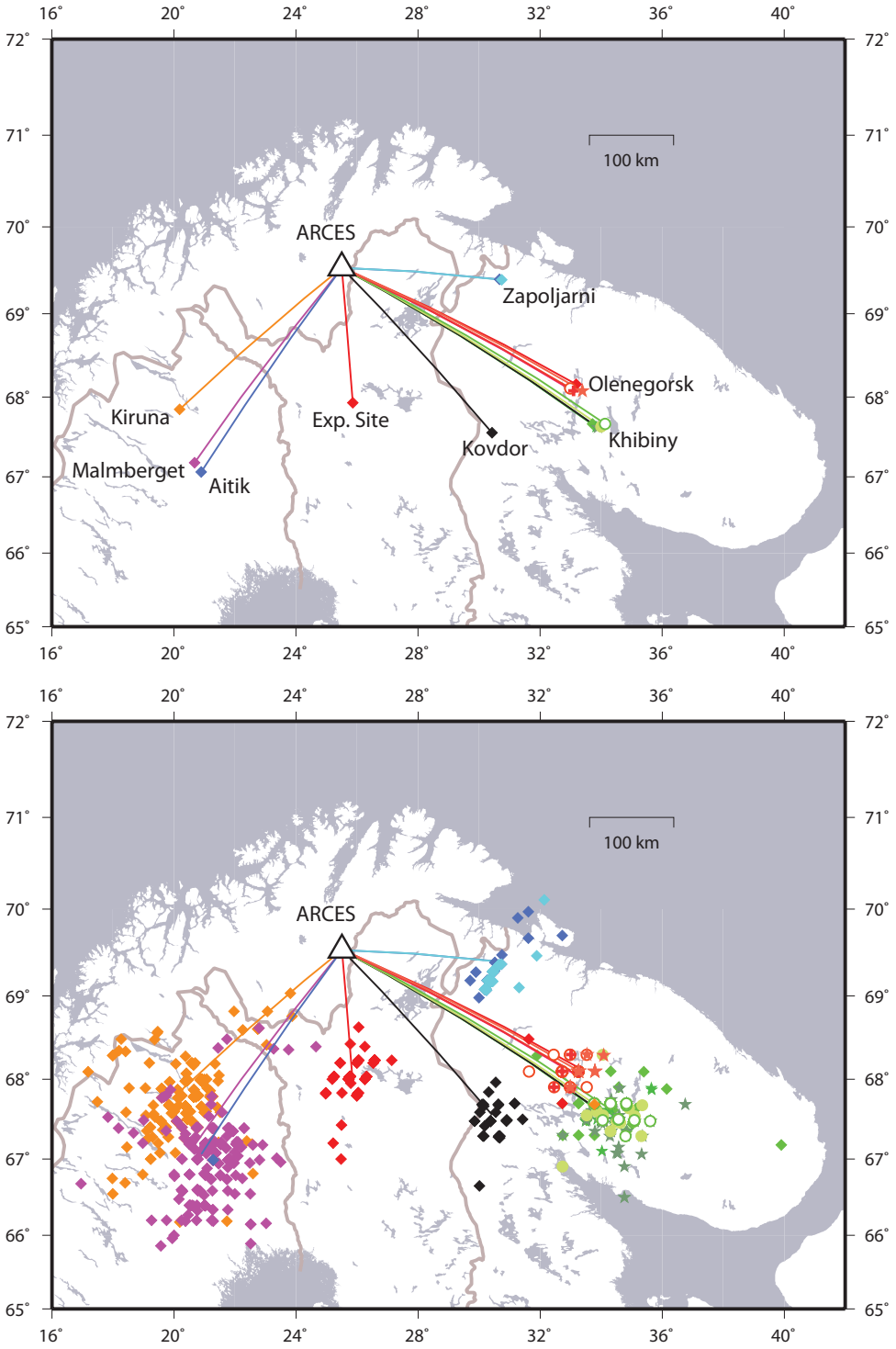

Figure 1: Upper panel: site of the ARCES regional seismic array in northern Norway together with mining regions in north-west Russia and northern Sweden, and a military ammunition destruction site in northern Finland. Lower panel: GBF automatic event location estimates for events which are known to have occurred at the sites in the upper panel.

The regions of Fennoscandia and North West Russia constitute an ideal natural laboratory for the investigation of automatic procedures for the detection and location of low-magnitude seismic events. The region is characterized by a reasonably low level of natural seismicity and contains many sites with frequent artificial seismic events. The majority of these sites are mines although military activity (predominantly the destruction of old ammunition) at several locations is also frequently observed by seismic stations in the region. The uppermost panel of Figure 1 displays the locations of several mining regions on the Kola Peninsula of NW Russia and in the north of Sweden. These sites are the source of a huge proportion of the regional signals registered at the IMS Primary seismic array station ARCES and also at the non-IMS array at Apatity in Russia. Also shown in Figure 1 is the location of an ammunition destruction site used by the Finnish military; approximately 20 explosions are conducted here each year, all being well-recorded by the ARCES array.

For each of the locations named in Figure 1, we have been able to obtain lists of seismic events confirmed to have occurred within the confines of the site within given periods. This provides us with knowledge of the source location for such events to within a maximum uncertainty of approximately 2 km. Such confirmed events allow us to evaluate the existing automatic event detection and location procedures, to calibrate parameters for the development of new algorithms, and to test the reliability and accuracy of the new procedures. For the mining sites on the Kola Peninsula (mine clusters at Zapoljarni, Olenegorsk, Khibiny, and Kovdor), lists of industrial explosions were provided to colleagues at the Kola Regional Seismological Center (KRSC) at Apatity by the Russian mining authorities. These lists were compiled and provided to us under the DoE-funded contract "Ground-Truth Collection for Mining Explosions in Northern Fennoscandia and Russia" (Harris et al., 2003). Such detailed information was not available for the sites in Sweden, although the mining authorities there have kindly confirmed the times and locations of a small number of events known to have taken place at these mines. Using the signals from these selected events as waveform templates, a cross-correlation procedure has been applied to identify subsequent events which, due to the waveform similarity, are guaranteed to have originated within a very close proximity of the locations of the master events (see, for example, Geller and Mueller, 1980). Using good signals from detected events as new master events, quite large databases of events have been accumulated for these sites. Events from the explosion site in Finland are generally easily identified due to the time of year and time of day; the signals from all such events also correlate very well with each other confirming a common source location.

The lower panel of Figure 1 shows automatic location estimates for events confirmed to have occurred at the sites indicated using the Generalized Beam-Forming (GBF) procedure (Kværna and Ringdal, 1989). GBF is a method of associating regional phases detected and characterized by a network of seismic array stations which, using a grid of trial epicenter locations, creates a list of hypothesized events which fit best the associated phase detections. GBF has now for many years formed the basis of the reviewed regional event bulletin at NORSAR; the approximate epicenter and origin time provided are usually sufficient for an analyst to reassign any spurious phase classifications, modify arrival times, and subsequently and efficiently relocate the event. Figure 2 displays manual location estimates for events known to have taken place at these sites, together with the fully

automatic GBF solutions which formed the basis for each of these analyst relocations. Whilst providing an adequate initial solution for an analyst location, it is clear from Figure 1 that GBF is inadequate for associating seismic signals generated by industrial explosions with their respective source locations automatically. Limited resources mean that it is not possible (or desirable) that every single such event be subject to manual review and somewhat arbitrary selection criteria are employed to determine which events should be subject to analyst relocation. The reasons for the large variability in location estimates provided by the GBF method are well understood and are discussed in the following section where we describe the formulation of the template-based method which has been developed under the current contract.

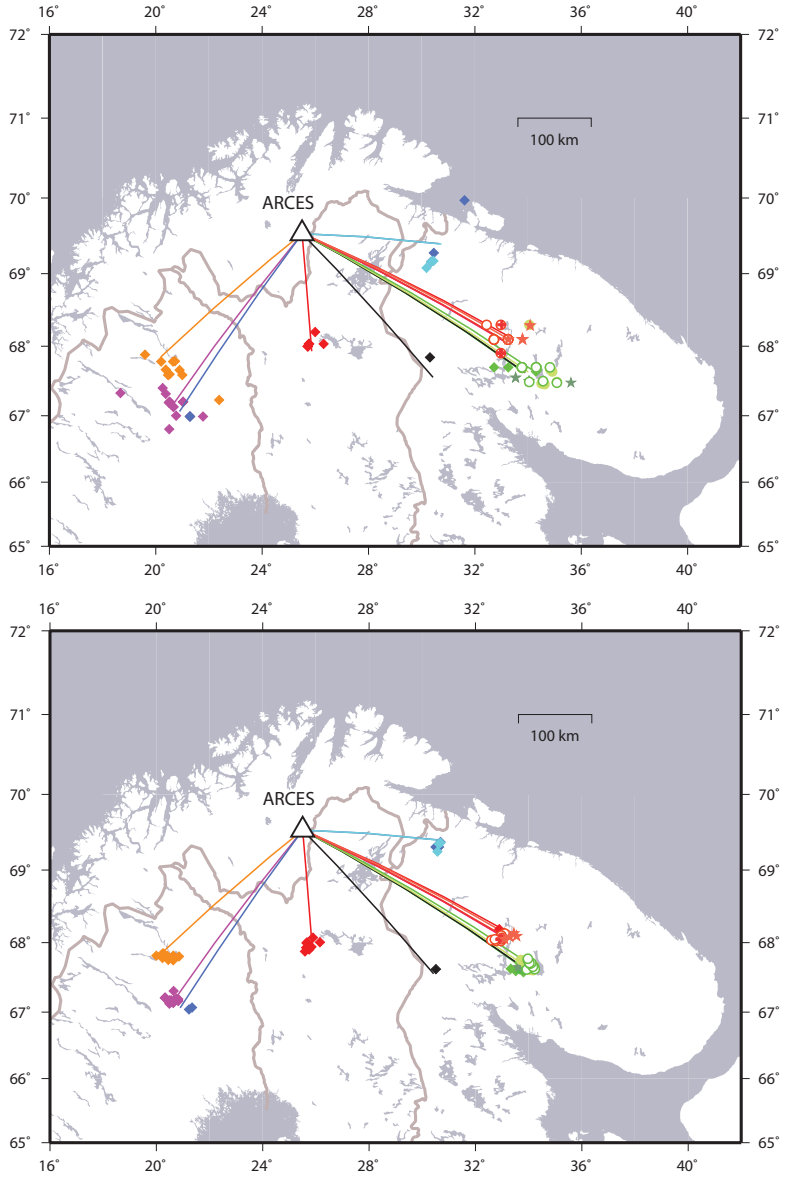

Figure 2: The upper panel displays the GBF locations of events displayed in Figure 1 which have been subsequently relocated by an analyst at NORSAR. The lower panel displays the manual locations for the same set of events. Note that only a small percentage of the automatic detections were selected for manual relocation.

The principal aim of the current contract has been to develop and test a new fully-automatic procedure for the detection and identification/location of low-magnitude seismic events which provides a significant improvement in reliability and location accuracy compared with current procedures.

1.3 Report overview

Section 2 describes the principles of the template system for the identification and location of events from specific sites of interest. There are two principal components to this procedure. Firstly (Section 2.1) is the definition of a template for a given seismic source region which specifies the set of phase arrivals which are likely to be observed at a single regional seismic array or a network of arrays and 3-component stations. Secondly (Section 2.2) is the definition of phase-templates which assess how observations of the seismic wavefield at a given array in an appropriate time-window compare with corresponding measurements from confirmed events from the site being monitored. Whilst both types of template are based upon predictions from 1-dimensional Earth models, they may need to be modified significantly in response to observations of confirmed (Ground Truth) events.

Section 3 provides details of the calibration of site and phase templates for a variety of sites in Fennoscandia and NW Russia. Details are provided of how representative events were identified (either by the provision of Ground Truth or the application of waveform correlation methods to small sets of verified master events). Characteristics of slowness measurements for phase arrivals are examined for relevant phases from the sites of interest as a function of different processing parameter specifications.

Section 4 discusses the improvement to event location estimates resulting from the application of site-specific processing parameters.

Section 5 discusses the transportability of these results, both to different configurations of seismic array but also to different tectonic settings. The example demonstrated is at the regional ABK array in Kazakhstan.

Section 6 describes the application of Matched Field Processing to event detection and source identification for the purpose of seismic screening of events from repeating seismic sources. This is a narrow-band procedure which replaces the steering vectors of f-k analysis with empirically calculated steering vectors obtained from spatial covariance matrices calculated from training events confirmed to have taken place at the site of interest. The shortcomings of the plane-wave assumption in representing regional phase arrivals over seismic arrays are mitigated with the source-specific steering vectors facilitating coherent processing at higher frequencies than would be possible using the theoretical steering vectors. Problems associated with the complicated source-time functions of these ripple-fired mining events are mitigated to some degree due to the narrow-band nature of the processing which makes the calibrations more sensitive to the spatial properties of the wavefield and less sensitive to the temporal.

Section 7 provides an overview and recommendations for further development.

2. Development of a template system for automatic source identification and event location

Prior to the formulation of a new procedure for the automatic location of events from sites of recurring seismicity, it is worthwhile examining the reasons for the large variability in the automatic event location estimates provided by the GBF (see the lower panel of Figure 1). The following three reasons are deemed to be the most significant:

- Many of the events have complicated firing sequences which can lead to an incorrect association of phases. For instance, if two similar blasts follow within seconds of each other, it is possible that a secondary phase from the second event may be associated with the P-phase from the first event, leading to a location estimate at too great a distance from the station observing these phases. Other combinations of incorrect coda phase associations can lead to similar spurious location estimates. (This problem clearly diminishes when a large number of stations with a good azimuth coverage can be used; the P-observations from the different receivers will diminish the influence of the secondary phases. However, this luxury is rarely available when attempting to observe very small magnitude events with a sparse network of stations.)
- The GBF system employs a system of somewhat empirically determined rules which help to determine which of several candidate sources (hypocenter and origin time) is the most likely to have produced a given set of phases. A single trial hypocenter which fits a larger number of phases (albeit with a poorer fit for each phase) may score more highly than, for example, two hypotheses for different events which would give a more accurate description of the cause of the detected phases.
- Azimuth and slowness estimates are performed on data filtered in a frequency band which varies from detection to detection. The optimal frequency band is determined on a case by case basis to maximize the signal-to-noise ratio (SNR) and it has been demonstrated (see, for example, Kværna and Ringdal, 1986) that, for observations of a given phase from repeating events at a given site, slowness and azimuth estimates are far more stable if the frequency band is kept constant.

The template system formulated here aims specifically to circumvent or, at least, mitigate these problems.

2.1 Event hypotheses

Seismic waves from an event occurring at a given location at a given time arrive deterministically at any given station. This is to say that, were it possible to measure both origin time and phase arrival time perfectly, the observed travel time would remain constant from event to event (assuming that no change affecting wave propagation has occurred within the medium between any two events). For a site of interest, we should therefore be able to define a “template” which describes the properties of the anticipated wavefield at a given set of stations in a given set of time windows relative to a hypothetical origin time. The principle is illustrated in Figure 3. Given that our focus is upon regional array processing, the wavefield properties which we will be considering are almost invariably measure-

ments of the slowness and backazimuth in the time-windows of interest using frequency-wavenumber (f-k) analysis (Capon, 1969). The time-windows will almost certainly correspond to the deterministic phases (Pn, Pg, Sn, Lg) which are typically used to locate an event at regional distances. Although the times of such arrivals are often well-predicted by velocity models, the calibration of such templates will, in general, require the observation of signals resulting from many events which have occurred previously at the site in question. (Manifestations of the Lg phase are notoriously difficult to predict on the basis of velocity models.)

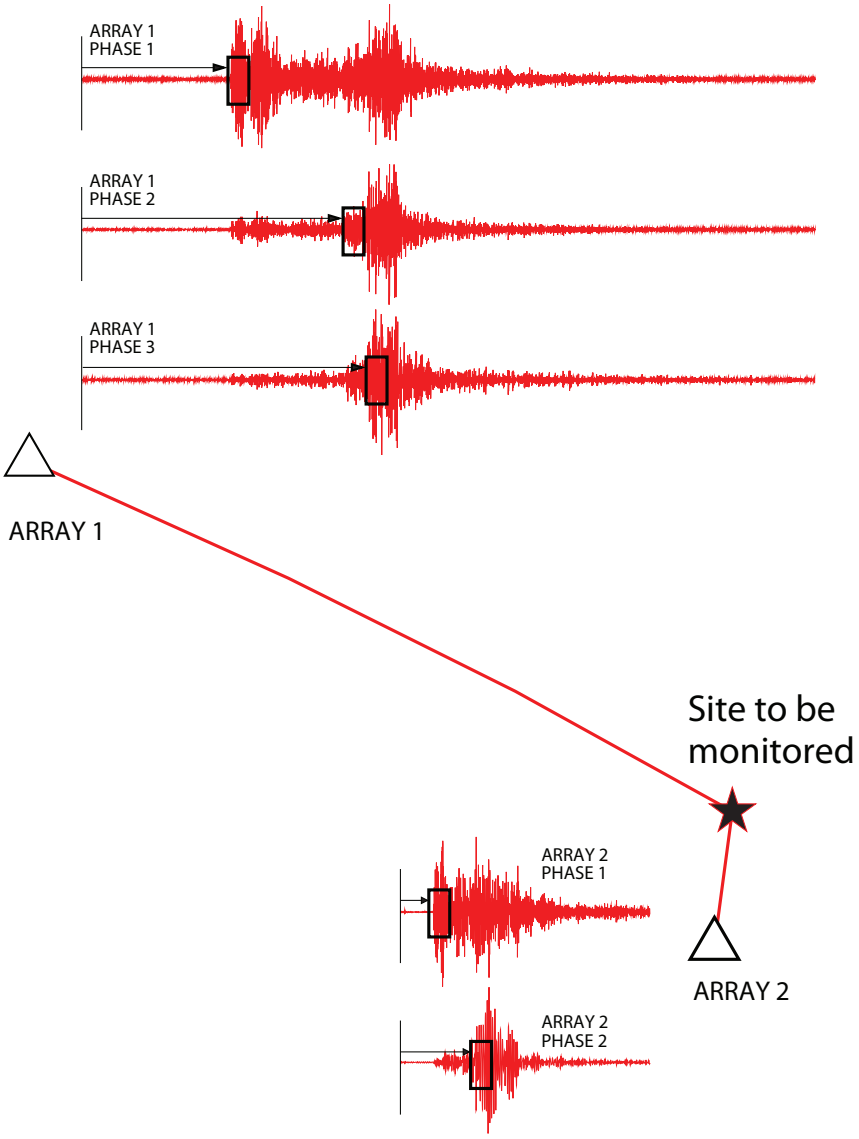

Figure 3: The concept behind a site template. Properties of the wavefield resulting from a seismic event should be observed at a selected number of stations at times fixed relative to the event origin time. A hypothesis that an event occurred at our site at a time t_0 can be tested by measuring the wavefield in a set of time-windows determined empirically from previous observations.

The most important criterion in selecting properties of the wavefield to measure is the degree to which that property varies for different events from the same site. Were the waveforms generated by each event identical, a cross-correlation calculation against a selected master waveform could confirm immediately whether or not the signals came from the same source. Indeed, whilst full waveform methods have been applied to the identification of quarry blasts (Harris, 1991, Rivière-Barbier and Grant, 1993), the majority of signals from such industrial explosions correlate quite poorly, either as a result of varying ripple-firing mechanisms and sequences, or as a function of source location within the quarry site (Bonner et al., 2003, McLaughlin et al., 2004). We consequently attempt to identify the most consistently observed properties of the wavetrain which can be measured using the traditional methods of regional array processing.

A pilot project started in the summer of 2002 had the objective of developing an online detector for seismic events from the Kovdor mine in NW Russia, using only the ARCES regional array at a distance of approximately 300 km. Given the prerequisite that any event at Kovdor should be able to be located using only phases recorded at a single array, reliable estimates of onset times and slowness for secondary phases were essential. The VESPA process (Davies et al., 1971) is ideal for illustrating the times at which coherent packets of energy are observed at an array, and a typical firing sequence from this site is shown with the corresponding vespagram in Figure 4. The presence of the Pn, Pg, Sn, and Lg phases is indicated by maxima of coherent energy with the anticipated slownesses at the anticipated times. This vespagram highlights at a glance one of the greatest challenges to the automatic processing of such industrial events; there is frequently more than one event within a short time interval, resulting in a multiplicity of primary and secondary seismic arrivals which makes any such automatic location estimates prone to error through a spurious association of phases. It is exactly cases such as these which lead to the large range of site-to-receiver distances displayed in the lower panel of Figure 1. This is in spite of the fact that the location estimates in Figure 1 are network solutions with observations from typically 2 or 3 regional arrays. A multiple event sequence as shown in Figure 4 will lead to multiple arrivals at all the stations and, without careful constraints upon the solution, a spurious identification of phases is still likely to cause a significant error in location.

The vespagram visualization indicates that the complicated succession of phases observed on the seismograms in Figure 4 can possibly be accounted for by two co-located events occurring in succession, the second approximately 27 seconds after the first[1]. For each of the phases Pn, Sn, and Lg, local maxima of coherent energy with approximately the same slowness are observed with approximately the same time-separation. This provides some grounds for optimism that an event classification based upon analysis of the wavefield in predetermined time-windows (see Figure 3) would indeed be able to classify (if not provide single-array location estimates for) the events. Gibbons et al. (2005) demonstrate how such a template treatment was able to classify[2] a very high proportion of Kovdor events within a given trial period including many events within multiple firing sequences. In the current contract, we aim to generalize the procedure applied to the Kovdor mine to a

1. Even describing the event as a “double event” is an oversimplification since each of the shots is a multiple ripple-fired salvo.

rather more general situation whereby a slightly larger source area may be considered (thus requiring a carefully controlled degree of flexibility in the definition of the time windows) and where observations from more than one seismic array may be considered.

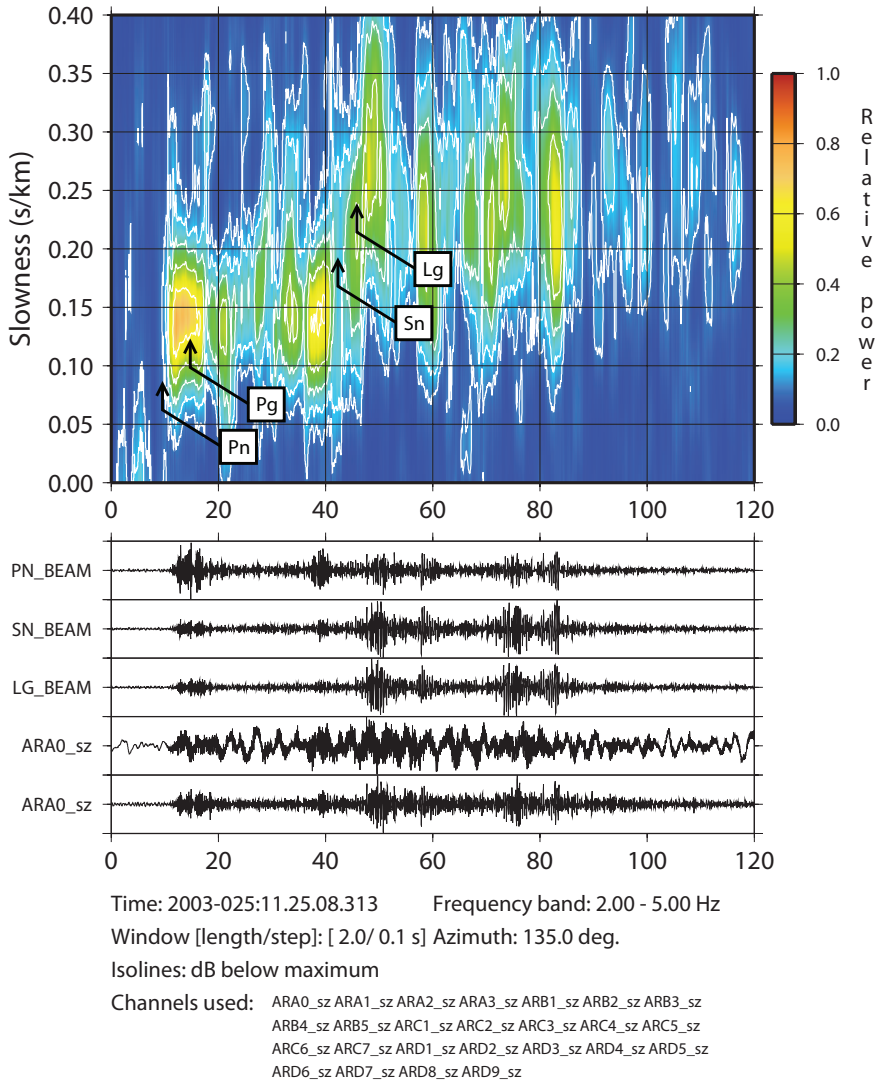

Figure 4: Vespagram for a blast at the Kovdor mine on January 25, 2003. This visualization of the wavefield indicates that the rather complicated wavetrain observed is probably the result two very similar events from approximately the same location. The coherent energy is observed within rather short time-windows corresponding to the arrivals of the deterministic regional phases as indicated; the coda appears to contain very little coherent energy. Taken from Gibbons et al. (2005).

2. Events were classified as being “very likely Kovdor events” if slowness estimates using broadband f-k analysis in fixed frequency bands, in pre-determined time-windows, fell within an empirically determined set of tolerance bounds. For a single array location estimate to be made, a satisfactory onset time estimate was also required for at least one secondary phase and this was not deemed possible for many complicated sequences. For a full discussion see Gibbons et al. (2005).

The "site template" concept (Figure 3), whereby the presence of phase arrivals is sought only in a finite number of predetermined time-windows, essentially mitigates the first two listed shortcomings of the GBF system. The presence of unrelated events or secondary events from the same site (providing multiplicity of similar phases) can be unproblematic provided that the slowness and arrival time measurements within the narrow time-windows are not too greatly compromised by the presence of the foreign signal. (An excellent slowness determination is often possible for a coherent phase arrival in incoherent signal coda, especially if the intruding signal occupies a rather different frequency range.) This is to say that our event hypothesis is unconcerned with what exists outside of these time-windows and will not attempt to incorporate phase detections from other times into the location estimate. Whereas the GBF attempts to determine which trial hypocenter best fits a set of associated phases, the site template system will simply reject an event hypothesis if insufficient evidence is found within the relevant time-windows for observations consistent with previous measurements of events from the given site.

To determine what constitutes "sufficient evidence" for the presence of an event from a given site is an enormous undertaking and studies of which conditions can reasonably be imposed to produce the desired level of confidence that we have an event from our site of interest is possibly the most challenging aspect of this work. In the schematic example[3] displayed in Figure 3, the site template defines five so-called "phase templates", each of which will be tested at the requested time relative to the hypothetical event origin time. It could be insisted that the data in each one of these time windows passed all the conditions imposed by the phase template (these conditions will be discussed in the next section). However, the likelihood is high that an event from the site being monitored would occur and fail to match one or more of the phase templates (for example because of a data outage, a poor signal-to-noise ratio, or a foreign signal). In the Kovdor study (Gibbons et al., 2005), it was found that many Sn phases were obscured by strong coda from secondary events from the same site; it was therefore decided only to insist that there was evidence for either the Sn or the Lg phase, and not both. As with most approaches to signal detection and event location, a balance needs to be achieved between detectability and the occurrence of false alarms.

2.2 Phase hypotheses

The automatic system is abstracted into two types of templates, site templates and phase templates. The site template states which phase hypotheses will be tested at which stations at which times, and contains a set of rules which attempt to evaluate the event hypothesis on the basis of the results reported from each of the phase hypotheses. A phase hypothesis postulates that the waveforms within the specified time-window display properties which are consistent with the corresponding observations from events confirmed to have taken place at the site being monitored. If measurements indicate that the specified time-window does appear to contain data consistent with the hypothesised phase, then we must also attempt to make the best possible evaluation of the phase arrival time.

3. The site is actually the Kirovogorsk mine of the Olenegorsk cluster displayed in relation to the ARCES and Apatity seismic arrays. The waveforms are taken from a routine industrial blast.

2.2.1 Slowness estimation

For the regional seismic array scenario which we focus on, the most applicable property is that of the slowness and backazimuth, or equivalently the vector slowness (s_x,s_y), measured by frequency-wavenumber analysis. This indicates the direction of arrival which provides the greatest array gain on the beam. An example of the relative beam power as a function of slowness is provided in Figure 5.

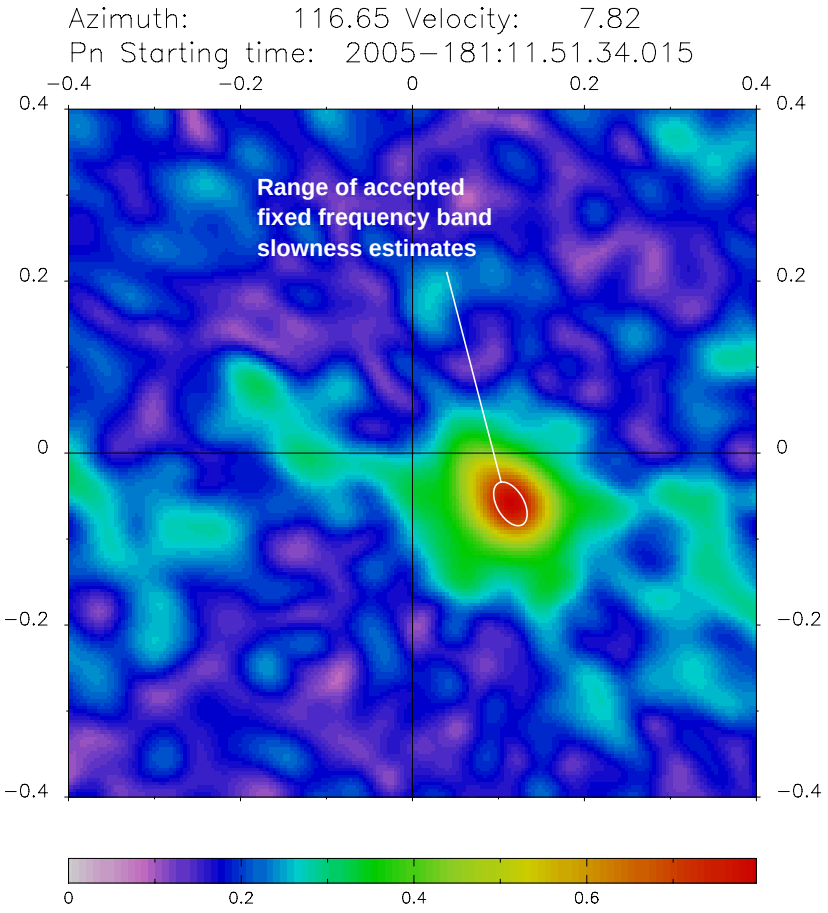

Figure 5: Relative beam power as a function of slowness (s_x,s_y) for a Pn phase recorded at ARCES from an industrial blast at a mine in the Olenegorsk cluster on the Kola Peninsula. This determination was performed in the 4.0-8.0 Hz frequency band which had been demonstrated to give highly stable estimates for events from this site. The observation of many events from the site being monitored allows acceptance bounds to be drawn within which the maximum relative power can be expected to fall if indeed the time window does contain the required phase from the required site.

The original narrow band method of Capon (1969) provides in principle the greatest accuracy, although Kværna and Ringdal (1986) demonstrated that, for a sequence of events that had occurred at the same location, the slowness estimates provided by taking the average over a range of adjacent wavenumbers was more stable. The mean and standard devi-

ation of azimuth estimates are often quite strong functions of the frequency band used to analyze the signal (see, for example, Bame et al., 1990) and very stable azimuth determinations are often made which indicate a significant deviation from the geographically predicted backazimuth (see, for example, Kværna and Doornbos, 1991[4]). The azimuth estimation capability of the ARCES array was specifically addressed by Carr (1993) and Schweitzer (2001b) displays slowness corrections calculated for a set of test events.

The optimal frequency band in which to process slowness estimation is not a foregone conclusion. Although Carr (1993) shows general trends for different pass-bands and array configurations, the situation may vary significantly for different sites and source types. Figure 6 indicates how the slowness estimates for initial Pn-arrivals from Kovdor explosions vary in different frequency bands. The top left panel in this figure shows the variation of the slowness estimates for the variable frequency bands. The large spread of these estimates is another of the principal reasons for the large spread of the GBF locations illustrated in the lower panel of Figure 1, and an obvious strategy for the mitigation of event mislocation due to such errors is to apply one of the more stable frequency bands. However, Figure 7 indicates an additional potential difficulty. The frequency band producing the most stable slowness estimates for large (high SNR) signals may produce spurious results for weaker signals (which is clearly the motivation for using variable frequency bands in the routine processing system). Figure 6 suggests that the most stable frequency band for measuring the slowness of Pn-arrivals from Kovdor is the 2-5 Hz band; however, the background noise in this frequency band is generally far stronger than at higher frequencies and a lower magnitude event from the same site could quite conceivably return a misleading slowness estimate in this frequency band and yet a qualitatively correct estimate for a higher frequency. Figure 7 illustrates the conflicting trends of signal coherency over the array (which decreases with increasing frequency) and SNR (which, in this case, increases with increasing frequency). At the highest frequencies, the coherence is lowest and large sidelobes often lead to qualitatively misleading slowness estimates (see the lower right panel of Figure 6).

For each of the sites to be considered, we have studied extensively the stability of slowness estimates for key phases as a function of frequency band.

4. This study interpreted consistent deviations in the measured backazimuths as an indication of scattering by Moho topography.

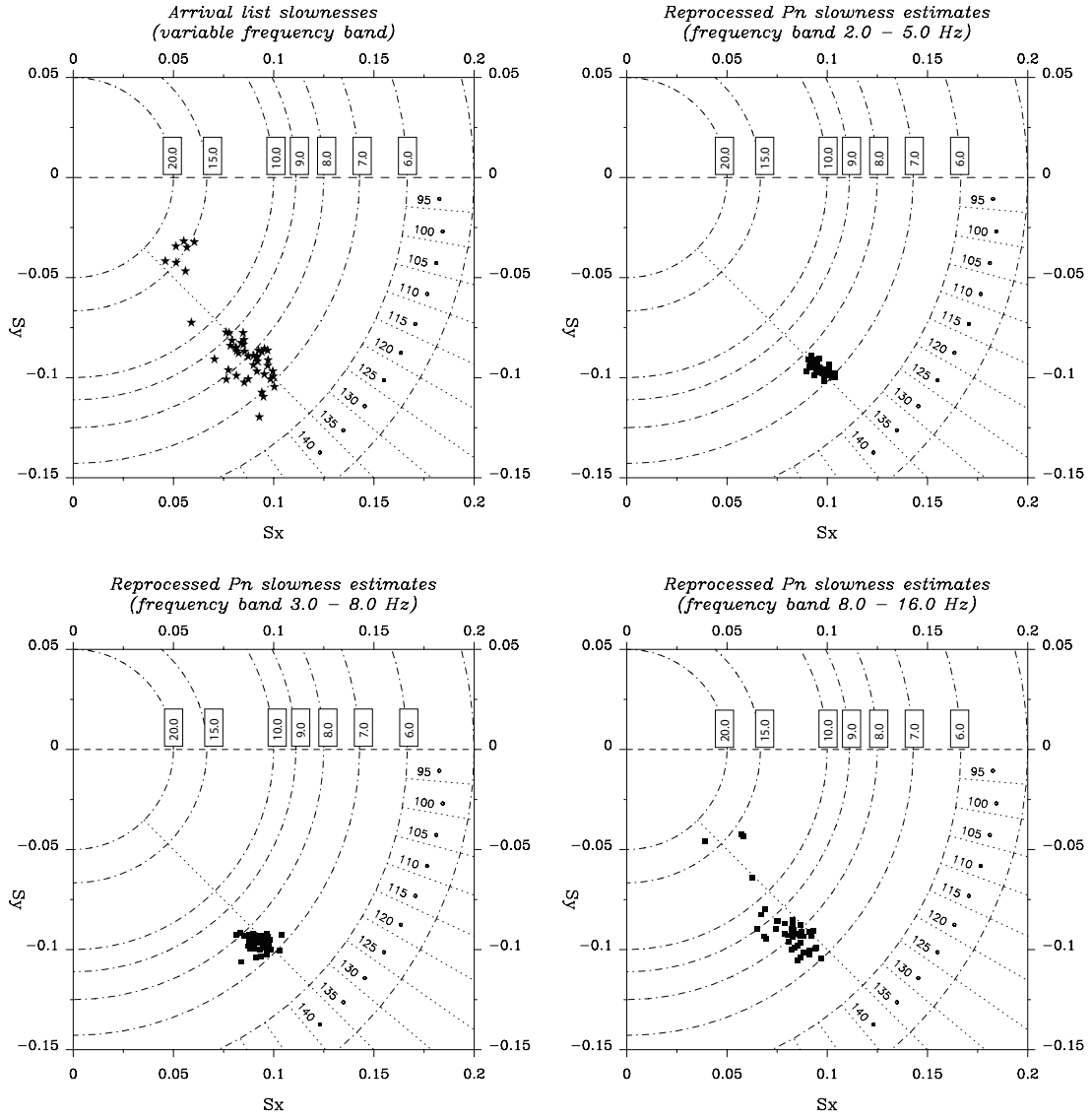

Figure 6: Slowness estimates for wide-band f-k analysis for first Pn arrivals at ARCES from confirmed blasts at the Kovdor mine between October 2001 and September 2002. The geographical backazimuth is 135^{o}. The top left panel shows variable frequency band estimates from the automatic detection lists and the remaining panels are for fixed-frequency band reprocessing as indicated. Taken from Gibbons et al. (2005).

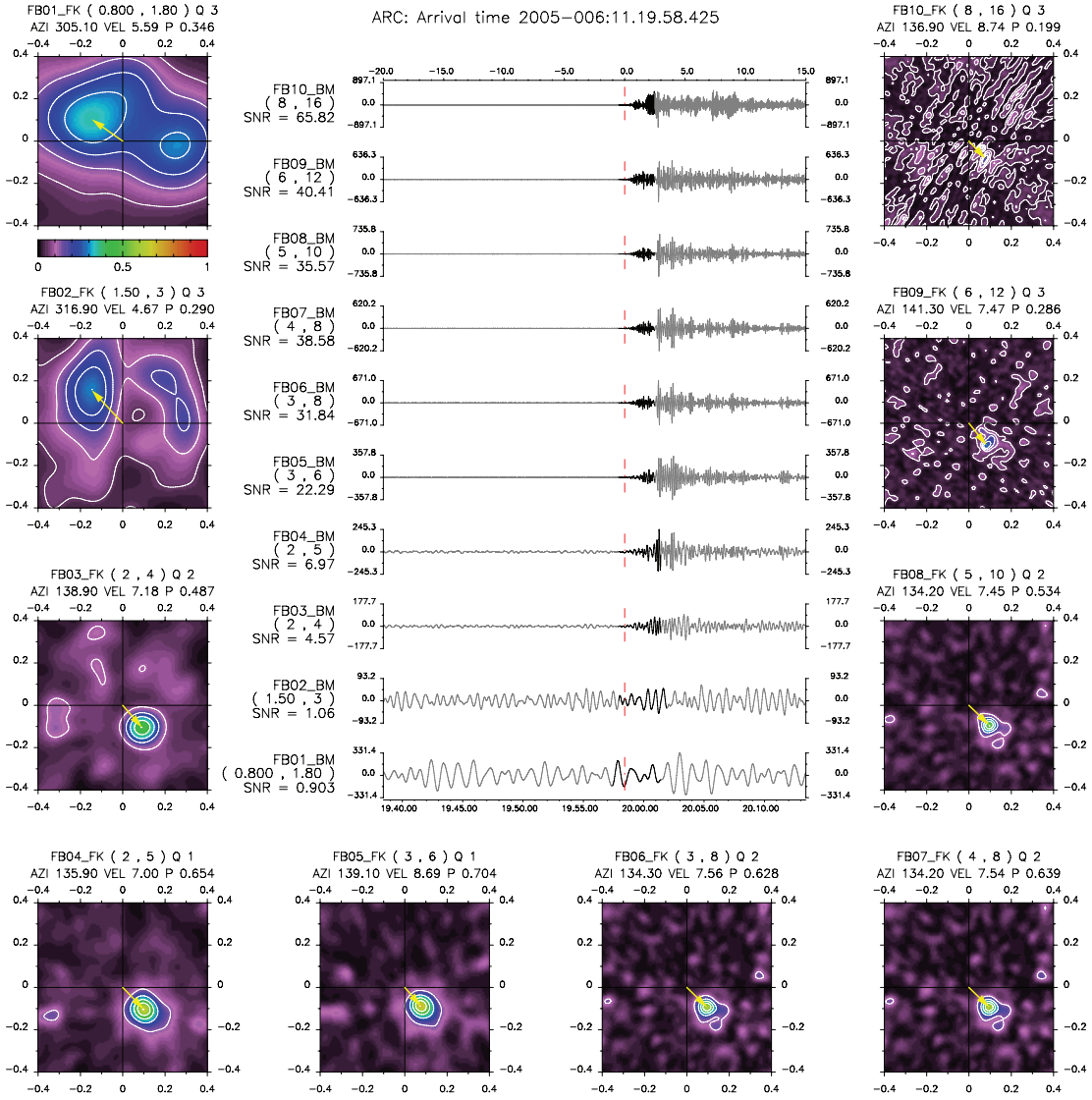

Figure 7: Relative beam power as a function of slowness for the initial Pn-arrival at ARCES from an event at the Kovdor mine, in ten different fixed frequency bands as indicated. The waveforms show the beams corresponding to the maximum relative beam power, filtered in the relevant frequency band.

2.2.2 Re-estimation of phase arrival time

Whilst slowness analysis facilitates the identification of a phase, a satisfactory arrival time estimate is necessary if the phase is to be used for obtaining an event location estimate. Gibbons et al. (2005) applied the AR-AIC (Autoregressive - Akaike Information Criterion) method (Akaike, 1973; GSE/JAPAN/40, 1992; Leonard and Kennett, 1999) and found that this provided excellent estimates for the Pn-arrivals from Kovdor events due to the large contrast in amplitudes over a wide range of frequencies.

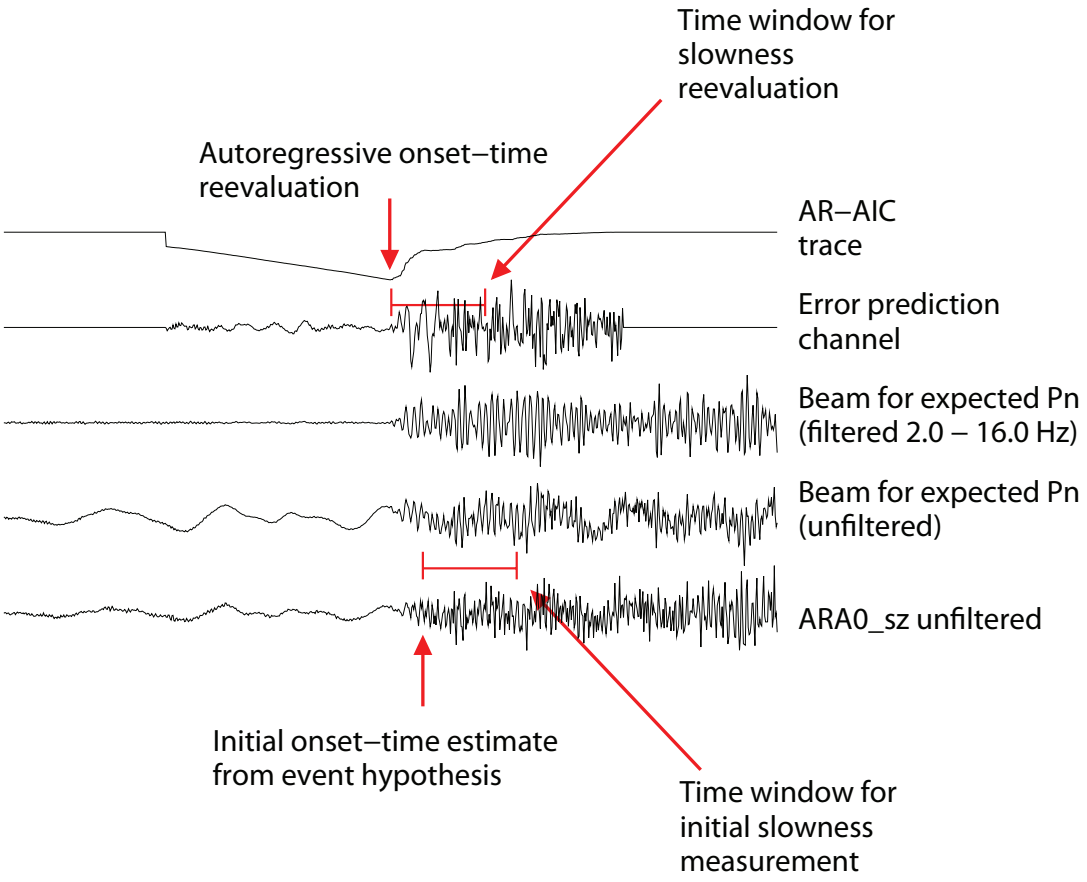

Figure 8: Illustration of an iterative refinement to the arrival time estimate. The slowness is first evaluated using broadband f-k analysis in a time window as indicated, dictated by the initial onset estimate. The slowness value is subsequently tested to see if it falls within the bounds of expectation (c.f. Figure 5). A new beam is formed according to the slowness parameters corresponding to the maximum beam gain and this trace is subsequently band-pass filtered in a wide frequency band, error-prediction and subjected to an auto-regressive onset time estimation. If the new time satisfies a set of quality-control tests (testing values of the Akaike Information Criterion, the Signal to Noise Ratio, or the deviation from the expected arrival time) then a new slowness determination is made relative to this onset time. The procedure may be repeated, although it is not recommended to perform many iterations since any workable convergence tolerance is limited by the standard error anticipated within each iteration.

Given the limited source region of interest, and the fact that the study was limited to a single array station, Gibbons et al. (2005) fixed a time-frame relative to the autoregressive Pn- arrival time estimate and measured slowness for the secondary phases in time-windows fixed relative to the Pn onset estimate. Arrival time estimates for the secondary phases were also attempted using AR-AIC using fixed beam definitions and fixed initial estimates. In order to provide a limited degree of flexibility, we introduce an iterative refinement to the onset time estimate as is displayed in Figure 8. Whilst this in principle allows for a slightly wider source region to be considered, in practice, the method is still limited to geographical confines as indicated by Figure 3. The dual control checks that, for an acceptable phase determination, the slowness estimate must fall within carefully determined boundaries and that the beam at the onset time estimated must show evidence of a phase arrival (for instance by displaying an SNR which exceeded a specified threshold value) mean that no phase identification used in an event location is ever likely to deviate greatly from that specified in the template.

3. Development of site-templates for locations NW Russia and Fennoscandia

All templates for site-specific monitoring require calibration. In the following sections, we cover three different cases.

3.1 Mining sites in NW-Russia confirmed by mining operators

The sites in NW Russia displayed in Figure 1 have been amenable to calibration for site-specific monitoring due to the provision of high-quality Ground Truth (GT) information from the operators of the mines. The information was collected under the DoE-funded contract "Ground-Truth Collection for Mining Explosions in Northern Fennoscandia and Russia" (Harris et al., 2003). The names of the mines are listed together with coordinates in Table 1; their positions in relation to the ARCES array are displayed in Figure 10.

Table 1: List of mines and quarries in NW-Russia for which Ground Truth data for routine industrial events was provided.

Name	Code	Latitude (degrees N)	Longitude (degrees E)	Distance from ARCES (km)	Azimuth from ARA0	Approximate diameter (km)
Zapoljarni						
Zapadny	zp1	69.404	30.682	203	91.696	1.0
Central	zp2	69.397	30.742	205	91.837	2.0
Olenegorsk						
Olenegorsk	ol1	68.154	33.192	345	112.83	1.0
Kirovogorsk	ol2	68.106	32.996	341	114.29	1.0
Bauman	ol3	68.057	33.145	349	114.53	1.0
Oktjabirsk	ol4	68.078	33.106	346	114.34	1.0
Komsomolsk	ol5	68.075	33.385	356	113.41	2.5
Khibiny						
Kirovsk	kh1	67.670	33.729	393	117.97	2.0
Rasvumchorr	kh3	67.631	33.835	400	118.10	2.5
Central	kh4	67.624	33.896	402	117.98	3.0
Koashva	kh5	67.632	34.011	406	117.47	3.0
Norpakh	kh6	67.665	34.146	408	116.58	1.5
Kovdor						
Kovdor	kv1	67.557	30.425	298	135.38	2.0

GT events during the period October 1, 2001, to September 30, 2002, were used to calibrate the phase- and site-templates. Subsequent GT events were used only to verify and evaluate the reliability of the detection and location algorithms developed. The GT events used for template calibration are listed in their entirety in Appendix 1. The observation of vespagrams for the identification of characteristic phase arrivals as performed for the Kovdor mine (Gibbons et al., 2005) was repeated for each of the sites listed in Table 1 for large numbers of the GT events. Representative waveforms for each of the mining regions are displayed in Figure 9 together with indicators of the arrival times deemed to be

observed consistently for the characteristic phases. A few comments need to be made regarding Figure 9. Firstly, whilst the signals displayed are not atypical, they were chosen because they indicate a relatively simple source-time function. Many other events were clearly multiple events (c.f. Figure 4) and, whilst these cases will need to be dealt with by any robust detection/location algorithm, they are not helpful for illustrating phase occurrence. Secondly, the plot from the Olenegorsk event displays a clear Pg arrival approximately 8 seconds following the initial Pn-arrival (confirmed by slowness analysis). However, for none of the sites was the Pg arrival deemed sufficiently robust to be used as an identification criterion for the site (usually due to the presence of high-amplitude P-coda from multiple arrivals).

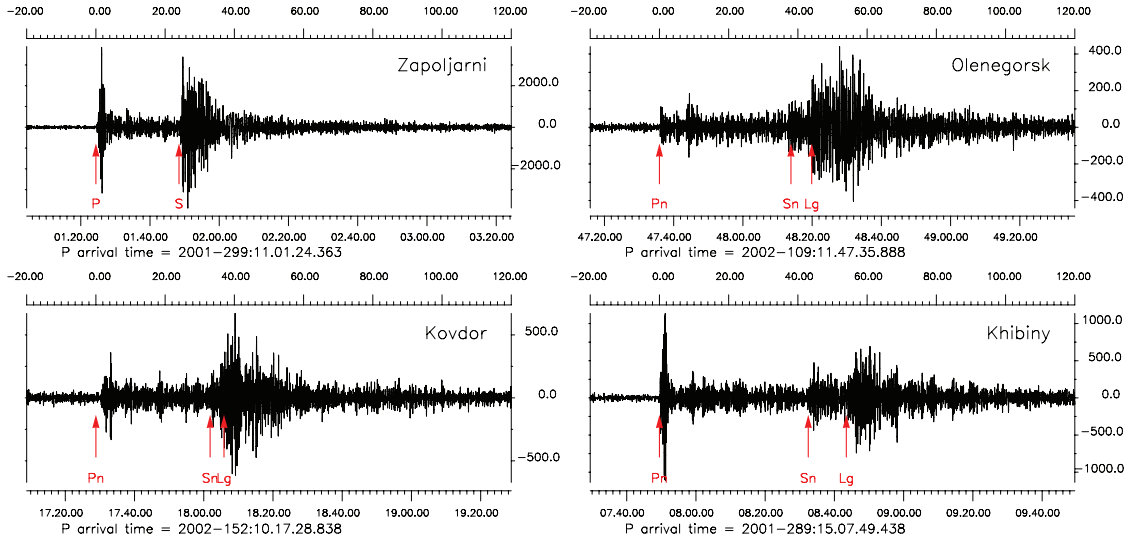

Figure 9: A waveform from one event from each of the four mining regions studied. The trace from the central ARA0_sz array element is displayed filtered in the frequency band 2.0 - 5.0 hz. According to the *barey* velocity model (as tabulated by Hicks et al., 2004), the Pb, Pg, and Pn phases all arrive within a second of each other for events from the Zapoljarni mines (distance 204 km from ARCES), as do the Sb, Sg, and Sn phases; we therefore simply denote first arrivals P and S. For the more distant mines at 298 km (Kovdor), 345 km (Olenegorsk), and 400 km (Rasvumchorr, Khibiny), Pn and Sn are the first arrivals and are indicated as predicted by barey. The time for the Lg phase is based upon observations of the Ground Truth events.

We first need to investigate the variability of slowness measurements for each of the characteristic phases. Figure 10 shows the mining sites in relation to the ARCES array together with the fully automatic (variable frequency band) slowness estimates for the initial phase arrivals from the GT events for the sites as indicated by the color codes. In most cases, the direction estimate is qualitatively correct but the variability is very large and it is easy to see how the errors inherent in these estimates will have consequences for automatic location estimates given the small number of constraining phases (c.f. Figure 1).

The black symbols in Figure 10 (corresponding to initial P-arrivals from the Kovdor events) are exactly the same data points displayed in the upper left panel of Figure 6. Since the remaining panels of Figure 6 indicate the dramatic improvement to the stability of the

slowness estimates resulting from the processing in fixed frequency bands, the next step is to investigate the extent to which the same pattern is observed for the remaining sites.

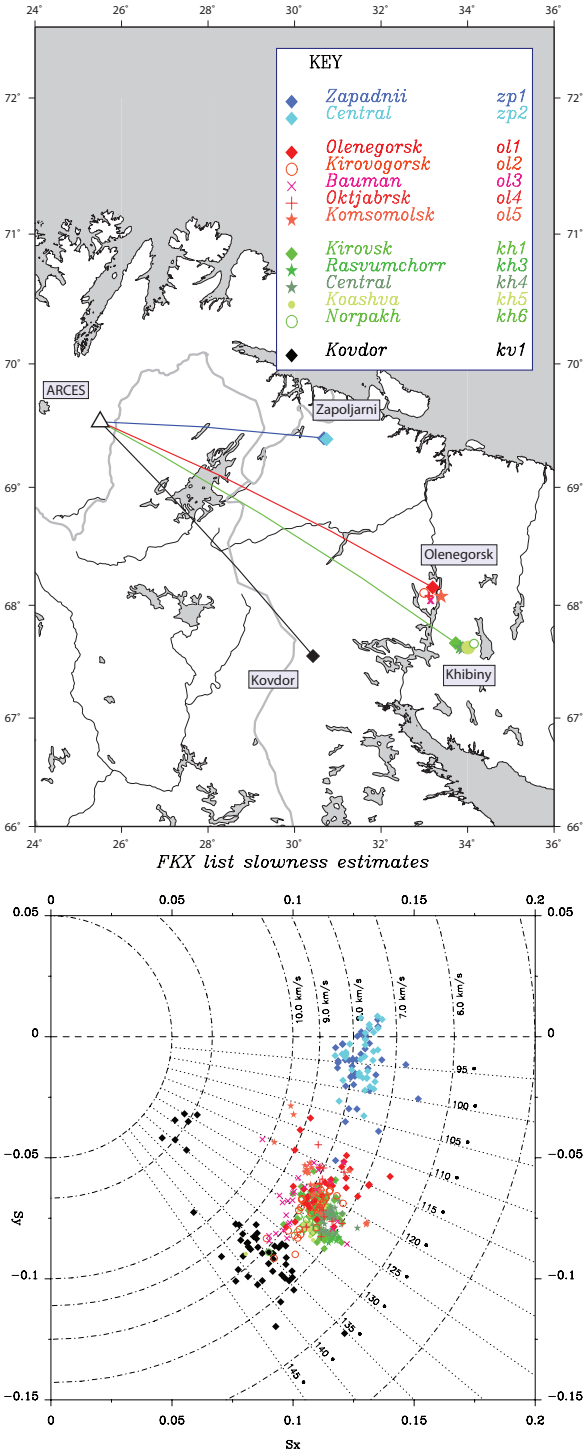

Figure 10: (Upper panel) Mines within the Zapoljarni, Olenegorsk, Khibiny, and Kovdor clusters in relation to the ARCES regional seismic array. (Coordinates are provided in Table 1.) (Lower panel) direction estimates for the initial P-arrivals for each of the trial GT events taken from the fully automatic ARCES detection lists.

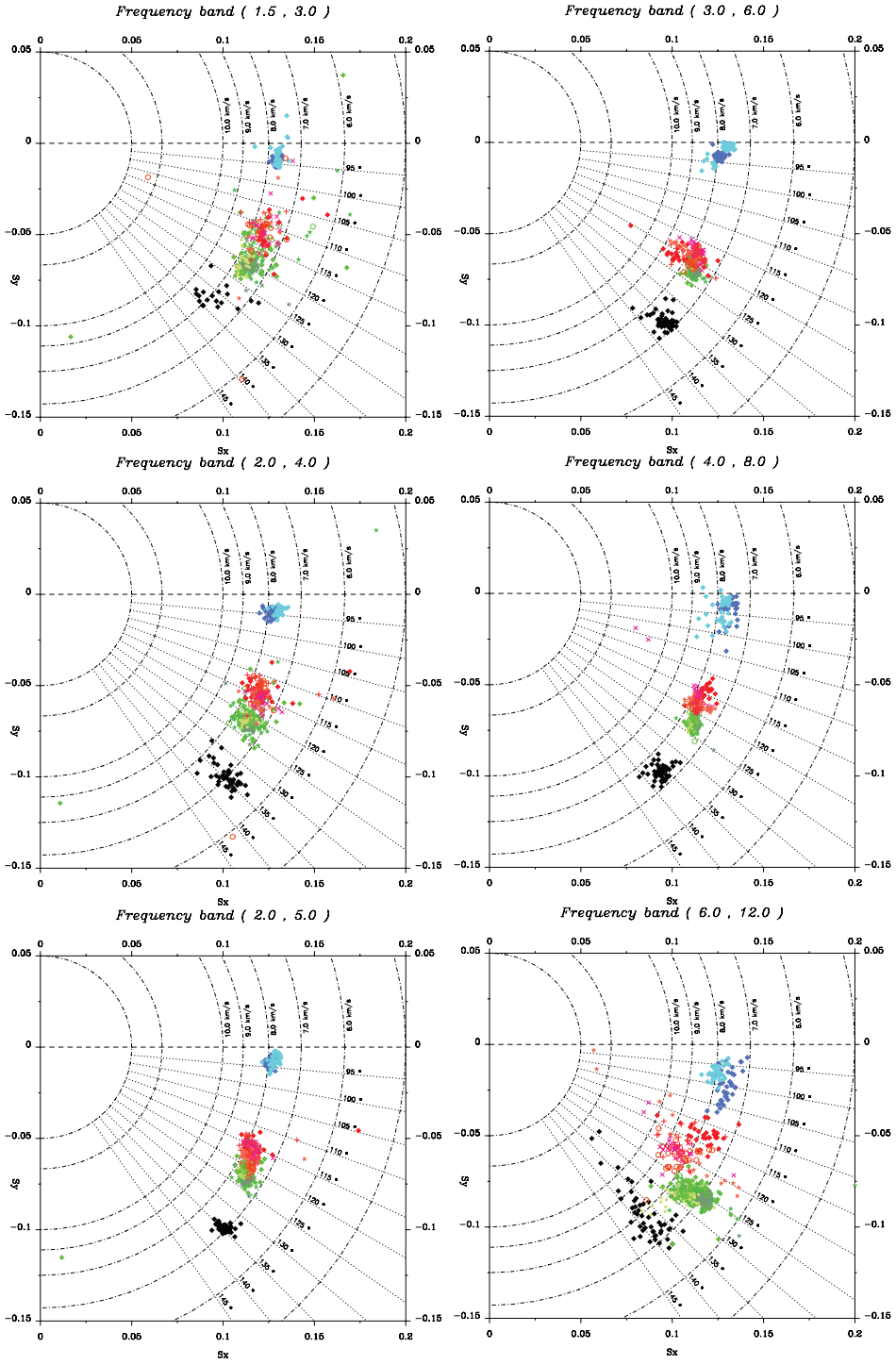

Figure 11: Fixed frequency band slowness estimates using broadband f-k analysis in the frequency bands indicated for initial P-arrivals from the GT events from the mining sites on the Kola Peninsula (see Appendix 1). Color codes are identical to those displayed in Figure 10.

Figure 11 displays directional estimates in the fixed frequency bands as indicated for the initial P-arrivals from the mining events displayed in Figure 10. It should be noted that the time-windows in which the slowness measurements in Figure 11 were made are all defined relative to the manually picked phase arrival times provided in Appendix 1. The automatic estimates in Figure 10 are made relative to automatically determined phase onset times which do not necessarily coincide with the reference times listed. In many cases, several P-detections with similar slowness estimates occur in rapid succession of each other and the initial P-arrival as determined by the multi-array GBF solution is not always the first in a given sequence. This situation is exacerbated by the complicated firing sequences employed in the execution of many of these events.

The upper left panel of Figure 11 shows the fixed-band results for the 1.5 - 3.0 hz frequency band. There are clearly far fewer points in this panel than in the corresponding panels for the higher frequency bands. This is because the SNR in this frequency band is very small for the majority for the majority of these signals and the waveforms in the specified time-windows are frequently dominated by high-amplitude coherent microseisms from the Barents Sea to the North. It is clear that with such a high “miss rate”, the 1.5 - 3.0 hz frequency band would not support effective diagnostic tests for any of these phases.

The center-left panel of Figure 11 contains a far higher percentage of the data points - almost certainly the result of a significantly higher SNR in the 2 - 4 hz frequency band. It is particularly noteworthy how much smaller a region of slowness space the fixed-band P-arrival estimates from the Zapoljarni mines (blue symbols) occupy than for the variable bands. Using the 2-4 hz band azimuth estimates in the event location procedures as opposed to the estimates from Figure 10 would almost certainly reduce significantly the standard deviation of estimates displayed in Figure 1. The variation for the estimates for P-arrivals from the Khibiny, Olenegorsk, and Kovdor events is also lower for the 2-4 hz measurements than for the variable-band results although the spread is larger than for the Zapoljarni events.

Increasing the upper frequency limit from 4 hz to 5 hz (lower left panel) reduces the variation for all of the mining clusters. The center-right and upper-right panels indicate however that considering higher frequencies does not result in a uniform improvement to the stability of the phase estimates. Comparing the 2-4 hz band (center-left panel) to the 4-8 hz band (center-right panel) shows that the P-estimates for the Zapoljarni mines are far more stable for the lower frequencies whereas the Pn-estimates for the Khibiny events are far more stable for the higher frequencies. This result cannot be predicted from simply studying the coherence of waveforms at different frequencies between different array sensors and can only be observed given significant numbers of confirmed events from the sites of interest. This is clearly a difficulty in the challenge of accurate event-location in regions where good calibration data is not available.

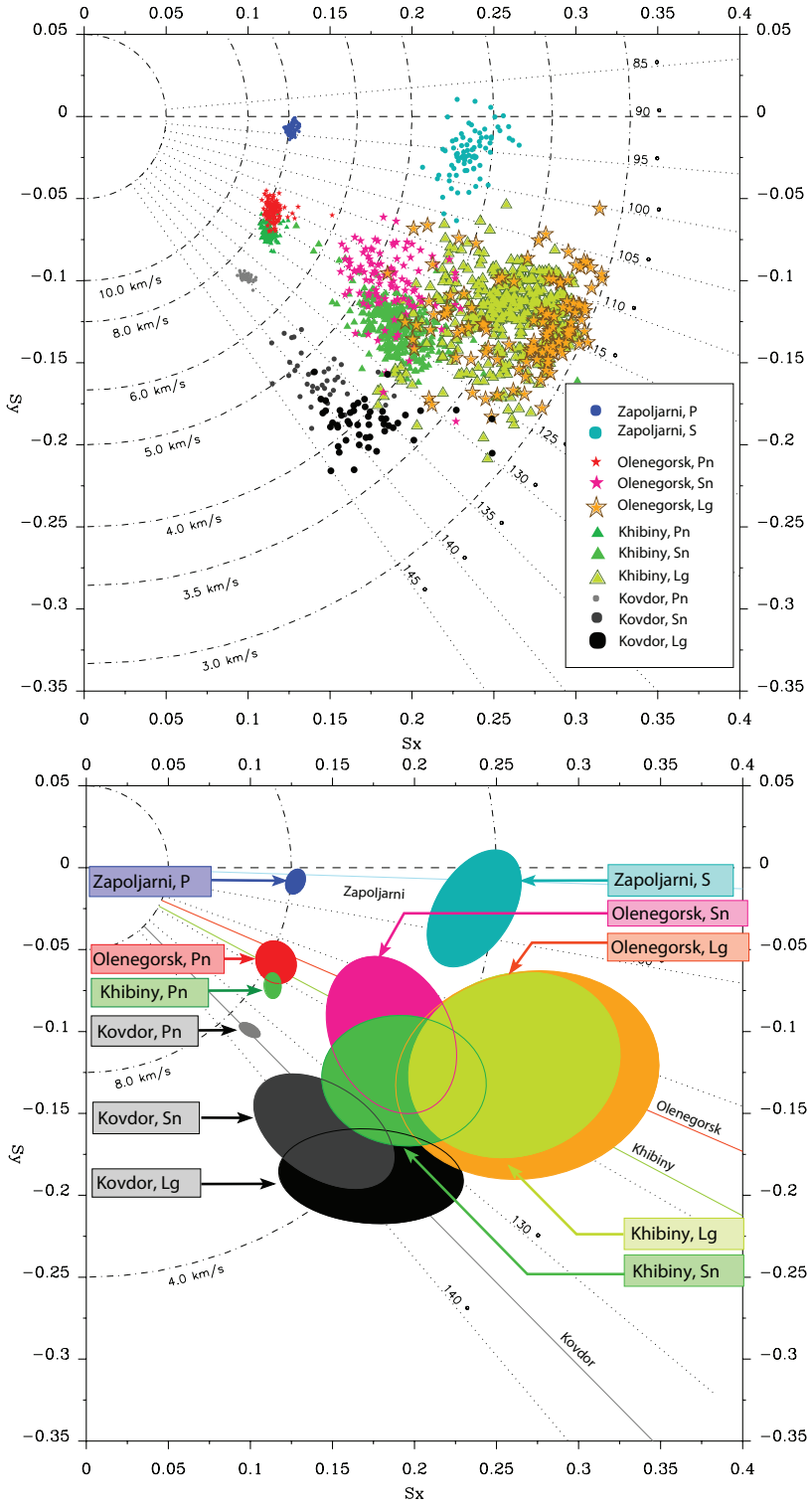

Figure 12: Summary of fixed frequency band slowness estimates for the 2.0 - 5.0 hz frequency band. The upper panel displays the individual measurements and the lower panel displays the 95% confidence ellipses. Phases from the different mines in the Zapoljarni, Olenegorsk, and Khibiny clusters are grouped.

The lower-right panel of Figure 11 shows the corresponding estimates for the 6 - 12 hz frequency band. The spread is notably larger than for the intermediate frequency bands and inspection of the f-k grids (c.f. Figure 7) suggests strongly that this is the result of incoherence of the smaller length scale wavefield. It should be noted that this is in spite of the removal of the outermost nine elements of the array (the so-called D-ring) for f-k calculations in this frequency band. However, it is interesting to note that many of the slowness estimates from the different source regions actually separate out in slowness space. This is especially notable for the two mines in the Zapoljarni cluster. The mines are so closely spaced that a seismic array with the dimensions of ARCES at this distance should not able to resolve the different slowness vectors from these two sources. It is most likely that the general direction is determined by coherent waveforms recorded on the closely-spaced innermost sensors and that the nuances result from deviations from planarity which result from small-scale source or path-specific features of the waveforms on other subsets of sensors. The consequences are that care must be taken when interpreting f-k results measured in high frequency bands, but also that there is cause for optimism for the effectiveness of full-waveform methods in classifying the events (c.f. Harris, 1991).

The absence of a “universally optimal” frequency band means that the processing in multiple frequency bands is unavoidable if estimates are to be made optimal for any particular target phase. A judicious selection of frequency bands is necessary for each phase for each site monitored. Comparing the different P-arrivals for the various phases in Figure 11 indicates that the 2 - 5 hz frequency band provides the smallest summed variance, even if a different band is likely to provide a better result for any single phase. The results for both P- and S- phases in the 2 - 5 hz band are displayed in Figure 12. The first observation is how much larger the confidence ellipses for the S-phases are than for the P-phases. The f-k estimates for the S-phases are made in time-windows fixed relative to the initial P-onset time for each site (c.f. Gibbons et al., 2005). The windows chosen were picked based upon observations of many vespagrams and filtered beams (on both vertical and rotated seismograms). Ringdal and Husebye (1982) observed how the coherence over arrays of the more highly scattered and more slowly propagating S-phases diminished more rapidly with increasing frequency than the corresponding P-phases. In this case, this property is compounded by the complicated time series which emerge as a result of these industrial firing sequences. Many of the S-arrival observations are corrupted by high-amplitude coda phases from different events in a given sequence. If the events are to be located by a procedure which uses the azimuth as a parameter (e.g. HYPOSAT, Schweitzer, 2001a) then we need to ensure that the azimuth associated with the fixed frequency band P-slowness estimate is given a higher weighting than the azimuth associated with the corresponding S-phases.

The final observation from Figure 12 is that the mean values of the slowness distribution lie significantly away from the geographical backazimuth meaning that a slowness correction needs to be applied prior to the location routine (c.f. Schweitzer, 2001b). In the Kovdor case study, Gibbons et al. (2005), although a slowness correction was applied, the effect was very small. The lower panel of Figure 12 shows how the azimuth biases observed for the Zapoljarni, Olenegorsk, and Khibiny mining regions are substantially greater than that observed for the Kovdor mine. If these measurements were applied uncorrected, this would lead to a large mislocation error in the single array case.

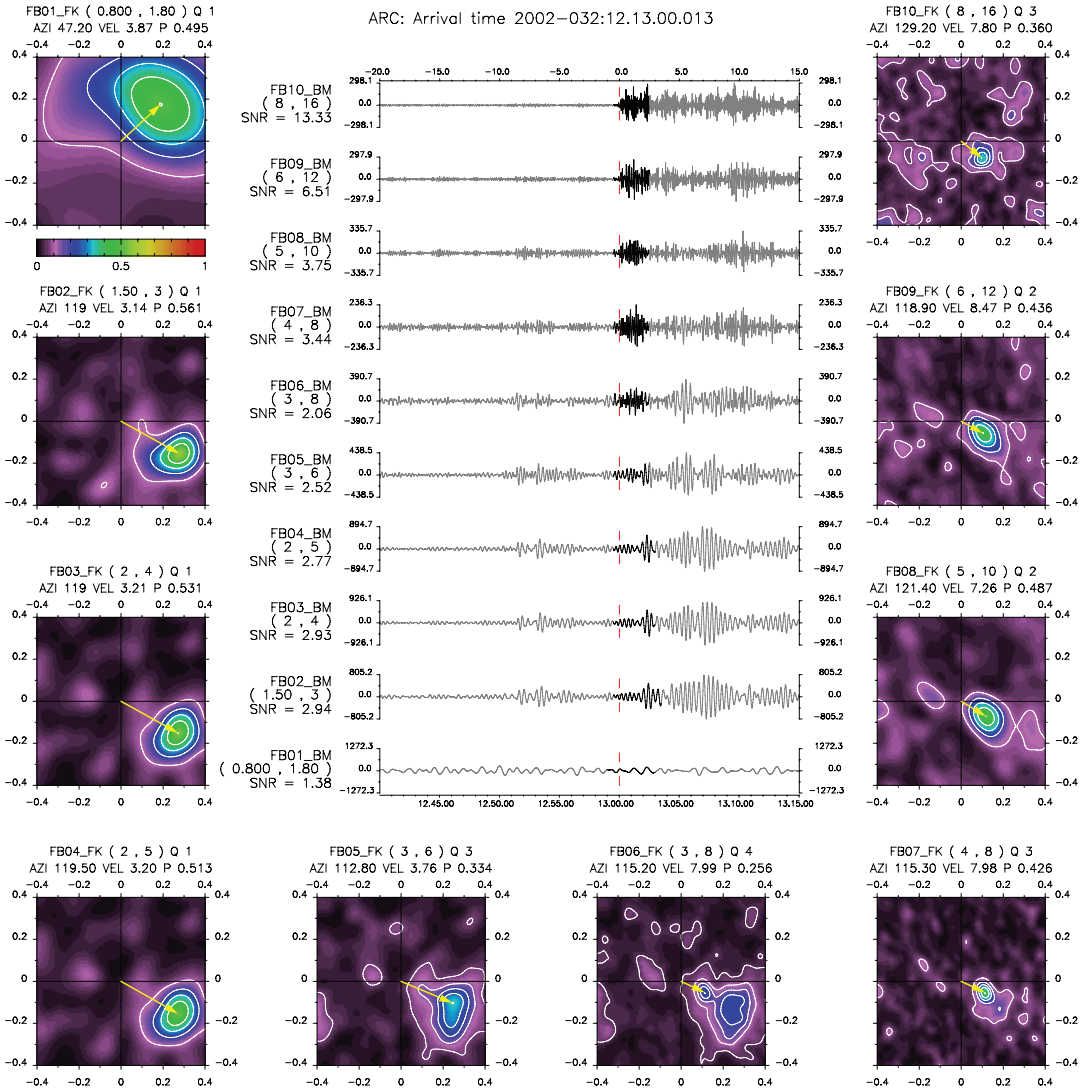

Figure 13: An illustration of the need to consider multiple frequency bands in order to reduce the risk of non-identification of key phases due to the presence of foreign signals in otherwise optimal frequency bands. The above figure is for the ARCES array with a reference time of 2002-032:12.13.00.013. The arrival is a Pn phase from a GT-mining event from the OL3 mine (Olenegorsk: see Table A1.9) and the interfering signal is coda from a GT-mining event at the Khibiny Central mine (KH4: see Table A1.3).

Figure 13 highlights the possibility of missing a key phase if only a single optimum phase is selected for examination. The signal of interest may be well recorded in a different frequency band - in this case one which is higher than the interfering coda signal.

3.2 Military Ammunition Destruction Explosions in Northern Finland

Each year between mid-August and mid-September, a series of explosions in the north of Finland is recorded by the stations of the Finnish national seismograph network and also by the seismic arrays in northern Fennoscandia and NW Russia. Based upon event locations given in the seismic bulletin of the University of Helsinki, the geographical coordinates of the explosion site are assumed to be approximately 68.00^{o}N and 25.96^{o}E. The explosions are carried out by the Finnish military in order to destroy outdated ammunition and are easily identified from the automatic seismic bulletins at NORSAR for several reasons. Firstly, they are always detected with a high SNR on the ARCES array, secondly they register very stable azimuth estimates on the detection lists, and thirdly they take place at very characteristic times of day (the origin time indicated by the seismic observations almost invariably falls within a few seconds of a full hour, or half-hour in the middle of the day). A preliminary list of candidate events was obtained by scanning the GBF (Kværna and Ringdal, 1989) automatic detection lists for events which appeared to come from the correct region at appropriate times of day. A typical example is shown in Figure 14.

CENTRAL LAPLAND FINLAND

Origin time	Lat	Lon	Azres	Timres	Wres	Nphase	Ntot	Nsta	Netmag
2001-228:14.00.01.0	68.03	25.77	2.88	0.87	1.59	4	9	2	1.23

Sta	Dist	Az	Ph	Time	Tres	Azim	Ares	Vel	Snr	Amp	Freq	Fkq	Pol	Arid	Mag
ARC	168.0	176.2	Pn	14.00.28.7	0.7	175.9	-0.3	6.6	88.9	1503.1	8.06	2		596316	
ARC	168.0	176.2	Lg	14.00.49.4	0.4	177.4	1.2	4.0	21.1	492.3	4.77	4	2	596321	0.92
ARC	168.0	176.2	s	14.00.53.8		169.8	-6.4	3.9	7.7	478.6	3.68	3		596324	1.02
ARC	168.0	176.2	s	14.00.58.0		174.6	-1.6	4.1	3.8	280.2	3.17	3		596327	
APA	308.4	282.3	Pn	14.00.45.7	-0.7	291.0	8.7	9.8	10.7	670.8	6.67	2	1	596317	
APA	308.4	282.3	p	14.00.51.8		286.0	3.7	8.2	6.0	299.2	6.43	3	1	596318	
APA	308.4	282.3	s	14.01.21.0		284.0	1.7	4.1	11.3	683.4	5.02	2	-2	596322	
APA	308.4	282.3	s	14.01.24.1		282.4	0.1	4.1	4.7	487.5	3.30	1	-2	596323	1.44
APA	308.4	282.3	Lg	14.01.27.4	-1.6	283.6	1.3	4.1	4.7	393.8	4.43	3		596325	1.21

Figure 14: Automatic event location estimate from the GBF list
http://www.norsar.no/NDC/bulletins/gbf/2005/GBF05242.html
The event is characterized by a high SNR for the P- phase at the ARCES array, an S-P time of approximately 20 seconds for ARCES, and a backazimuth from ARCES of ~177^{o}. The location estimate incorporates detections from the ARCES and Apatity arrays.

Between 2001 and 2005 (up to and including day 254), a total of 108 events were found which appeared to fit the general attributes of explosions from this site; the GBF location estimates for these events are displayed in Figure 15. Whilst the reasons for errors from the GBF algorithm are well understood (page 9), the spread observed in Figure 15 is disappointing. Both P- and S- phases are detected with a high SNR on the ARCES array and the simplicity of the source-time functions (there is no ripple-firing and no multiple shots) should prevent the confusion of multiple phase arrivals. A factor which may be significant is that the events frequently result in detections at the Apatity array which show a far greater variability than the automatic phase estimates at ARCES. This is due to a combination of a far lower signal to noise ratio, far greater competition from interfering signals, and a far less advantageous array response function. Not only are the azimuth and apparent velocity estimates from the Apatity array far more varying, but the arrival times show a far greater variation and phase misidentification is often pivotal in defining poor epicentral distance estimates.[5]

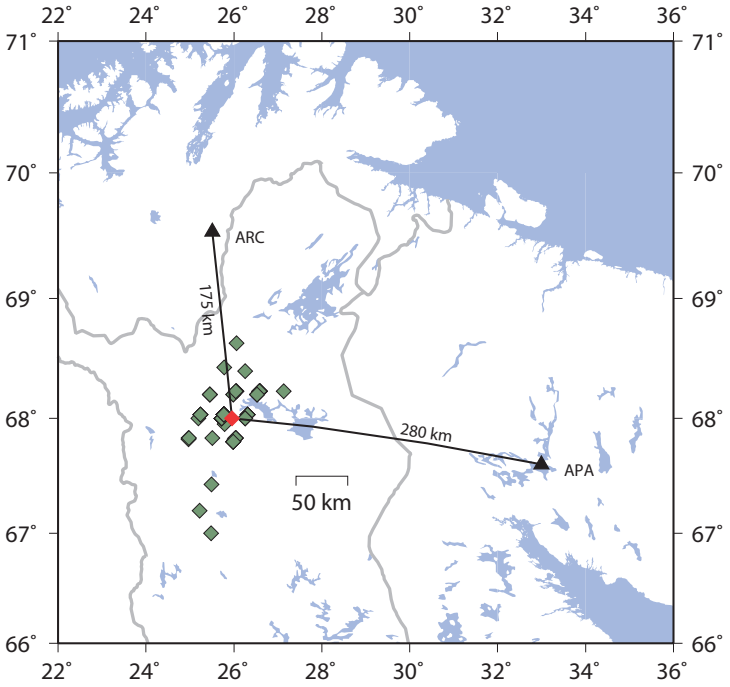

Figure 15: Estimated location of explosion site (orange diamond) in relation to the seismic arrays ARCES and Apatity together with the GBF fully automatic location estimates for 108 candidate events between August 2001 and September 2005 (green diamonds). The regular pattern of event location estimates is due to the fixed-grid trial epicenter procedure employed by the GBF.

Figure 16 (left) illustrates the direction estimates for the defining P-phase from the ARCES array for each of the Finnish explosions displayed in Figure 15. These display a considerable spread in both azimuth (up to ten degrees in each direction of the assumed true direction) and in apparent velocity (low values are likely to result in a Pg phase classification and high values are likely to result in a Pn phase classification). The panel to the right shows broadband f-k measurements for the same arrivals in the listed fixed frequency bands. We observe that for any single frequency band, the slowness estimates are far more stable than for the variable band estimates. Whilst this is to be expected from previous results, the improvement in the stability is nonetheless surprising. A second observation is that the populations of estimates from the different frequency bands are almost entirely mutually exclusive and so, if restricted to the current set of fixed frequency bands, the apparent direction of the incoming phase is almost entirely defined by the frequency band used. The spread of the FKX-list slowness estimates is considerably worse than would be anticipated from a “random fixed frequency band” selection algorithm. This could be due to competing contributions to different components of wider frequency bands, and also due to the selection of slightly different sections of the wavetrain under the automatic procedure.

5. The events are problematic due to the essentially simultaneous arrival of Pn/Pg and Sn/Sg (Hicks et al. 2004)

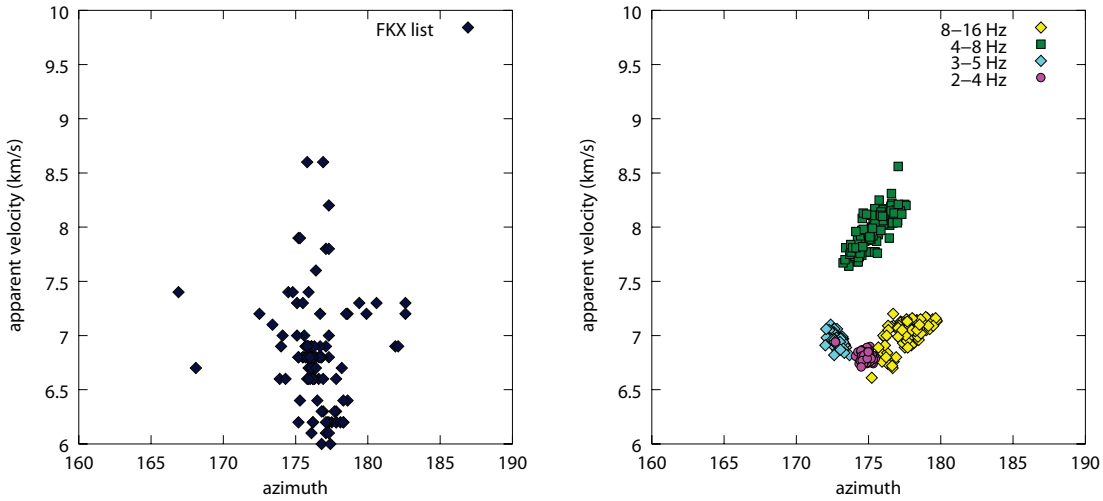

Figure 16: (Left) Slowness estimates in the routine automatic processing for the defining P-arrival at the ARCES seismic array for each of the 108 ammunition destruction explosions at a military site in the north of Finland, at a distance of approximately 175 km. (Right) slowness estimates in the indicated fixed frequency bands for the same arrivals, albeit measured in an identical time-window for each event.

Figure 17 displays how the waveforms vary with frequency band. As for many signals in Fennoscandia, the SNR improves as the frequency band increases at the expense of signal coherence over the array. The slowness estimates for the 4-8 hz band in Figure 16 show a far greater variability than those in the 2-4 hz band and this is indeed unfortunate from the point of view of consistency in event analysis. A seismic analyst will attempt to choose a frequency band with an optimal combination of a good signal to noise ratio and a high beam-gain, and based on these criteria is likely to choose the 4-8 hz band over the 2-4 hz band. The higher values of the apparent velocity recorded in this higher frequency band suggest that it is primarily the Pn phase which is being observed at the higher frequencies and primarily the Pg phase being observed at the lower frequencies.

A slight modification to the f-k procedure was implemented whereby, instead of integrating the energy in the beam directly over the Fourier coefficients, the beam was transformed back into the time domain and the energy present within each of many narrow frequency bands was obtained using the multitaper method of Thomson (1982). These results are displayed in Figure 18. These plots indicate that the variation in apparent slowness space with increasing frequency varies in quite a continuous way - at least for the lower frequencies. The variance of the slowness estimates increases with increasing frequency as the waveform coherence over the array diminishes. A discontinuity occurs between 8 and 10 Hz whereby it is assumed that the slowness estimates are dominated by small parts of the wavetrain on subsets of closely spaced sensors.

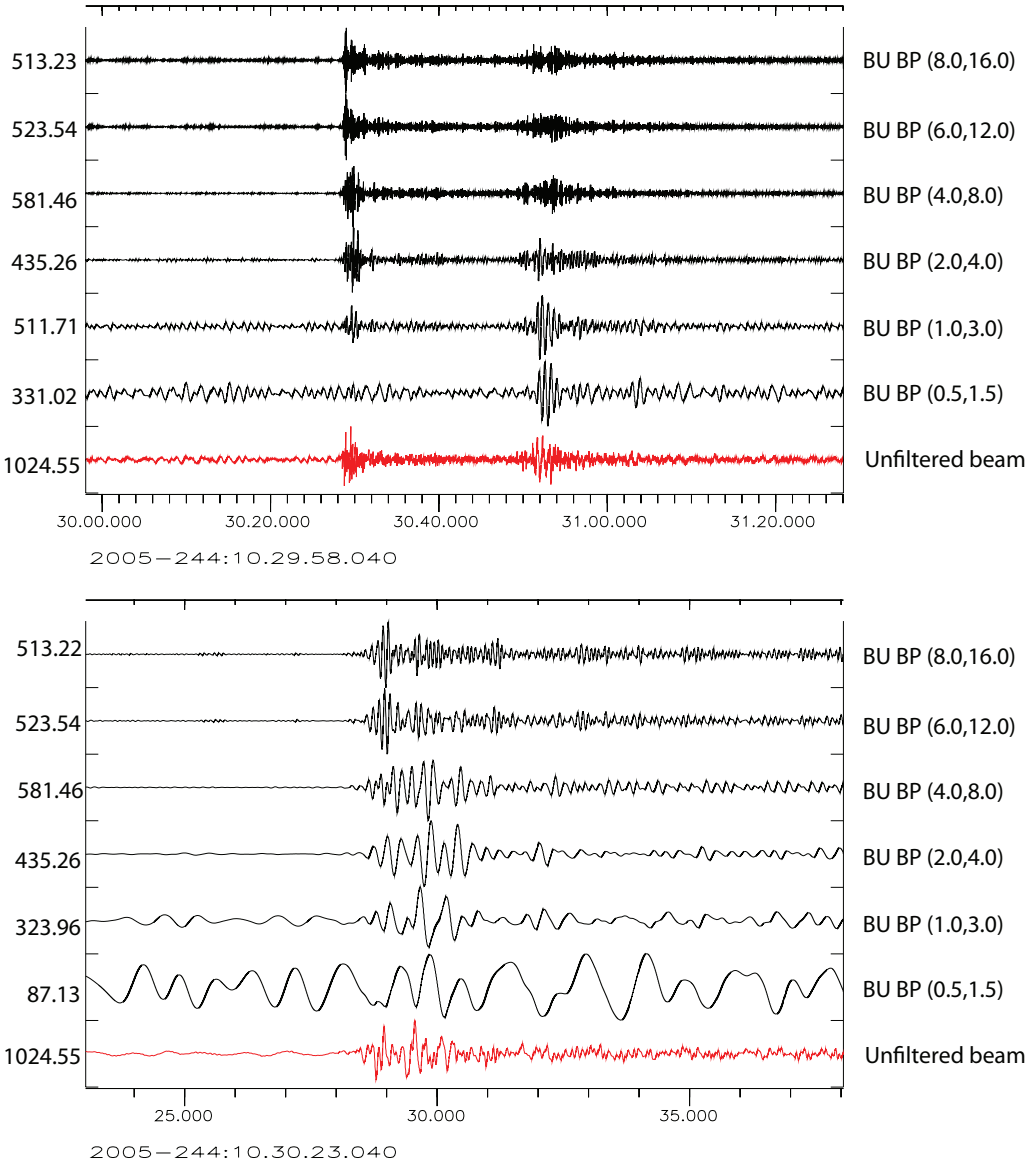

Figure 17: Beams at ARCES of signals from an event in Northern Finland at approximately 10:30 GMT on September 1, 2005. The beam is steered with an apparent velocity 6.72 km/s and a backazimuth of 173^{o}. The onset time of the initial P-arrival is estimated to be 2005-244:10.30.28.380.

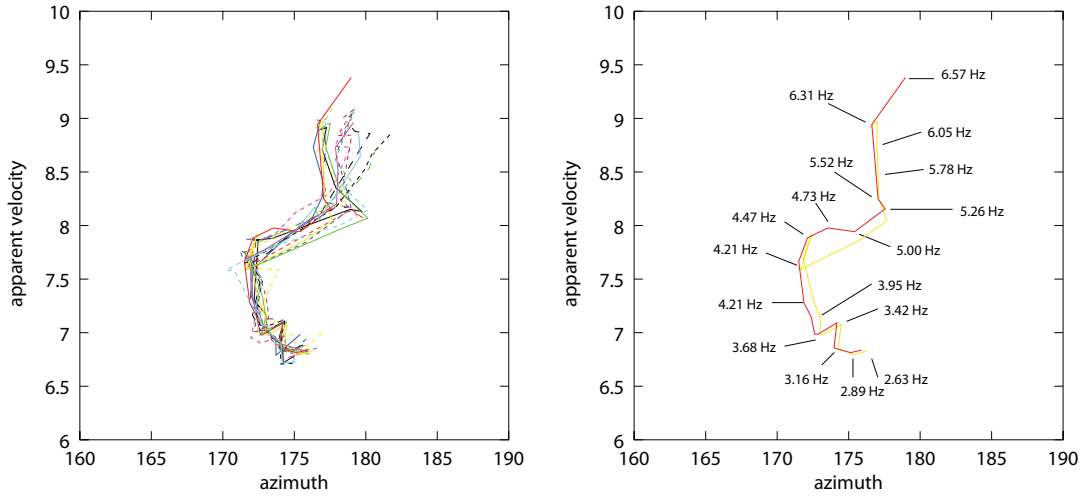

Figure 18: Slowness estimates for selected explosions from the Finnish data set obtained by measuring the energy in the beam in very narrow frequency bands using the multitaper method of Thomson (1982). These plots may be compared directly with Figure 16.

3.3 Mining events in Northern Sweden

The DoE-funded collection of Ground Truth mining data for NW-Russia provided a unique and, to the best of our knowledge, complete dataset of events by which to calibrate templates for sites in the region. Such a comprehensive list of events has not as yet been made available to us for the mining regions in northern Sweden. However, the waveform correlation procedure applied for the identification of the Finnish explosions can also be applied to events from Kiruna, Malmberget, and Aitik. The mining companies have confirmed the presence of a small number of events (primarily rockbursts) which have occurred at the various sites and signals from these events have been used as initial waveform templates. High SNR signals from events detected by this method can then be used as waveform templates and a large collection of events can be constructed iteratively in a bootstrap procedure. A possible limitation is that, due to the lack of independent confirmation of events, the conditions upon the waveform similarity are very strict in order to ensure that signals from distant sites are not included spuriously. This may have the effect that datasets include only signals of a very specific kind (for example roof-collapses) or from a very limited part of the source region. The limited datasets may therefore not be representative of the whole mining complex. An example of a convincing correlation detection is displayed in Figure 19.

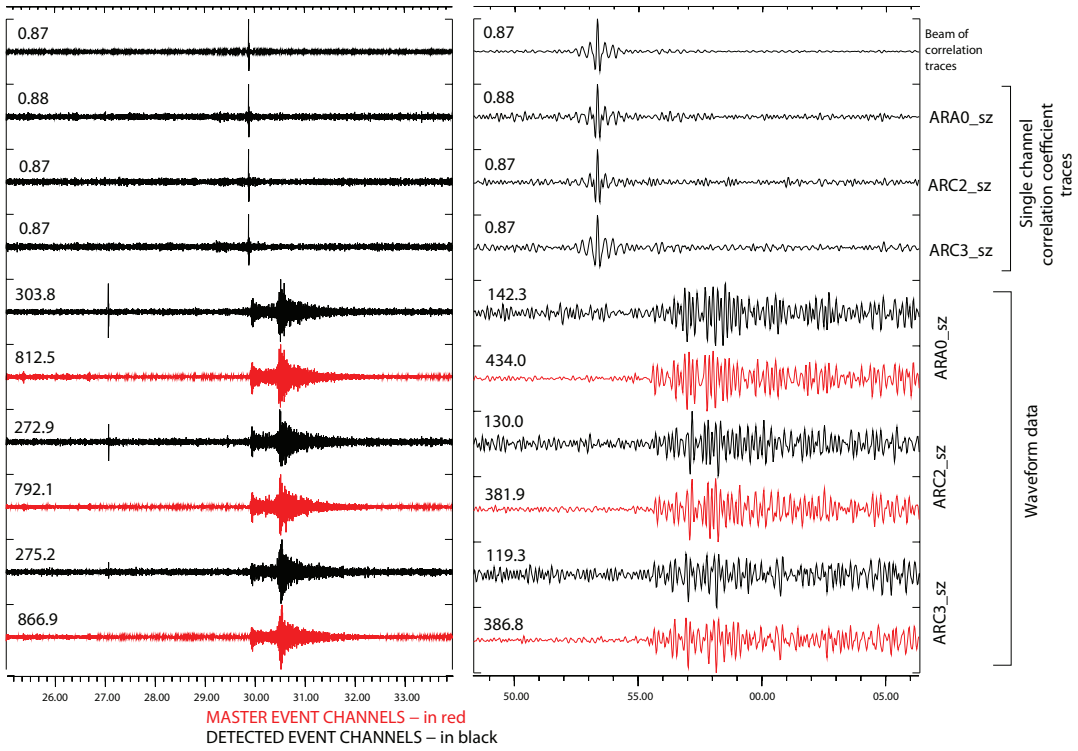

Figure 19: Demonstration of the simultaneous detection and identification of an event at the Malmberget ore mine in northern Sweden using waveform correlation on array data from the ARCES array (see Gibbons and Ringdal, 2006, for details). The waveforms are band-pass filtered between 4.0 and 8.0 hz. The master waveform consists of 60.0 seconds of data beginning at a time 2004-116:06.29.55.000 and the time of the maximum array correlation coefficient is 2004-085:12.12.51.870.

4. Comments on Event Location Accuracy

Events which are selected as likely candidates for a given source region need to be located automatically using processing parameters and (optionally) bias corrections derived from the sets of calibration events. A useful routine for location estimates using arrays with few observations is the HYPOSAT program (Schweitzer, 2001a) since the backazimuth estimates can be used to constrain the solution estimates with weightings chosen according to the consistency and accuracy of previous measurements.

Figure 20 shows event location estimates obtained for the Finnish ammunition destruction explosions using a variety of different procedures. The solutions with the greatest error are the fully automatic GBF solutions for the reasons discussed in Section 3.2. The analyst-reviewed solutions show an enormous improvement due to the manual repicking of phase arrival times, the reidentification of phases (and in many cases the rejection of spurious phase associations), and the recalculation of direction estimates in time-windows consistent with the reassessed seismic phases. The bulletin from the University of Helsinki has the solutions very tightly constrained in the North-South direction and very poorly constrained in the East-West direction which is a direct consequence of the sparse configuration of the 3-component stations available in this region.

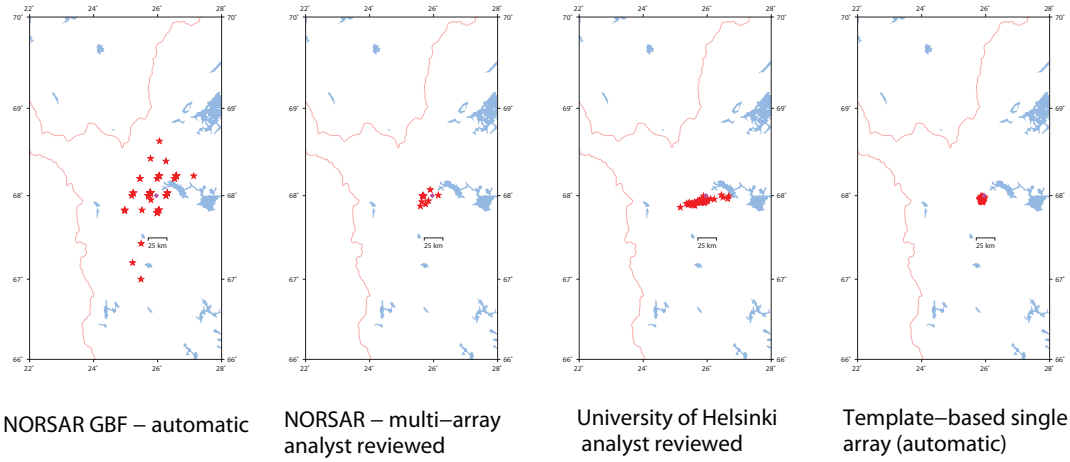

Figure 20: Comparison of location procedures for the military ammunition destruction explosions in northern Finland. The NORSAR analyst reviewed solutions cover a relatively small subset of the events since the reviewed bulletin includes only events exceeding magnitude 2 unless there is special interest in particular events. The majority of the Finnish analyst solutions are obtained using two three-component stations without azimuth estimates. The template-based solutions use azimuth estimates from the 2-4 hz frequency band for both P- and S- arrivals.

By far the most accurate event locations in Figure 20 are those obtained from the fully-automatic template algorithm using autoregressive re-estimated P- and S- arrival times within specified target windows (see Gibbons et al., 2005) and f-k slowness estimates calculated in the 2-4 Hz frequency band which was demonstrated in Figure 16 to provide the most stable measurements, despite the non-optimal SNR and beam-gain in this frequency band. There are two important lessons from this case-study:

- The accuracy of analyst-reviewed event location solutions will in many cases never match that available using fully automatic algorithms if the analyst is not able to apply the same consistency to the choice of processing parameters. Unfortunately, it takes relatively large populations of confirmed events to be able to determine useful statistics from which an enlightened choice of processing parameters can be made. Figure 11 indicates that not only is there no single optimal frequency band but that it is probably not possible to extrapolate the behavior over any extended geographical region. This means that the optimal automatic event locations displayed in Figure 20 are probably only available for sites for which excellent calibration information is available.
- An SASC (Slowness and Azimuth Station Correction) cannot be applied optimally without taking account of the frequency band in which the measurement is made. A single bias correction may reduce the offset somewhat for a range of frequencies but it is clear from Figure 16 that a well-tuned SASC optimized for one frequency band will not correct measurements made in a different frequency band and may also lead to a greater offset than would result from applying the uncorrected slowness and azimuth estimates.

Figure 21 shows corrected and uncorrected automatic template location estimates for the confirmed mining events from Figure 1. The upper panel indicates how, without the application of SASCs, the location estimates can be mislocated consistently by quite large distances when the single-array procedure is used.

A serious shortcoming of the template procedure is that events from the site-regions of interest which fail any of the necessary diagnostic tests will not be able to be located automatically and will have to be marked for manual review. Figure 21 displays a far smaller number of events than Figure 1, the remaining events being excluded due to an insufficient number of accepted measurements for the location procedure. Gibbons et al. (2005) found that, for the Kovdor mine, only 32 out of 53 confirmed events during one calender year could be located fully-automatically using the selected tolerance criteria. This is serious shortcoming considering that one of the main purposes behind the system is to perform screening without the need for analyst resources. In almost all cases, the reason for failure was the inability to measure an arrival time for a secondary phase within the permitted time-window with an acceptable SNR. This is almost inevitably a consequence of the complicated firing sequences occurring at these sites[6] and the analyst is confronted by the same fundamental problems as the automatic system.

6. It is worth noting that the Finnish ammunition explosions exhibited a 100% success rate in automatic event location (Figure 20). It is assumed that the most important reason for this is the simpler source-time function which allows a reasonable SNR for the S-phase in the absence of strong coda phases.

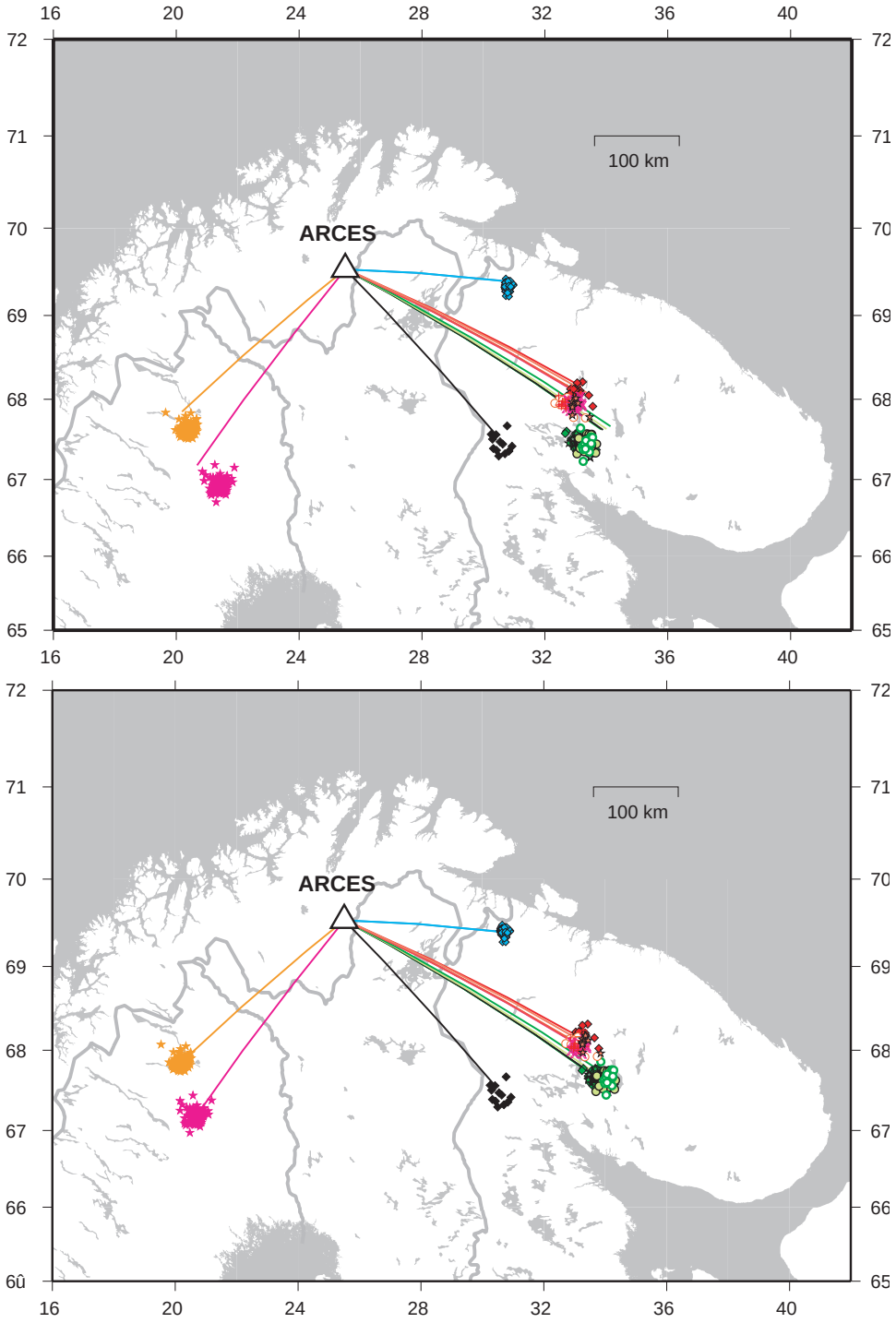

Figure 21: Location estimates for events from the Kiruna, Malmberget, Zapoljarni, Kovdor, Khibiny, and Olenegorsk mining regions using a template scheme which only considers a single P- and a single S- phase at the ARCES array. All azimuth and apparent velocities are taken using a frequency band deemed optimal for the given site. In the upper panel, no corrections for bias in azimuth estimates have been applied and the single-station location estimates are in some cases mislocated by up to 50km. The application of slowness corrections in the lower panel results in estimates which are almost symmetrically distributed around the known source regions.

5. Transportability of Results: An Example from Kazakhstan

The design of regional array conceived for the NORESS station in southern Norway, and applied subsequently to the GERESS and ARCESS arrays, has become a standard for new installations worldwide. However, primarily from economic considerations, the four concentric ring, 25 element design has in general been replaced with a two concentric ring, 9 element reduced version. Kazakhstan is in a part of the world where there is strategic interest in observing low-magnitude seismic events at regional distances and a network of four such regional arrays is now operational (see Figure 22). The previous chapters have demonstrated the degree to which event location estimates can be improved by applying optimal processing parameters for slowness and azimuth measurements and corrections which are specific to the processing parameters with which the measurements are made.

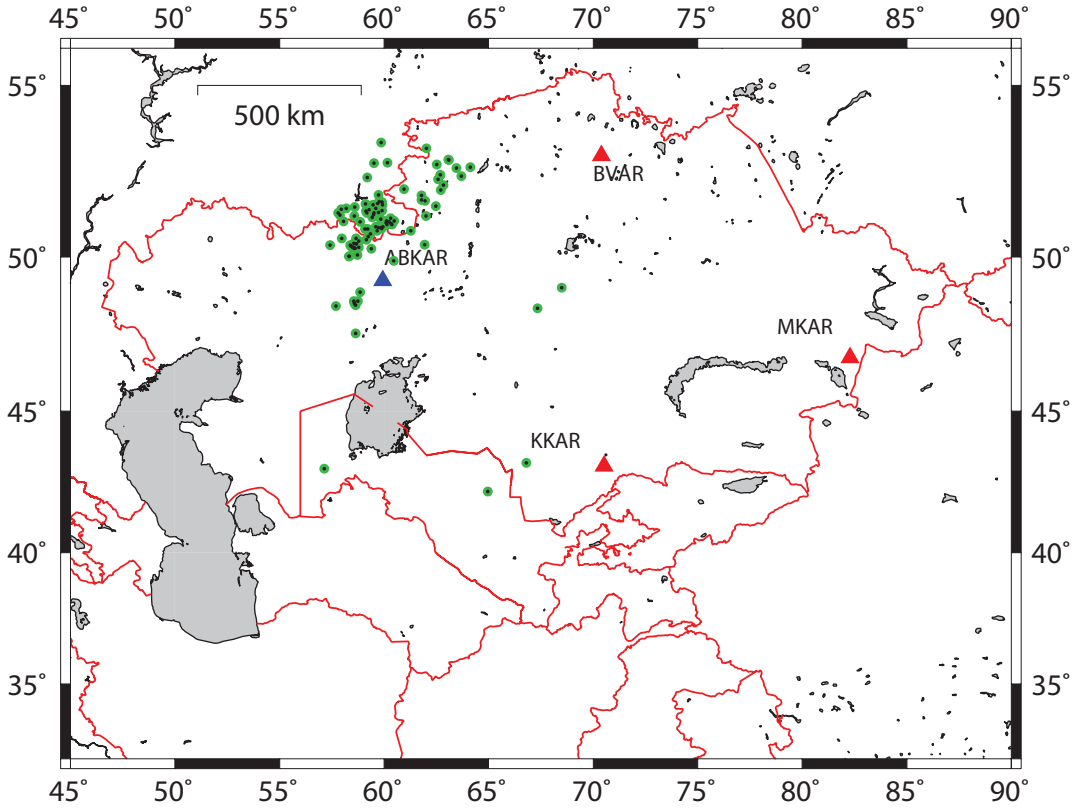

Figure 22: Location of the four 9-element arrays in Kazakhstan together with locations from the Kazakhstan NDC reviewed event bulletin from May 2004 for which regional phases were recorded at the Akbylak array (ABKAR). Also shown are the arrays at Borovoye (BVAR), Makanchi (MKAR), and Karatau (KKAR).

It is important to assess how well these results apply to arrays with different geometrical configurations and in a different tectonic setting. Figure 23 shows the geometry of the ABK array in North East Kazakhstan. It has a slightly wider aperture than ARCES and with significantly fewer sensors.

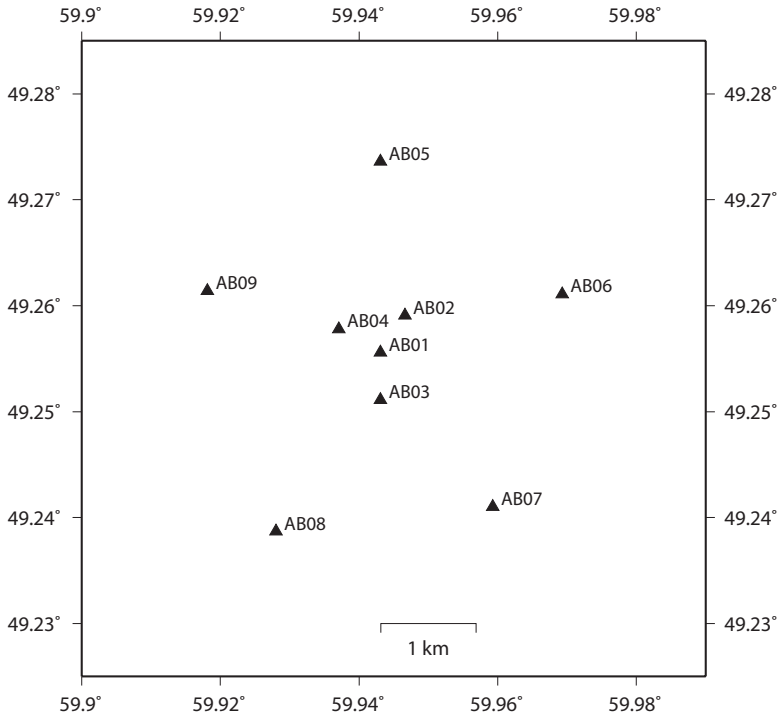

Figure 23: Geometry of the 9-element ABK array in Kazakhstan.

The multiple frequency f-k analysis panel for an initial P-arrival for a presumed mining explosion at a distance of approximately 150 km from ABK is displayed in Figure 24. This is clearly a very different situation to that displayed in Figure 7 for the ARCES array for a regional Pn-arrival for a mining explosion. The wavefield at the lowest frequencies in the European Arctic is dominated by high amplitude ocean-generated microseisms which make measurement of all but the strongest regional phases impossible below 2-3 Hz due to the competing coherent background noise. This is not the case for this arrival in Kazakhstan which (despite a lower SNR than at higher frequencies) gives a qualitatively correct slowness estimate in the lower frequency band considered. As the frequency band is increased, the resolution of the slowness estimate appears to improve although the decreasing wavelength and associated coherence problems lead to an increase in the energy in the sidelobes diminishing the significance of the main lobe. In the 4-8 Hz frequency band, although a qualitatively correct slowness vector is chosen, the maximum beam gain is marginal and the estimate could easily result in a spurious estimate given less favorable noise conditions. In the 5-10 Hz frequency band and above, a spurious estimate is indeed chosen and it could be assumed that useful coherent processing using the ABK array is limited to frequencies below 4 Hz. Figure 25 shows an analogous plot which differs from Figure 24 only in the removal of two sites, AB08 and AB09. Despite this relatively small change to the array configuration, a qualitatively correct slowness vector is now chosen for all frequency bands up to 12 Hz.

Within the month of data examined, several signals were observed at a similar time of day which exhibited a satisfactory waveform similarity within the low frequency band 0.8 - 2.0 Hz. Whilst this is less conclusive evidence that the events are co-located than the

high-frequency band cross-correlation displayed in Figure 19, it provides a clear indication that both wavefronts are incident from a similar direction. The multiple frequency band f-k grids for the subsequent detected events show a remarkable degree of similarity to those displayed in Figure 24 and it can be assumed that frequency-dependent SASCs would need to be applied to correct for different biases in the different frequency bands.

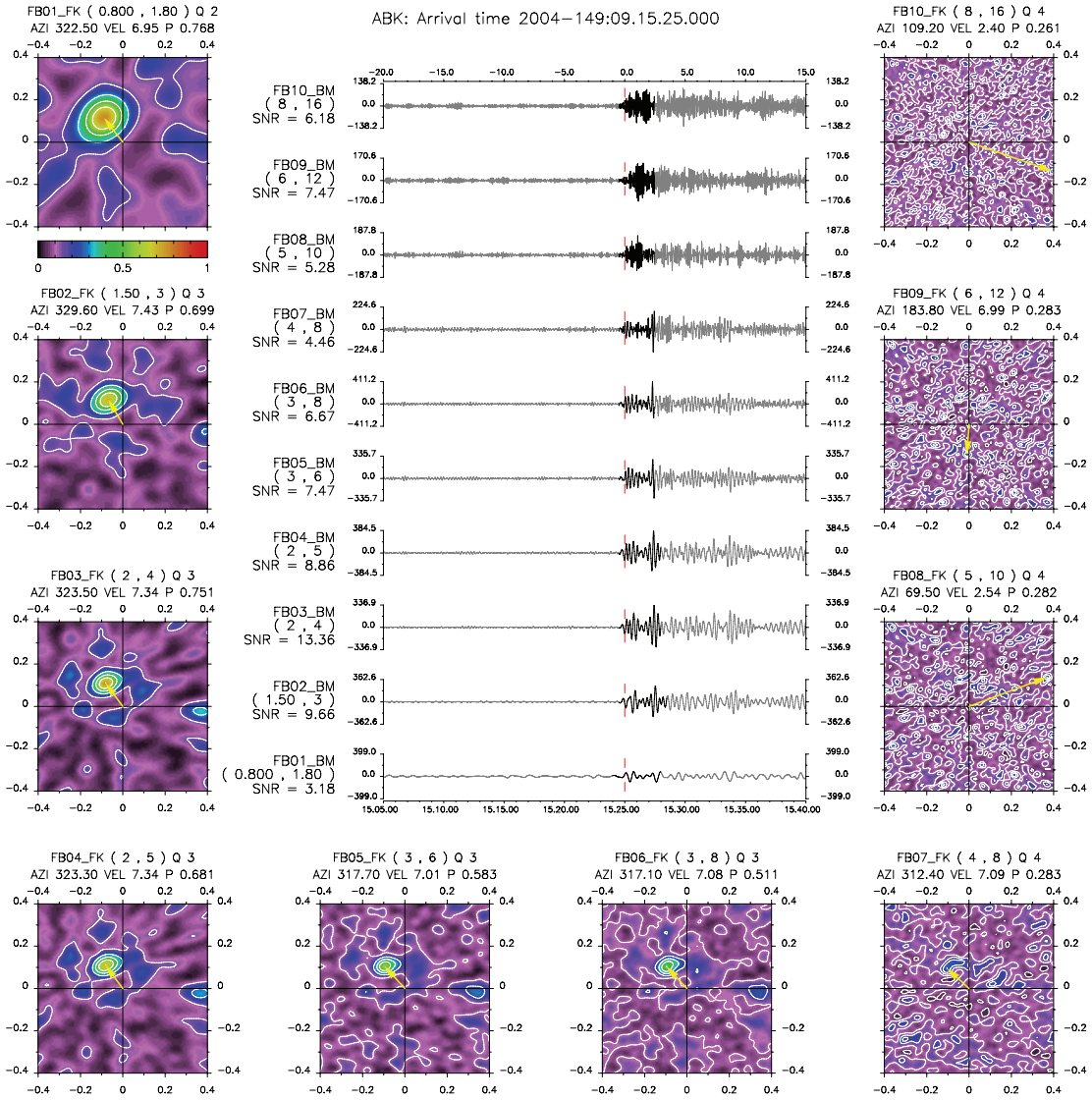

Figure 24: Relative beam power as a function of slowness for the initial P-arrival at the ABK array in Kazakhstan from a mining event at a distance of approximately 150 km. All fixed frequency bands and processing parameters are as displayed in Figure 7.

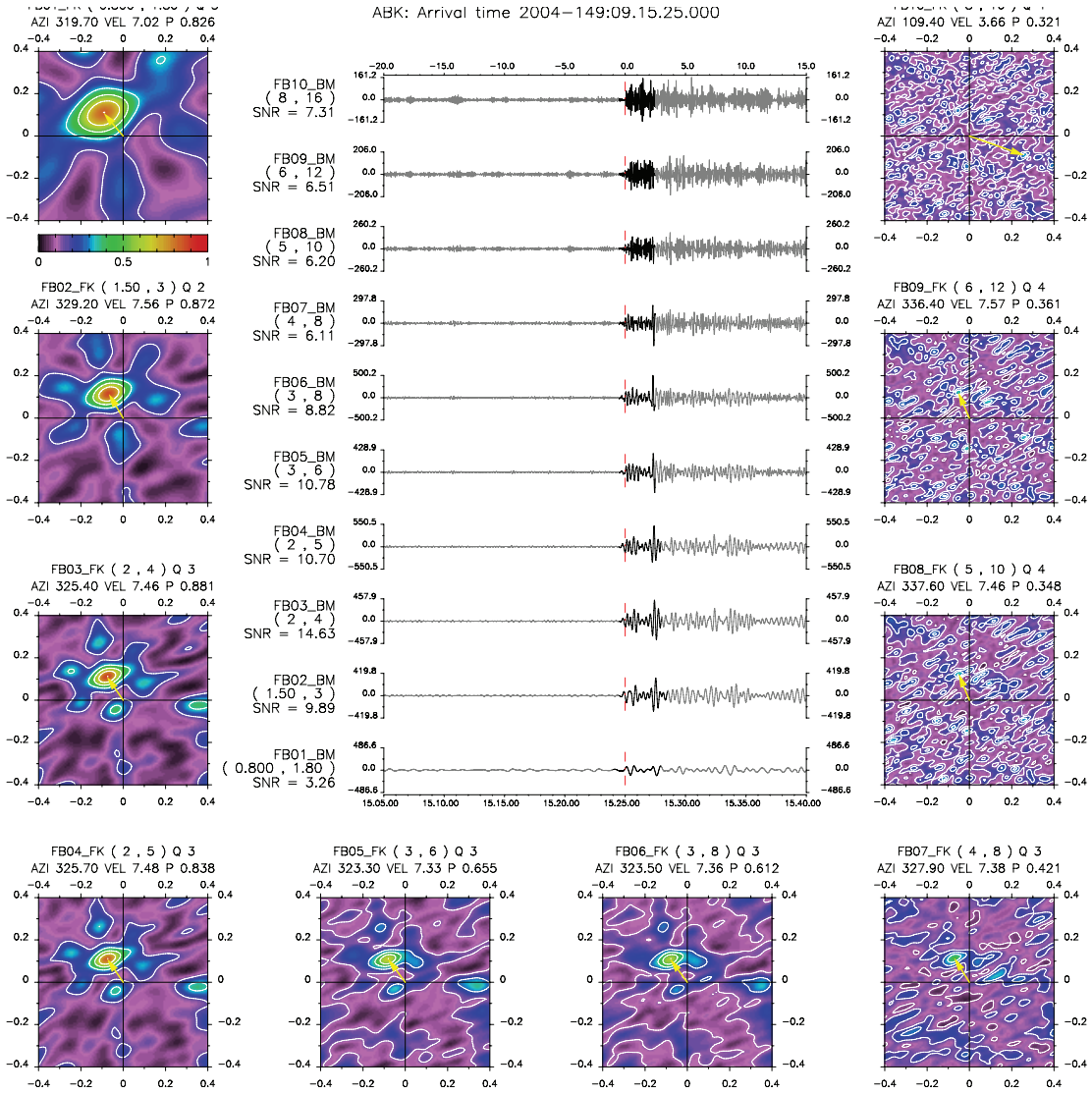

Figure 25: An identical plot to that shown in Figure 24 except that the AB08 and AB09 site traces have been removed from the calculations. Whilst the trend towards low beam-gain and multiple side-lobes at high frequencies is still observed, the situation has been helped by the removal of these two peripheral stations and a qualitatively correct estimate is returned in the 5-10 Hz and 6-12 Hz frequency bands.

6. Empirical Matched Field Processing: Rethinking Frequency-Wavenumber Analysis

We examine empirical matched field processing as an alternative to conventional f-k (frequency-wavenumber) analysis in situations where calibration event observations are available. Conventional f-k analysis maps the wavenumber distribution of energy incident upon an array using theoretical plane-wave steering vectors as the wavefield representation kernel. Empirical matched field processing replaces the plane-wave kernel with empirical steering vectors derived as the principal eigenvectors of narrowband spatial covariance matrices estimated from ensembles of signals from distinct sources. Using ground truth information for mines in the vicinity of the ARCES array, we have been able to calculate stable covariance matrix estimates for eight mines by averaging sample covariance matrices over event ensembles. Two ensembles in this study contain over 200 events.

Using just Pn observations at the ARCES array from 768 ground-truth mining explosions in the Khibiny Massif and Olenegorsk regions of the Kola Peninsula, we demonstrate the ability of matched field processing to distinguish between explosions from closely-spaced mines. Explosions are correctly classified (~5% error) by source for mines separated by as little as 3 kilometers at observation ranges up to 400 kilometers. The performance of the empirical matched field processor is considerably superior to even calibrated plane-wave FK analysis in separating closely-spaced sources. It does so by extending coherent processing to higher frequencies than is possible with plane wave assumptions.

6.1 Introduction and Review of Mathematical Background

Frequency-wavenumber analysis is the principal tool in seismic array signal processing for estimating the azimuth and apparent velocity of incident waves, and thereby distinguishing seismic phases and the events they represent by direction and phase speed. As originally conceived (see, e.g. Capon, 1969), f-k analysis treats the incident seismic wave field as a homogeneous random field of stationary propagating plane waves, the spatial equivalent of a stationary random process model for temporal signals. Under this model, f-k analysis consists of estimating indirectly the power wavenumber spectrum of the random field as a function of frequency. The approach is indirect in that the spatial covariance function of the wavefield is estimated first (as samples on the coarray of the observing array), then the spatial Fourier transform of the sample covariance function is computed to estimate the distribution of power in wavenumber.

The estimate of power in the indirect approach assumes the quadratic form

$$\hat{P}(f) = \underline{\varepsilon}^{H}(f)\underline{\hat{R}}(f)\underline{\varepsilon}(f) \tag{1}$$

where the covariance matrix is estimated from $M = m_1 - m_0 + 1$ complex analytic narrowband samples of the waveforms incident upon the array:

$$\hat{\underline{\underline{R}}}(f) = \frac{1}{M} \sum_{m = m_0}^{m_1} \underline{r}[m] \underline{r}^H[m] \tag{2}$$

The superscript H denotes the Hermitian transpose operation. Here the sample-data form of the received signals have been represented as the vector

$$\underline{r}[n] = \begin{bmatrix} r(\underline{x}_1, n\Delta t) \\ r(\underline{x}_2, n\Delta t) \\ \\ r(\underline{x}_N, n\Delta t) \end{bmatrix} \tag{3}$$

where the signal observed on the i^{th} array sensor ($i = 1, \ldots, N$ sensors) is $r(\underline{x}_i, n\Delta t)$ and $\underline{x}_i$ is the position of the sensor in the array. Here, again, the signals are complex-analytic representations of the observed waveforms filtered into a narrow band centered about a frequency of f Hz.

We remark further that if the incident wavefield is comprised of a single plane wave characterized by the slowness vector $\underline{s}$, a reasonable model for the received signal is:

$$\underline{r}[n] \sim s(n\Delta t | f) \begin{bmatrix} e^{-i2\pi f(\underline{s} \cdot \underline{x}_1)} \\ e^{-i2\pi f(\underline{s} \cdot \underline{x}_2)} \\ \bullet \\ \bullet \\ e^{-i2\pi f(\underline{s} \cdot \underline{x}_N)} \end{bmatrix} \frac{1}{\sqrt{N}} = s(n\Delta t | f) \underline{\varepsilon}(f) \tag{4}$$

This is the common-signal model for the incident wavefield, and is accurate provided the inverse bandwidth of the filters used to filter the data into narrow bands is much larger than the characteristic time of propagation across the array. That characteristic time is approximately 3/8 second for Pn phases traversing the ARCES aperture. The filter bandwidth should be much less than 1 Hz in this case. The model consists of the product of a slowly time-varying, complex envelope function $s(t|f)$ [see e.g. Baggeroer et al., 1993] common to all sensors of the array with a so-called *steering vector* $\underline{\varepsilon}(f)$ that collects the complex phase delays occasioned by the time delays to each sensor resulting from wave propagation across the array aperture. The model becomes exact in the limit for incident plane waves as the bandwidth of the observation becomes infinitesimal.

The sample covariance matrix (Equation 2) is rank one in the limit of large observation times when the observed wavefield consists of a single plane wave:

$$\hat{\underline{R}}(f) \sim \sigma_s^2(f)\underline{\varepsilon}(f)\underline{\varepsilon}^H(f) \tag{5}$$

where $\sigma_s^2(f) = E\{|s(n\Delta t|f)|^2\}$. In suggesting the equivalence of (5) and (2) in the limit as $M \to \infty$, we have made use of the stationarity assumption. We note that this matrix structure has a single eigenvalue $\sigma_s^2(f)$ with associated eigenvector $\underline{\varepsilon}(f)$.

We note that the estimate of incident wavefield power made with Equation (1) uses the theoretical plane-wave steering vector defined in (4). The quadratic form of Equation (1) represents a discrete Fourier transform of the spatial covariance function sampled on the finite aperture of the co-array of the physical array.

While the assumption that the observed wave-field is a homogeneous random field is a useful abstraction for background noise or even long-duration transient signals such as highly-dispersed surface waves (Capon, 1969), it clearly is not an accurate representation of the situation that pertains for short-duration transient signals such as high-frequency regional body phases. For this latter case, an alternative is to treat the observed wavefield as a deterministic collection of incident plane waves with unknown vector slowness (Kvaerna and Ringdal, 1986). The vector slowness is estimated by computing direct-form estimates of the incident power (the squared magnitude of the Fourier transform of the signal) and integrating the resulting power over frequency. Mathematically this approach can be shown to be equivalent to the indirect approach with degenerate (rank one) estimates of the covariance matrix made from a short observation window. This form of spectral analysis is an implementation of the periodogram (Jenkins and Watts, 1968) and is known to be a high-variance estimate of incident power. Consequently, integration of the power over frequency is employed to stabilize the estimate.

A practical issue that arises in application of frequency-wavenumber spectra to locating events (and equivalently assigning them to specific sources) is the frequent occurrence of non-ideal propagation conditions such as significant refraction and scattering of the wave-field due to (unknown) heterogeneity of the propagation medium. The classical approach to dealing with this problem is to employ empirically-derived corrections to the slowness estimates obtained from f-k measurements (Schweitzer, 2001b). While frequently successful, particularly at low frequencies, this approach applies corrections after the strongly non-linear step of estimating slowness from a computed wavenumber spectrum. It seems intuitively desirable to apply corrections prior to the nonlinear step, by employing aperture-level corrections directly to the observed wavefield (in effect providing a set of spectacles to correct the vision of the array). Matched field processing is one mechanism for achieving just this kind of correction.

In this study, we explore the application of matched field processing to the estimation of incident wavefield power. Matched field processing (see e.g. Baggeroer et al., 1993) is quite similar to traditional frequency-wavenumber analysis in that it uses the same estimator (Equation 1) for incident power. However, it replaces the plane-wave steering vector with more general steering vectors appropriate to signals with spatial structure that

are not plane waves. In its original conception in underwater acoustics, the steering vectors were computed from the theoretical spatial modal structure of waves trapped in the SOFAR waveguide.

In the event that the medium is unknown, but observations of the wavefield are available, it is possible to estimate the steering vector as the principal eigenvector of sample covariance matrices (Equation 2) of the observed vector signal. This approach depends upon the dominance of a single source in the observed data leading to the rank-one structure of the sample covariance matrix as described in Equation (5). This method has been attempted with limited success in underwater acoustics (Fialkowski et al., 2000). Success was limited because the duration M of the observation window was limited by the stationarity assumption, leading to high-variance estimates of the covariance matrix and associated principal eigenvector. Only short-duration observation windows were available because the sources in underwater acoustics frequently are moving.

We have reason to believe that such empirical matched field processing can be more successful in seismic applications, because there are circumstances where we can obtain more stable estimates of the spatial covariance matrix. Stable estimates are possible, even though the observation windows of regional body phases are short, when repeated events from a particular source have been observed. It then is possible to replace the stable temporal average of Equation (2) with a stable ensemble average over the observed events. This is an innovation of this study and depends upon a new conception of seismic sources as random processes that produce transient signals that, while not temporally stationary, are at least stationary in the Green's functions that describe signal propagation from the source to a given receiver.

We note further, and will demonstrate in the results section, that empirical matched field processing offers the prospect of calibrating the fine spatial structure of the wavefield observed by an array for a particular repeating source. As such, it provides a means to capture some of the performance enjoyed by waveform correlation techniques applied across an array of sensors (Gibbons and Ringdal, 2006). Waveform correlation methods operate by matching both the spatial and temporal structure of an array signal given a previously-observed multichannel template. Consequently, matched field processing, which averages out temporal behavior, cannot achieve the full gain possible with waveform correlation methods. However, it should be more robust under circumstances when the source time history varies dramatically, as it only depends on the narrowband spatial structure of the signal.

Despite achieving stable estimates of empirical steering vectors through ensemble averaging, the matched field estimate of signal power for an individual event is a high-variance estimate. This situation is due again to the short observation interval. Thus, we adopt the same strategy as Kvaerna and Ringdal (1986) in stabilizing the estimate by computing the total wideband power

$$\langle \hat{P} \rangle = \sum_i \underline{\varepsilon}^H(f_i)\hat{\underline{R}}(f_i)\underline{\varepsilon}(f_i) \quad (6)$$

We note that this is an incoherent operation over frequency even while it is possibly coherent over the spatial aperture of the array. This observation again draws a fundamental distinction between this method and wideband waveform correlation methods, which are coherent over both frequency (equivalently, time) and spatial dimensions of the signal.

6.2 Results

Covariance matrix estimation and eigenvector characteristics

To test matched field processing and contrast it with conventional f-k methods, we assembled ARCES waveform data from 768 mining explosions from eight of the mines in the Khibiny Massif and the Olenegorsk group (Table 2 and Figure 26). The event data were chosen from a much larger event set, by manually screening the events for good signal to noise ratio, the absence of overlapping events and dropouts. The Pn phases were picked to within a few tenths of a second.

Table 2: Number of ground truth explosions acquired for each of 8 mines in the Olenegorsk Group and the Khibiny Massif

Mine	Number of Events
Bauman	52
Kirovogorsk	52
Komsomolsk	36
Oktjabirsk	24
Olenegorsk	73
Kirovsk	209
Central	99
Rasvumchorr	223

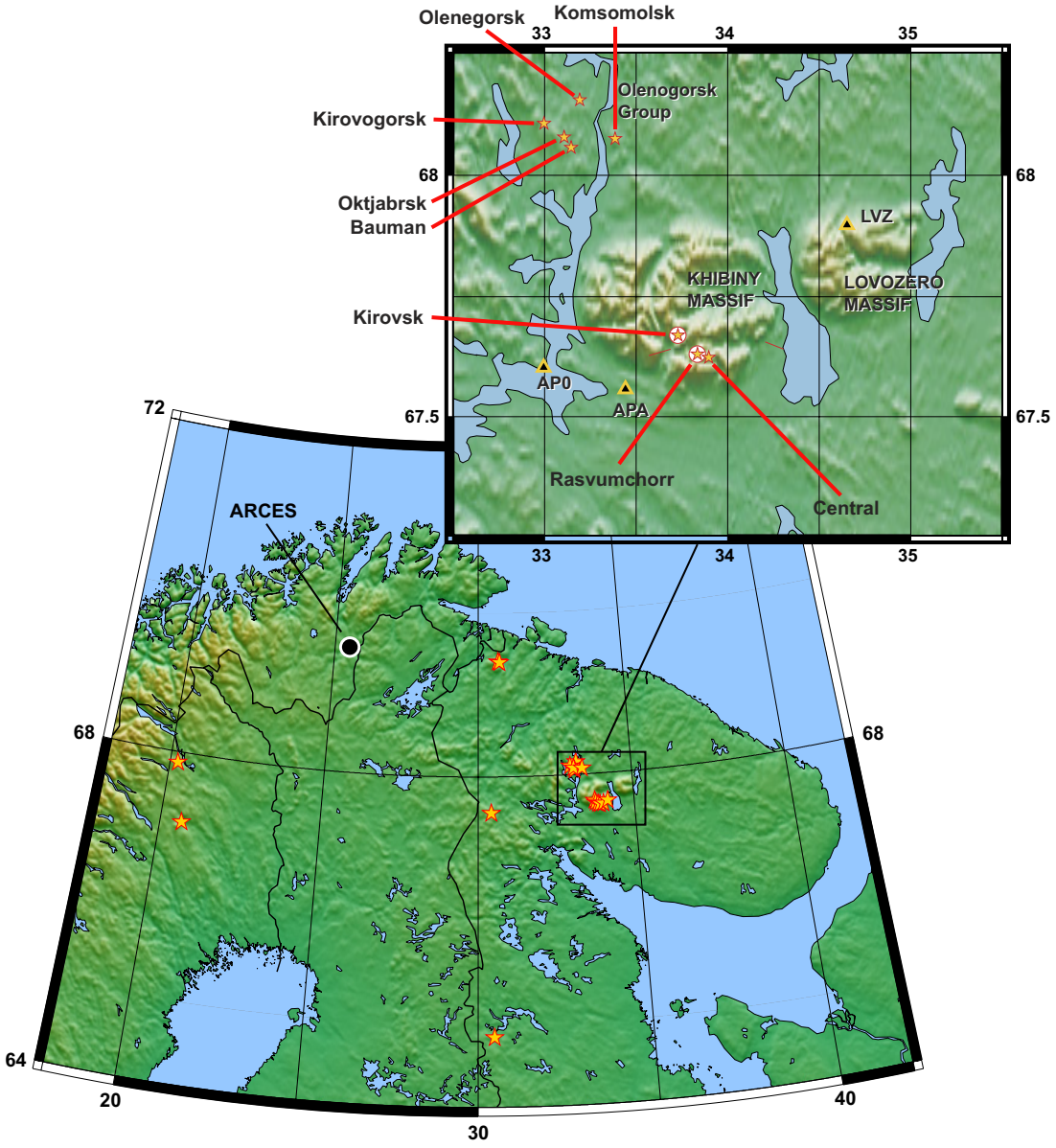

Figure 26: Map of the mines of the Khibiny Massif and Olenegorsk region and their relation to the ARCES array.

For each event within a particular mine, waveform data from the teleseismic configuration of the array (17 channels: A0, C ring and D ring) were filtered into 33 narrow (0.3125 Hz) frequency bands with center frequencies ranging from 2.5 to 12.5 Hz. The complex analytic forms of the resulting narrowband signals were used to estimate spatial covariance matrices (using Equation 2) in each frequency band. The resulting sample covariance matrices were stacked over the ensemble of all events at a given mine to form an ensemble average. These average covariance matrices then were used to derive calibrations for the individual mines. In the case of matched field processing, the principal eigenvector was extracted from each narrowband covariance matrix and retained as the steering vector calibration.

A number of questions arise concerning the characteristics of the covariance matrices. First among them is whether the eigenspectrum is concentrated in the largest eigenvalue as would be consistent with the assumption of a single source model for the incident Pn wavefields. Figure 27 displays the fraction of the energy in the eigenspectrum that is concentrated in the first eigenvalue, i.e

$$F = \frac{\lambda_1}{\sum_i \lambda_i} \tag{7}$$

Note that at low frequencies (especially below 7 Hz) the eigenspectral energies are highly concentrated in the first eigenvalue. There is a marked difference in behavior between the mines of the Olenegorsk and Khibiny groups. The Khibiny mines experience a more dramatic drop-off in eigenconcentration above 7 Hz than the Olenegorsk mines.

The second question is whether the principal eigenvectors (associated with the largest eigenvalues) are similar within a proximate group of mines. One may expect some continuity in steering vectors as a function of source location. One way of testing this expectation is to evaluate the inner products of eigenvectors among pairs of mines within a particular group. Figure 28 displays the quantity

$$\left| \underline{e}_i^H \underline{e}_j \right| \tag{8}$$

where the eigenvectors $\{\underline{e}_i\}$ are indexed to range over the individual mines in the Khibiny group (upper plot) and the Olenegorsk group (lower plot). Since the eigenvectors are normalized to have unit length, the norm of the inner product resembles a correlation coefficient in that it ranges between 0 and 1.

The very high degree of eigenvector similarity below 8 Hz among the Khibiny mines (upper plot) is remarkable, as is the sharp transition above 8 Hz to relatively strong dissimilarity. This effect is probably a consequence of the proximity of the mines (they all fall within a region 10 kilometers across). It is also notable that the Central eigenvectors strongly resemble those from Kirovsk and Rasvumchorr mines despite the fact that the firing practices differ substantially between the surface Central mine (with large, ripple-fired events) and the other two underground mines (which use relatively compact and smaller explosions). This similarity strongly suggests that narrowband matched field eigencalibrations are likely to be independent of source time history, one of the major motivations for developing narrowband matched field methods.

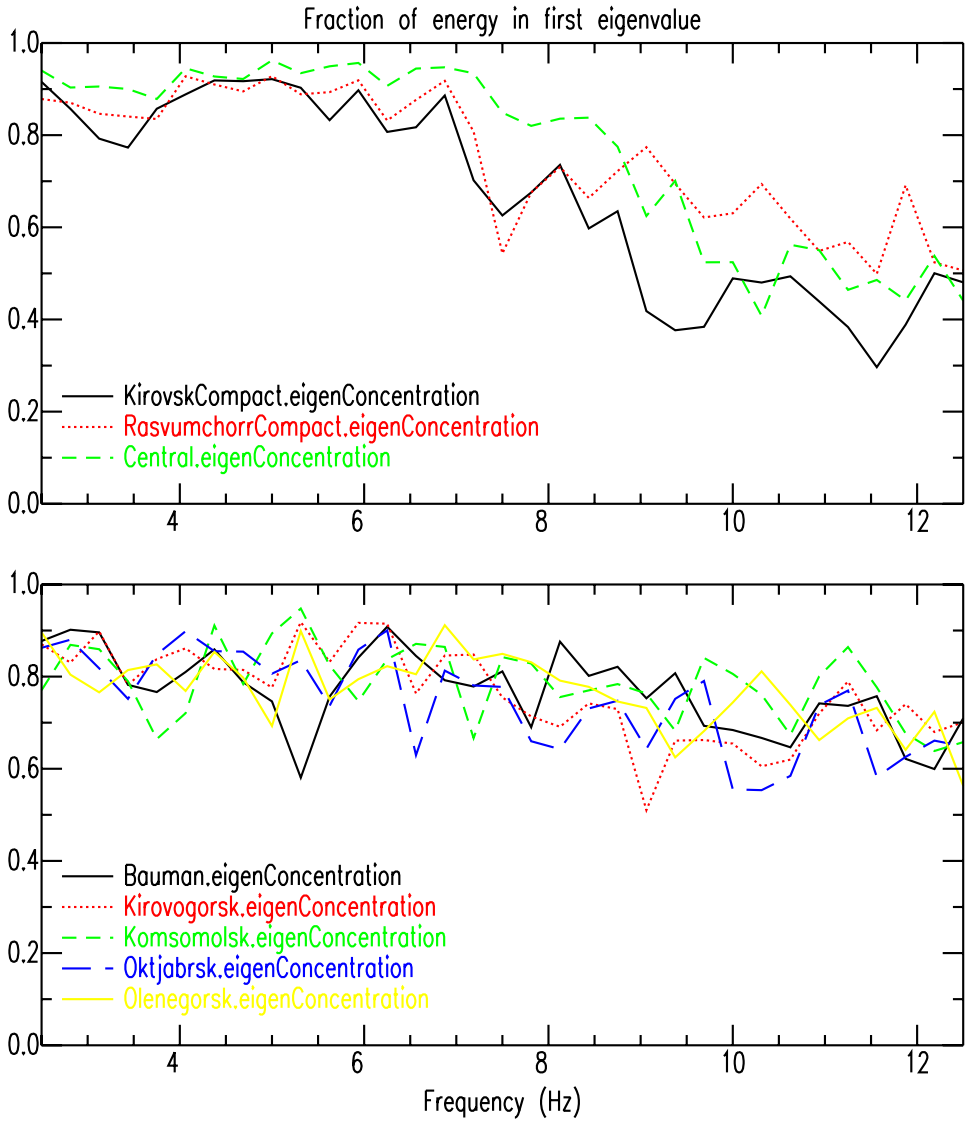

Figure 27: Signal energy is concentrated in the first eigenvalues of the spatial covariance matrices at frequencies below 8 Hz. Above 8 Hz the energy spreads out over more of the eigenvalues. This effect is most pronounced for the Khibiny Massif mines (top plot), and is less significant for the Olenegorsk group (bottom plot). See text for details.

By contrast, the eigenvectors corresponding to the Olenegorsk mines show much greater diversity (lowermost plot in Figure 28). Several factors may contribute to this phenomenon. The Olenegorsk mines are geographically more widely dispersed (Figure 26), perhaps leading to decorrelation among their eigenvectors. However, a subset (Bauman, Oktjabirsk, Kirovogorsk) of the Olenegorsk mines is not more widely dispersed than the three Khibiny mines, but still shows large diversity.

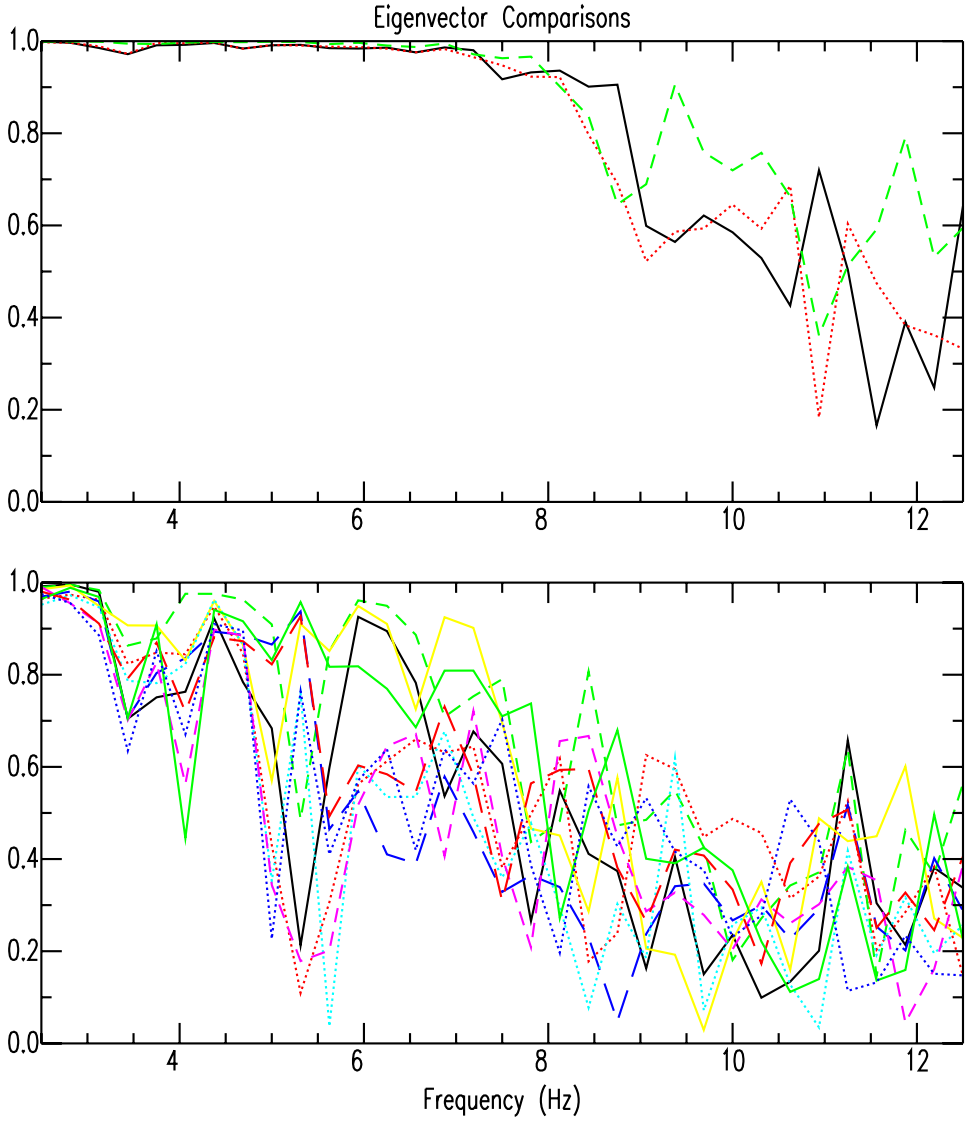

Figure 28: The principal eigenvectors of the spatial covariance matrices are very similar for the Khibiny mines (upper plot) up to 8 Hz, and become distinct above 8 Hz. The similarity of the eigenvectors probably is due to the proximity of the mines: the three mines lie within a region 10 kilometers across. The eigenvectors for the Olenegorsk mines (lower plot) are much less consistent, though still more similar below 8 Hz than above.

The Olenegorsk group eigenvectors may exhibit higher variance than their Khibiny counterparts because they are estimated from much smaller numbers of events (Table 2). However, as we will see later, this potentially higher variance does not appear to translate into poor classification performance among the Olenegorsk mines with matched field processing.

Finally, diversity among the principal eigenvectors could be a consequence of complex and variable source time functions or the presence of multipath interference with path lengths that vary across the source region. The Olenegorsk signals exhibit somewhat

greater complexity than the Khibiny signals. In addition, the Olenegorsk mines are up to 50 kilometers closer to the ARCES array than the Khibiny mines, which means that the separation between the Pn and Pg phases is correspondingly less (roughly 7 versus 9 seconds). It may be that the measured Pn Olenegorsk covariances are contaminated with some Pg energy and that this contamination does not occur with the Khibiny signals. An examination of the signals from both mine groups shows that the Pg phase is more strongly observed for Olenegorsk explosions (Figure 9). We intend to investigate this possibility further.

Another question of interest is whether the principal eigenvectors of the covariance matrices reproduce the theoretical plane-wave steering vectors assumed in conventional array processing. This question is addressed in Figure 29, which shows the inner products between the principal eigenvectors and theoretical plane-wave steering vectors. The theoretical steering vectors are constructed in this case using the theoretical backazimuths and nominal Pn phase velocities (8.0 km/sec for the Olenegorsk group and 7.8 km/sec for the Khibiny mines). The effect of elevation corrections was examined and found to be inconsequential. As in the previous two figures, the Khibiny mines are highly similar, with principal eigenvectors that match theoretical plane-wave steering vectors up to about 6 Hz. Above that frequency, the similarity declines rapidly. The rapid decrease presumably reflects the growing incoherence with increasing frequency of the signals across the full aperture of the ARCES array, though it may also result from increasing azimuthal bias (refraction) as frequency increases.

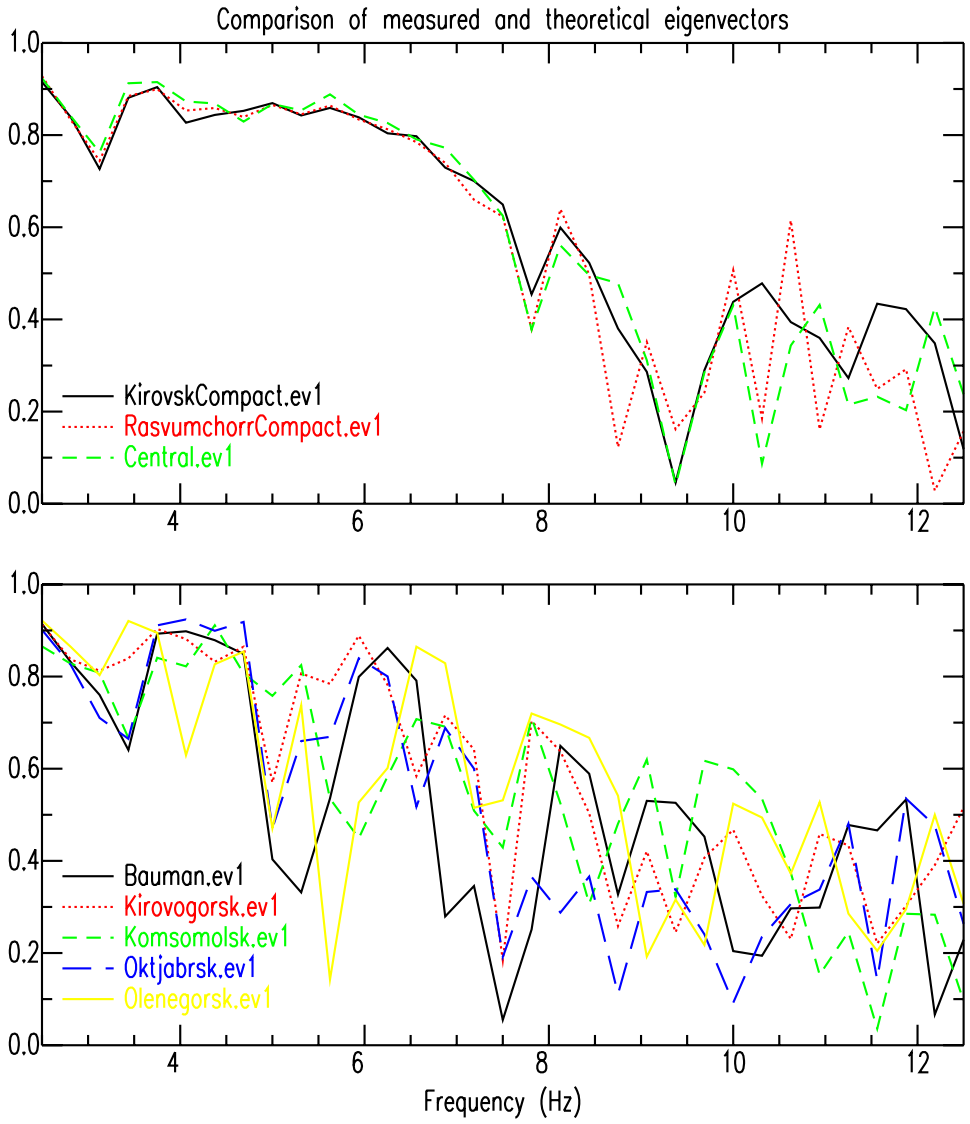

Figure 29: The first eigenvectors of the spatial covariance matrices are fairly consistent with steering vectors predicted by a plane wave model using a theoretical backazimuth and nominal Pn phase velocity for the Khibiny mines below 7 Hz (correlations above 0.7). The Olenegorsk mines produce less predictable eigenvectors, though the trend of decreasing correlation with theoretically predicted steering with increasing frequency is observed here as well.

The situation for the Olenegorsk mines (lower plot of Figure 29) is similar, though the correspondence between measured eigenvectors and theoretical steering vectors is much more variable, with significant drops in correspondence at several frequencies that appear somewhat consistent across the five mines in this group. This effect may be due to the same factors discussed above: mines more widely dispersed, high variance eigenvector estimates due to the smaller number of defining events or Pg contamination.

Application to event source classification

We now turn to examining the performance of f-k and matched field estimates of incident power as statistics for classifying events by originating mine. We consider three estimators of power: conventional f-k power estimation with theoretical plane wave steering vectors, calibrated f-k power estimation with plane wave steering vectors constructed with vector slowness corrections, and power estimation with empirical steering vectors estimated as the principal eigenvectors of the ensemble covariance matrices for each mine. We also examine two cases for each estimator: wideband power estimation over 2.5 - 12.5 Hz, and power estimation restricted to a higher frequency band: 7.8125 - 12.5 Hz. Estimation in the latter frequency band is intended to examine the effect of signal decorrelation on power estimation. We intentionally use the teleseismic ARCES configuration (A0, C ring, D ring, 17 elements total) in estimating spatial covariance matrices in order to test effects of decorrelation. As noted in the previous section, eigen-concentration declines above 8 Hz, and eigenvector diversity among mines of the two groups increases. This latter effect suggests that good matched field performance should be obtained in the high frequency bands if this processing style compensates signal decorrelation among the arrays. Matched field processing may, in effect, fingerprint the spatial structure of the signals across the ARCES aperture for each mine as a function of frequency to enable good classification performance.

Figures 30 and 31 show the classification performance of the broadband f-k estimator using theoretical plane wave steering vectors. This estimator closely resembles the wide-band f-k estimation approach of Kvaerna and Ringdal (1986), differing from it in unimportant details. This case is presented as a baseline for comparing the other two techniques. The histogram plots in these figures (and in Figures 33-36) display the number of events assigned to each mine by maximizing the incident event power estimated under the eight alternative hypotheses about the correct origin of each event. Eight histograms are presented in each figure, one for each population of events corresponding to each mine. For example, the top histogram in Figure 30 shows how the 52 Bauman events were assigned among the eight mines using theoretical plane wave power classifiers. The next histogram down shows the distribution of the 52 Kirovogorsk events and so forth. If classification were perfect, the collection of histograms would show a diagonal structure of single bars proceeding from upper left to lower right.

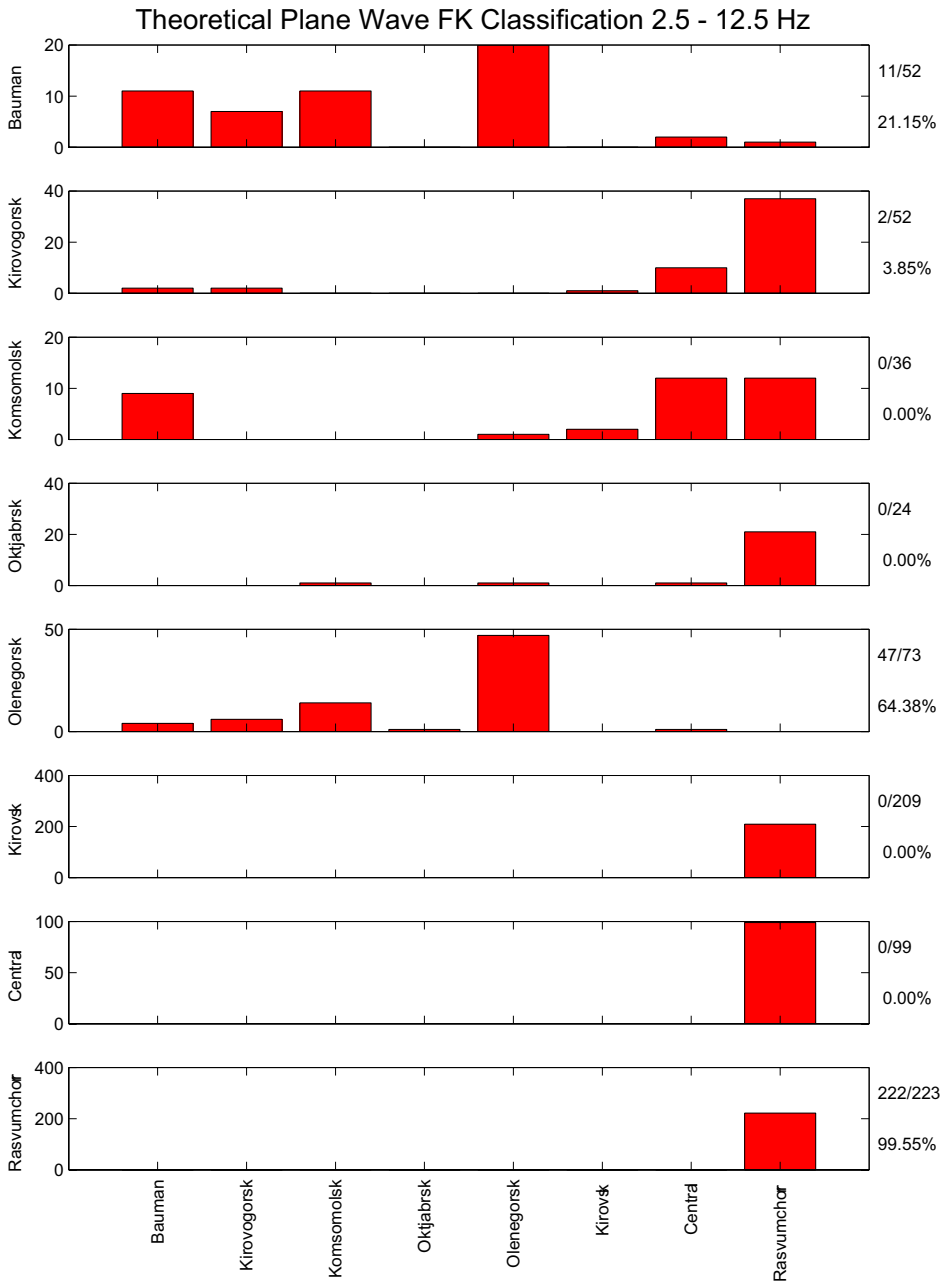

Figure 30: Event classification by broadband f-k spectral power estimation using theoretical steering vectors based on theoretical back-azimuths and nominal phase velocities fails to perform well due to biases in propagation and insufficient resolution to distinguish closely-spaced mines. See text for details.

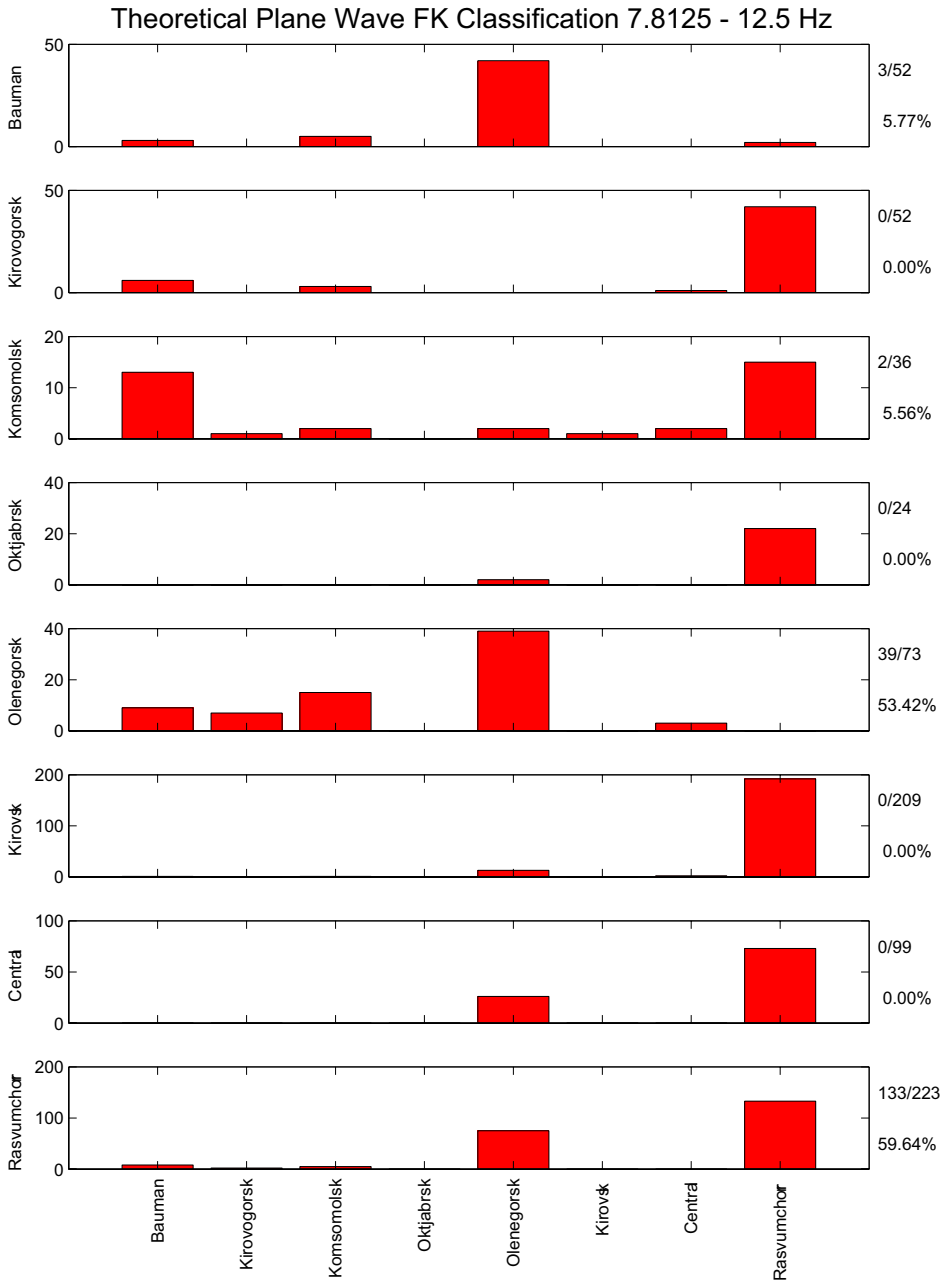

Figure 31: Event classification by conventional FK power spectral estimation deteriorates further as the frequency band is narrowed and the center frequency is increased. Poor performance is explained by the sparse array aperture employed in the calculations with the attendant decrease in signal coherence

However, classification results for the theoretical plane wave f-k method are far from perfect in the wide frequency band (2.5 - 12.5 Hz). The Olenegorsk group events frequently are misclassified within the group or even assigned to Khibiny mines. The Khibiny events are all assigned to the Rasvumchorr mine, which at least is within the correct group. The situation deteriorates further when the data are processed in the higher band (7.8125 - 12.5 Hz). In this case, even the Khibiny events frequently are misclassified to the other mine group.

Performance of the broadband f-k estimator improves considerably with slowness calibrations. We estimated slowness corrections for a particular mine by adjusting the theoretical slowness vector to maximize the power in the broadband plane wave f-k estimate for that mine, using the associated ensemble covariance matrices. A coarse grid search was conducted to initialize the search, with the grid centered on the theoretical slowness predicted by the backazimuth to the mine. The slowness estimate was further refined from the best grid value using Nelder-Meade optimization. The slowness calibrations are displayed in Figure 32.

The results of applying slowness calibrations over the wide band (2.5 - 12.5 Hz) are shown in Figure 33. Misclassification error is significantly reduced; Figure 33 has begun to show the diagonal structure characteristic of more accurate classification. The reduction in error probably results from the calibrations reducing slowness bias caused by refraction of the Pn phase. Significant misclassification errors remain among the mines of the two groups, but there is little crossover between the two groups. This effect is consistent with the interpretation that the mines within each group are too close to be resolved by this array, but the two groups are far enough apart to be distinguished once bias has been removed (c.f. Figure 11 and Figure 12 for a direct comparison of slowness estimates using conventional broadband f-k analysis).

The error increases significantly (Figure 34) if the analysis is carried out in the higher frequency band (7.8125 - 12.5 Hz). The loss of performance probably results from decreased Pn coherence across the teleseismic ARCES aperture.

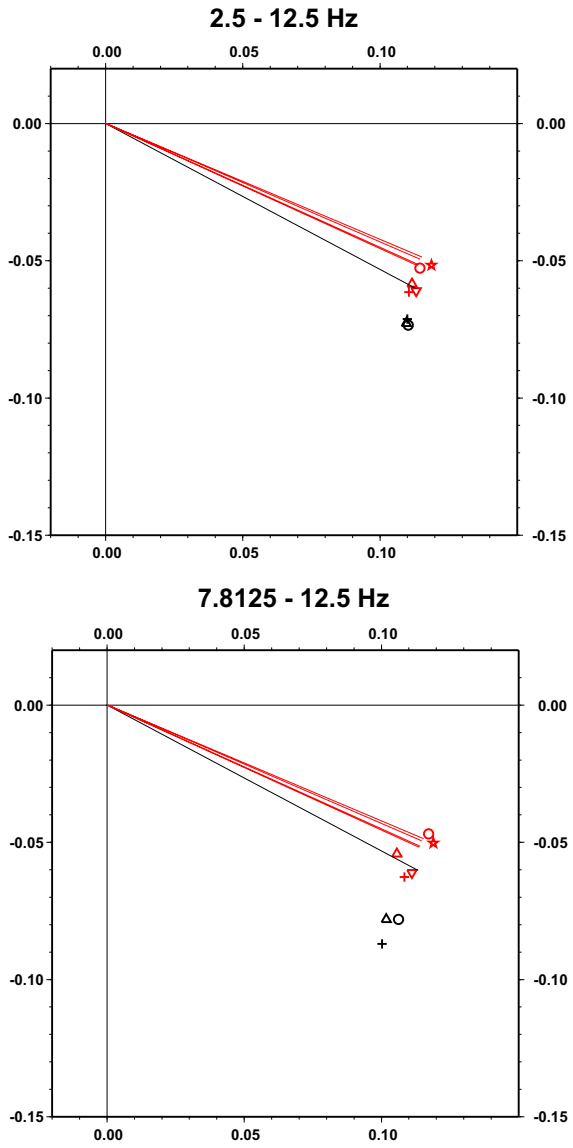

Figure 32: Plane-wave vector slowness calibrations for the eight mines of this study show biases and increasing scatter in the high-frequency band. Note the correspondence between the slowness corrections calculated between the new narrow-band code and the existing broadband code (Figures 11 and 12).

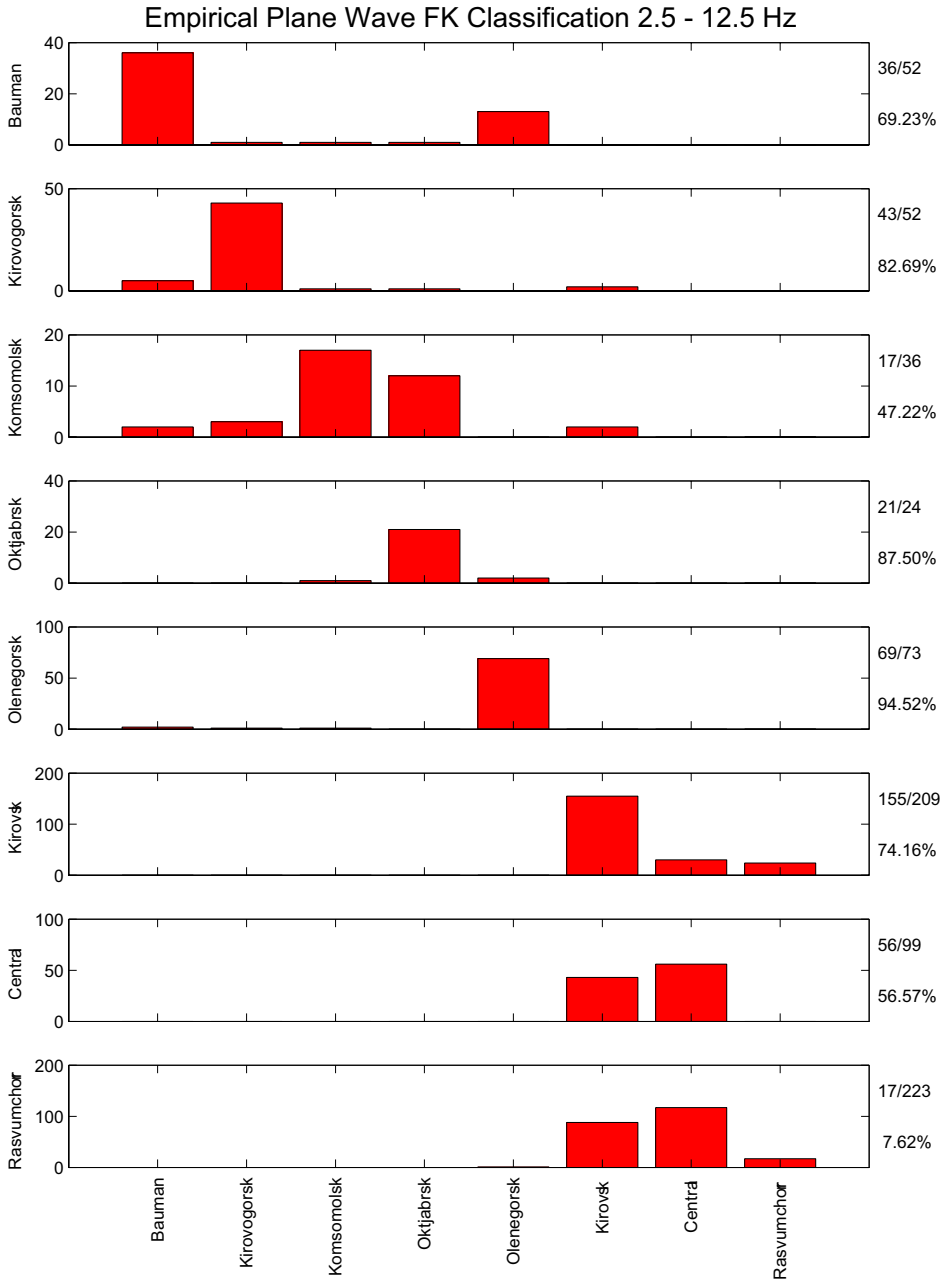

Figure 33: Event classification by calibrated FK power spectral estimation considerably improves performance by removing slowness biases caused by refraction in Pn propagation.

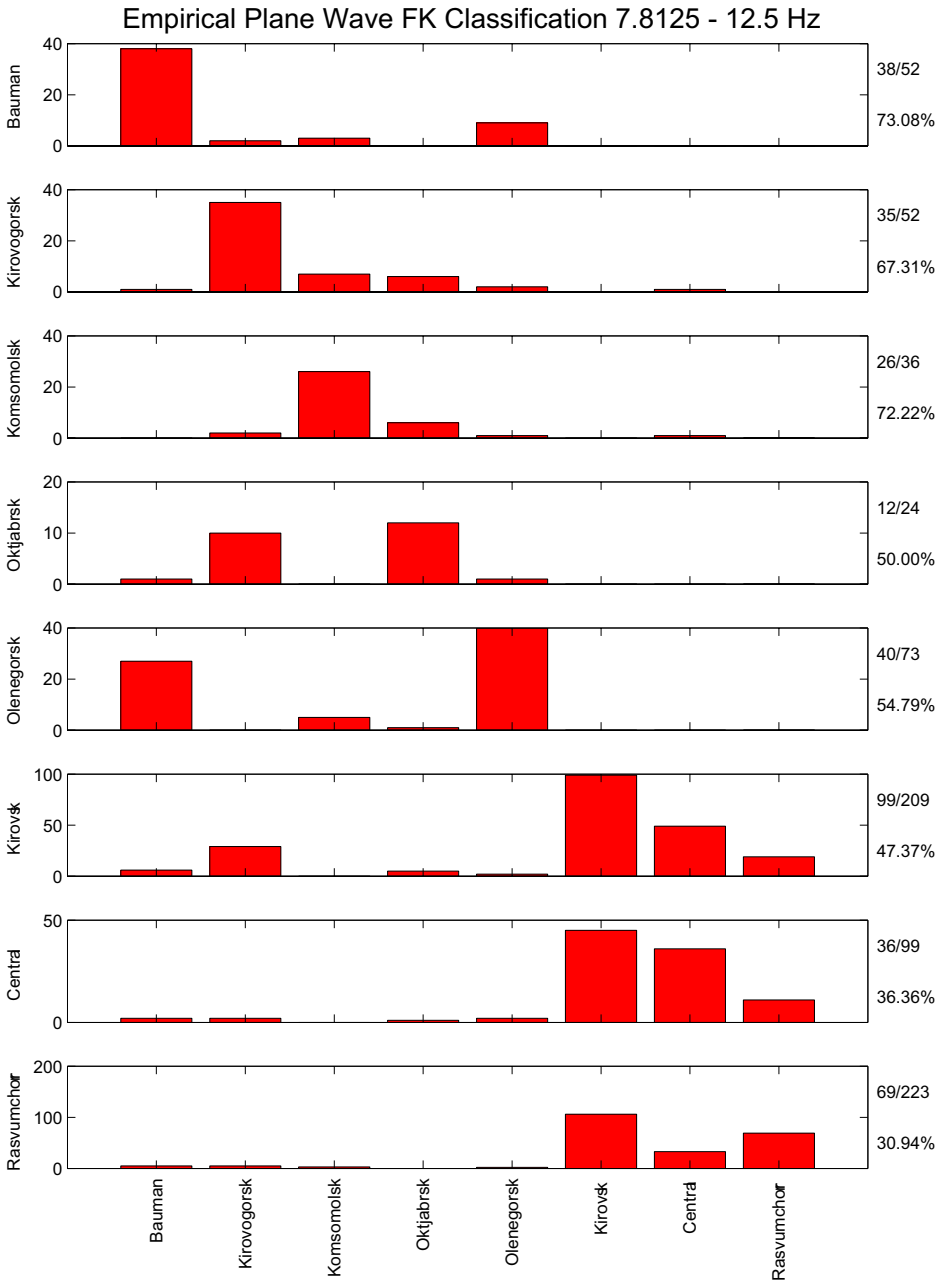

Figure 34: Event classification by calibrated FK power spectral estimation also deteriorates in the higher frequency band again due to the loss of coherence across the array aperture. The deterioration is not as severe as when theoretical backazimuths are used to define the steering vectors.

Misclassification error is dramatically reduced (to ~5% overall) with the use of matched field eigenvectors in the power estimation algorithm (Figure 35). This level of performance is consistent with the detailed characterization that the matched field calibrations represent of the spatial amplitude and phase structure of the Pn signals across the array aperture. Another significant observation is that the performance does not degrade appreciably when classification is carried out in the higher frequency band (Figure 36). This observation suggests that the empirical eigenvectors employed in matched field processing compensate for the effects of scattering and refraction that generally are understood to cause decorrelation across array apertures at high frequencies. Empirical matched field processing is the narrowband spatial equivalent of correlation matching that currently is employed in correlation detectors (Gibbons and Ringdal, 2006).

It is instructive to view the classification results in terms of a scatter diagram illustrating the marginal problem of classification between just two mines. Figure 37 shows the matched field processing classification statistics for compact underground explosions in the Kirovsk and Rasvumchorr mines under the two alternative hypotheses that the events are the Kirovsk mine or the Rasvumchorr mine. The statistics are computed in the high frequency band (7.8125 - 12.5 Hz). They show good separation between the two populations despite the fact that the mines lie on the same backazimuth viewed from ARCES (117.99 versus 118.15 degrees). That they can be separated at all at 400 kilometers range is an indication that some effect other than classical array resolution is at work. We speculate that the mines have different radiation patterns perhaps caused by differences in the topography surrounding them or different orientations of the underground shots. In any case, the scattering and refraction in the source regions may differ causing the energy incident upon the ARCES to approach for sufficiently distinguishable directions or combinations of directions. We note further that the two populations have few points directly between them but a few tens of points that fall directly in the main bodies of the alternative (incorrect) populations. We intend to examine whether these points represent incorrect ground truth event assignments to the two mines.

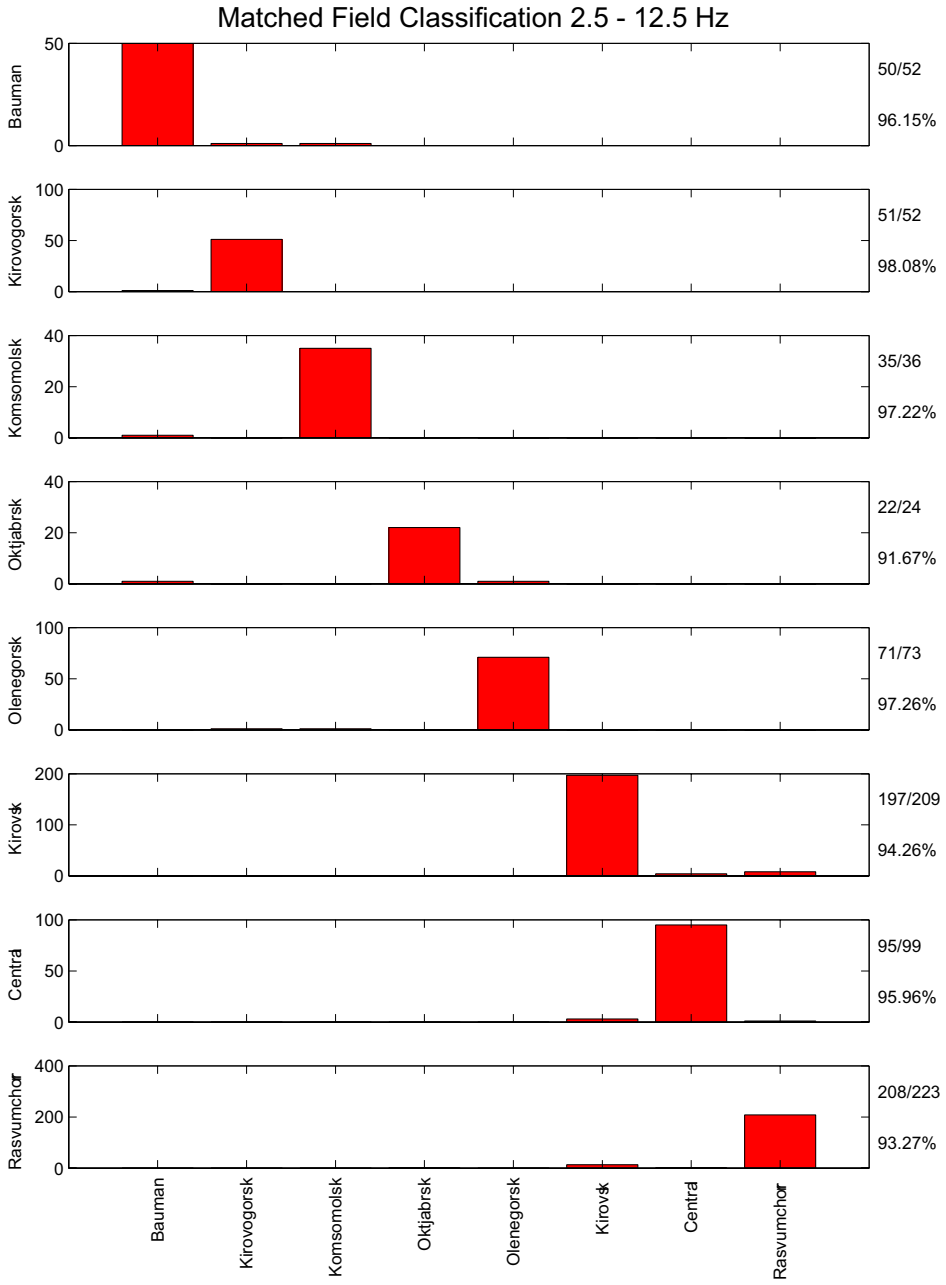

Figure 35: Event classification by broadband matched field processing is highly accurate due to the fact that it represents aperture-level calibration rather than a correction in slowness space.

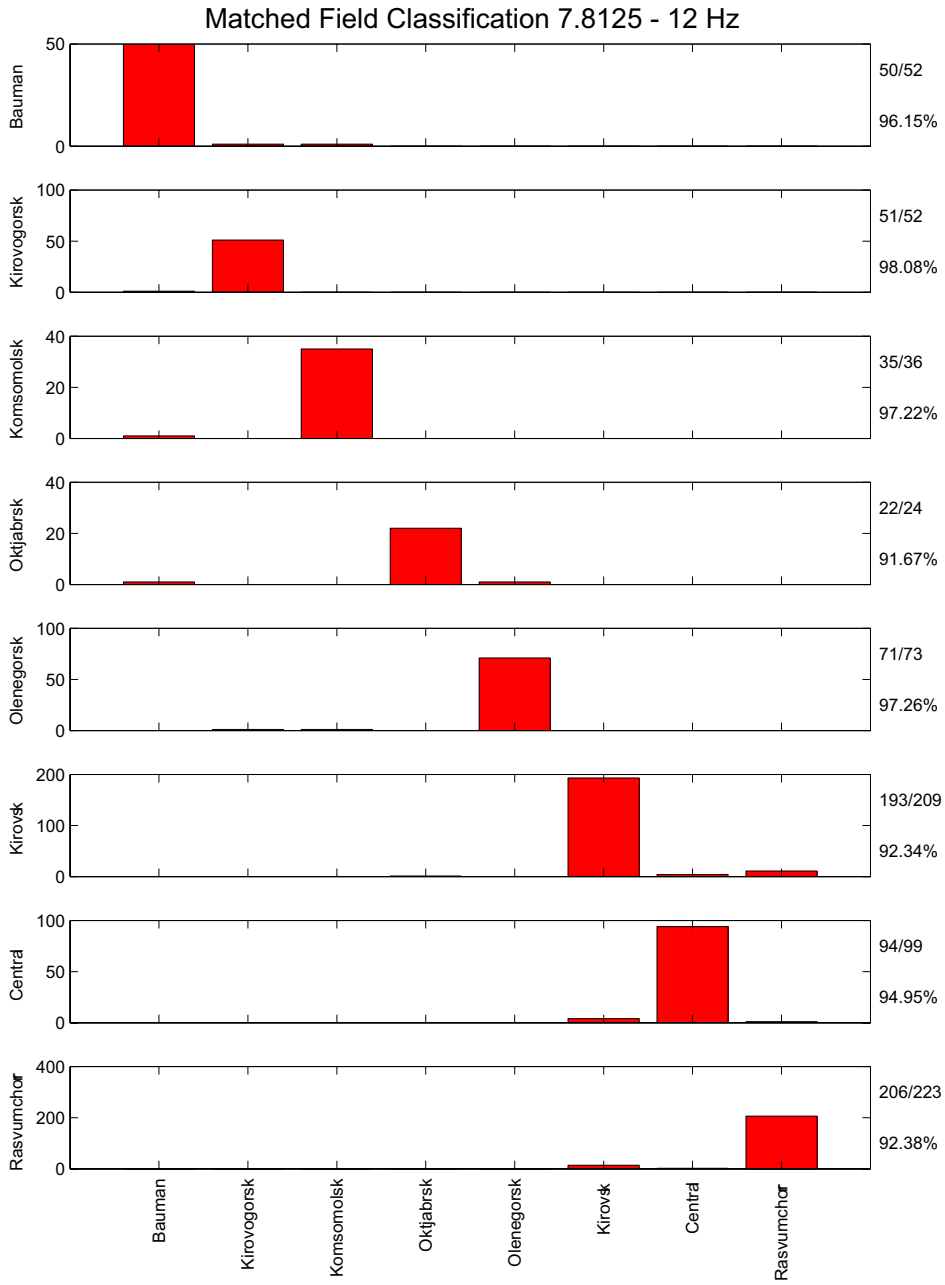

Figure 36: Matched field classification results do not deteriorate appreciably as the frequency band is increased due to the fact that aperture-level calibration compensates the effects of refraction and scattering, effectively turning an incoherent wavefield into a coherent wavefield.

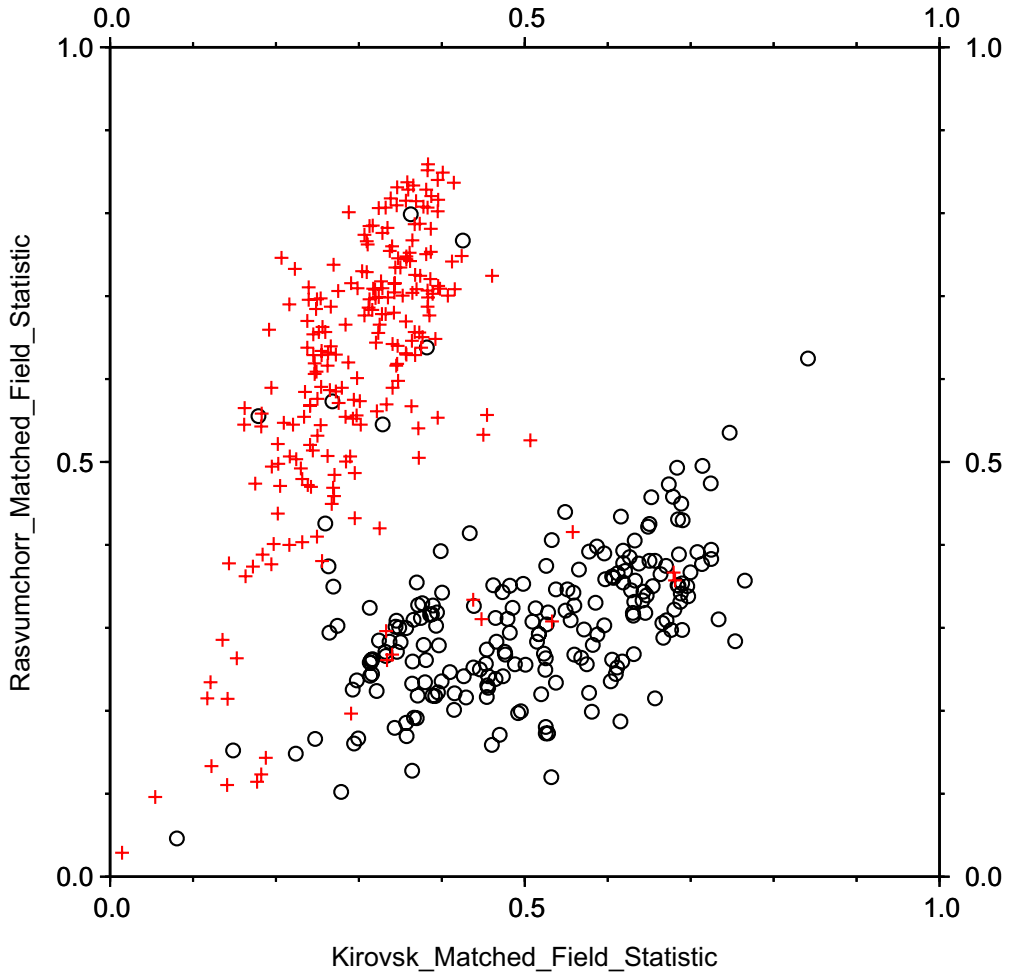

Figure 37: Populations of Rasvumchorr compact (red crosses) and Kirovsk compact (black circles) explosions separate well using matched field classification in the higher frequency band (7.8125 - 12.5 Hz). Relatively few points fall between the two clouds. This observation suggests that the Kirovsk events that fall solidly within the main Rasvumchorr population cloud (and vice versa) may have incorrect ground truth identities, an issue we intend to investigate.

Application to signal detection

A prerequisite to the association of a seismic signal with a given source is that the signal first be detected. Figure 7 indicates one of the fundamental difficulties with seismic array processing. The SNR for many signals improves with increasing frequency whilst, at the same time, the coherence over the array decreases. This is especially the case in the European Arctic where regional signals are characterized by high frequencies and the lower frequencies are dominated by high-amplitude ocean-generated microseisms. The selection of a frequency band in which to process a signal becomes an optimization problem whereby a compromise is sought between a high single-channel SNR and an optimal array-processing gain. It is subjective judgement of this trade-off from event to event which leads analysts to choose different and non-optimal frequency bands for taking measurements of seismic phases (c.f. Figures 16 and 20). A frequency band for signal detection should prioritize an optimal SNR over stability in parameter estimation (since the direction can be measured a posteriori), although the array-processing gain must be considered since signal-decorrelation can lead to a reduction of SNR by the same stacking process designed to improve signal observation.

Since we have demonstrated that empirical matched field processing can exploit the higher frequencies present in a signal in a way that the plane-wave model stacking cannot (compare Figure 36 with Figure 34) we can expect that a beamforming process which uses the empirically calibrated steering vectors will result in improved gain at the higher frequencies. Figure 38 shows that this is indeed the case for a low-amplitude signal from a Kirovsk underground compact explosion. The beamforming gain is especially high above 10 Hz, a frequency at which the matched field steering vectors and the plane-wave model steering vectors differ significantly (c.f. Figure 29).

This method may offer a technique for enhanced detection capability for sources of repeating seismicity where differences between successive signal waveforms may make full waveform matching (Gibbons and Ringdal, 2006) ineffective.

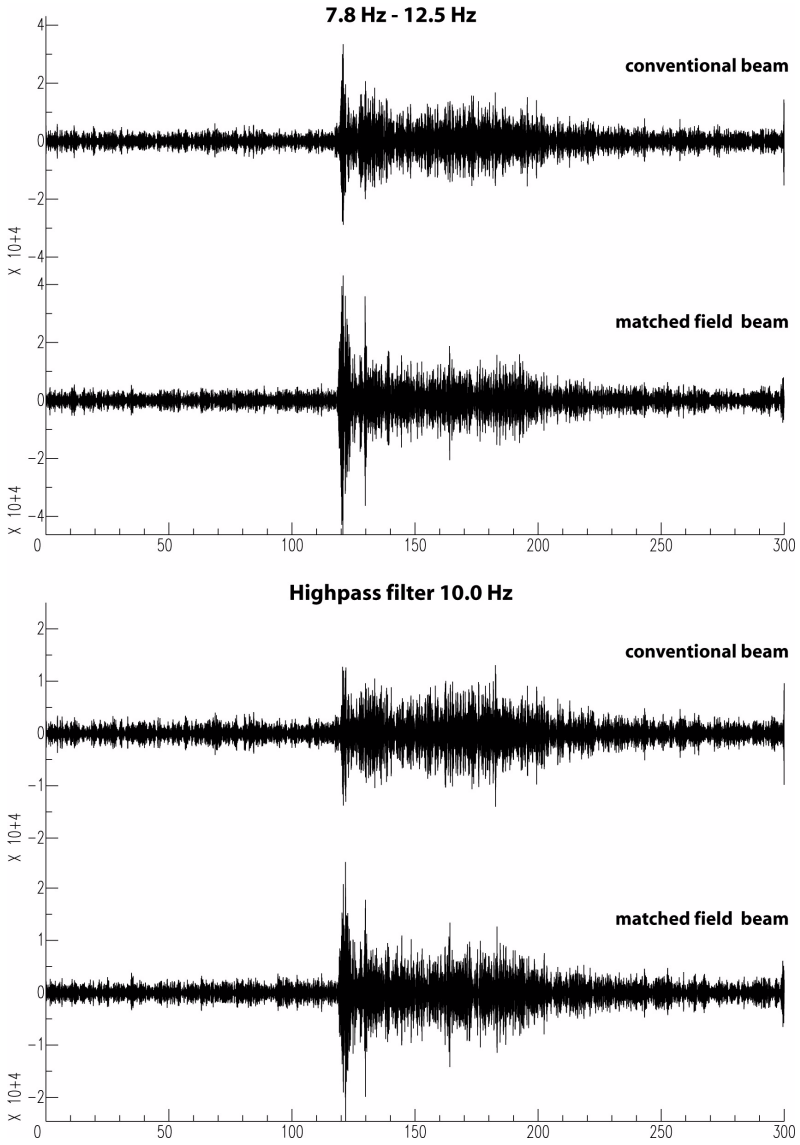

Figure 38: A comparison between beams constructed using theoretical steering vectors based upon the most appropriate plane wavefront solution and beams constructed from empirical steering vectors calculated from spatial covariance matrices for Pn arrivals for compact underground explosions at the Kirovsk mine on the Khibiny Massif.

7. Conclusions

We have examined approaches for the fully-automatic detection and identification of low-magnitude seismic events for small-aperture regional arrays which provide an improved location accuracy compared with current automatic approaches, combined with a low false alarm rate. The first approach identifies and locates events from sites of interest using a system of templates, which are calibrated using observations from previously observed events at the site of interest. The second approach is that of Empirical Matched Field Processing whereby the plane-wave steering vectors of broadband f-k analysis, applied for measuring the propagation parameters of incoming seismic phases, are replaced by a calibrated narrow-band steering vectors calculated from spatial covariance matrices from phase arrivals from events at the site being monitored.

Both approaches have resulted in significant improvements to automated event location estimates and/or source classification. The calibration efforts involved in designing the templates have raised many issues which have implications for event detection and location, both in the fully-automatic and analyst reviewed contexts.

A template system for automatic identification and location of events

The basic procedure followed is detailed in Gibbons et al. (2005). The system is defined in terms of two types of template: a *site template* defining which phases are likely to be (well) observed by one or several regional seismic arrays and, for each such phase, a *phase template* which specifies which processing parameters are expected to result in optimal propagation parameter estimates and which uncertainties and corrections should be applied to the results. The procedure was investigated for several sites within regional distances of the ARCES seismic array in Northern Norway. For each site, large numbers of confirmed events were identified: either from Ground Truth provision from the operators of mines, or using full waveform-correlation methods. These events were examined systematically in order to ascertain the variability of observations which could be anticipated for subsequent events from these sites. The following list emphasizes the most important results:

- The studies confirmed that broadband f-k slowness and azimuth estimates calculated in consistent, fixed frequency bands are far more stable than estimates made in variable frequency bands as is the current procedure for routine online detection.
- The frequency bands which result in the most stable slowness and azimuth estimates can vary greatly between different phase arrivals from different sites. No single frequency band was identified for which a different frequency band did not produce a better result for a different site. For example, for the Kola Peninsula mines, the Zapoljarni mines generated the most stable estimates in the 2-4 Hz band whereas the Khibiny mines generated the most stable estimates in the 4-8 Hz band.
- Slowness and azimuth estimates for secondary phases for most of the mining events were significantly poorer than the P-arrival estimates. The situation is especially acute for many of these complicated ripple-fired mining explosions since strong and variable coda phases often contaminate the S-phases significantly.

- The optimal frequency band for azimuth and slowness estimation is not necessarily the frequency band with the best signal to noise ratio or the best beam-gain.
- The bias associated with the optimal slowness vector for a given phase arrival can often vary greatly for different fixed frequency bands. This means that the SASCs (Slowness and Azimuth Station Corrections) applied widely in global seismic monitoring cannot be used optimally without considering the frequency band being studied. We recommend that substantial work be undertaken to develop a system for the correction of time-delays prior to the non-linear process for calculating slowness vectors.
- Both at ARCES and at the ABK array in Kazakhstan, it was observed that estimates deteriorated with increasing frequency due to loss of coherence.

The greatest shortcoming of the template system is that event hypotheses for real events are frequently rejected due to the failure to confirm secondary phase arrivals. This was discussed in detail for the Kovdor mine by Gibbons et al. (2005) and the failure statistics for other sites considered here was comparable to that case-study. The number of locatable events is linked to the simplicity of the source-time function and the SNR.

One interesting case was a site in northern Finland used for military ammunition destructions. This case was useful since the simple and repeating source-time function allowed the stability of f-k estimates and arrival times estimates to be considered without consideration of multiple events and other complications. In this case, all of the automatic template location estimates were successful and were far more reliable than the analyst reviewed solutions. This is a direct consequence of the stability of processing parameters used for measuring the phase arrival times and slowness vectors. The analyst tries to optimize frequency bands and other processing parameters on a case-by-case basis and the location estimates are dictated by the bias associated with the processing parameters chosen.

Empirical Matched Field Processing

Spatial covariance matrices were calculated for large numbers of confirmed events at mines in the Khibiny and Olenegorsk clusters on the Kola Peninsula. From these were derived empirical narrow-band steering vectors which can replace the theoretical plane-wave steering vectors applied in traditional f-k analysis. These resulted in the following advantages in terms of event detection and classification:

- A modified beamforming using the narrow-band calibrations results in a higher SNR for detection than the corresponding plane-wave beams. This is especially true at higher frequencies for which the plane wave assumption breaks down (even over small-aperture arrays) due to dissimilarity of waveforms over the array aperture.
- The matched field event classification resulted in only ~5% error in source identification - even between individual mines with less than 10km separation at a distance of over 400 km from the seismic array. For the few cases where the event classification failed, the selected source was always in the same cluster.

- The matched field event classification used only a short time-window at the beginning of the wavetrain. This means that we do not need to consider the secondary phases which are of paramount importance in the template system described above.
- The degradation in performance with increasing frequency is small which means that the method may be applied to weaker signals which are only well-observed at higher frequencies.
- The narrow-band nature of the matched field processing makes the procedure more sensitive to the spatial nature of the wavefield and less sensitive to the temporal properties. This means that the method may be more amenable to complicated seismic sources than full-waveform cross-correlation methods. It also suggests that the matched field processing will be well suited in cases of interfering events.

A significant disadvantage of the matched field method was that the empirical steering vectors for the different sites were quite dissimilar which suggests that calibrations will only be possible for sites with large numbers of confirmed events with strong signals. It is unlikely that the steering vectors will be able to be extrapolated to an extended source region. This suggests that the method will be more useful for source identification than for parameter estimation.

8. References

Akaike, H. (1973). Information theory and an extension of the maximum likelihood principle, In "*Proceedings of the 2nd International Symposium on Information Theory. Budapest Akademiai Kiado*", pp. 267-281.

Baggeroer, A. B., Kuperman,W. A., and Mikhalevsky, P. N. (1993). An overview of matched field methods in ocean acoustics, *IEEE Journal of Oceanic Engineering*, **19**(4), pp. 401-424.

Bame, D. A., Walck, M. C., Hiebert-Dodd, K. L. (1990). Azimuth Estimation Capabilities of the NORESS Regional Seismic Array, *Bull. Seism. Soc. Am*., **80**, pp. 1999-2015.

Bonner, J. L., Pearson, P. M., and Blomberg, W. S. (2003). Azimuthal variation of short-period Rayleigh waves from cast blasts in Northern Arizona, *Bull. Seism. Soc. Am*., **81**, pp. 724-736.

Breinzo, R. K. and W. S. Hodgkiss, W. S. (1993). Broadband matched-field processing, *Journal of the Acoustical Society of America*, **94**(5), pp. 2821-2831.

Capon, J. (1969). High-Resolution Frequency-Wavenumber Spectrum Analysis, *Proc. IEEE*, **57**, pp. 1408-1418.

Carr, D. B. (1213). Azimuth Estimation Capabilities of the ARCESS Regional Seismic Array, *Bull. Seism. Soc. Am*., **83**, pp. 1213-1231.

Fialkowski, L. T., Collins, M. D., Kuperman, W. A., Perkins, J. S., Kelly, L. J., Larsson, A., Fawcett, J. A., and Hall, L. A. (2000): Matched-field processing using measured replica fields, *Journal of the Acoustical Society of America*, **107**(2), pp. 739-746.

Geller, R. J., and Mueller, C. S. (1980). Four Similar Earthquakes in Central California, *Geophys. Res. Lett.*, **7**, pp. 821-824.

Gibbons, S. J., Kværna, T., and Ringdal, F. (2005). Monitoring of seismic events from a specific source region using a single regional array: a case study. *J. seismol.*, **9**, pp. 277-294.

Gibbons, S. J. and Ringdal, F. (2006). The detection of low magnitude seismic events using array-based waveform correlation, *Geophys. J. Int.*, **165**, 149-166.

GSE/JAPAN/40 (1992). A fully automated method for determining the arrival times of seismic waves and its application to an on-line processing system. In "*Proceedings 34th GSE session, Geneva, GSE/RF/62, G.S.E.*"

Harris, D. B. (1991). A waveform correlation method for identifying quarry explosions, *Bull. Seism. Soc. Am.*, **81**, pp. 2395-2418.

Harris, D. B., F. Ringdal, E. O. Kremenetskaya, S. Mykkeltveit, J. Schweitzer, T. F. Hauk, V. E. Asming, D. W. Rock and J. P. Lewis (2003). Ground-truth Collection for Mining Explosions in Northern Fennoscandia and Russia, in "*Proceedings of the 25th Seismic Research Review - Nuclear Explosion Monitoring: Building the Knowledge Base*", Los Alamos National Laboratory, LA-UR-03-6029, Tucson, AZ, Sept. 23-25, 2003, pp. 54-62.

Hicks, E. C., Kværna, T., Mykkeltveit, S., Schweitzer, J. and Ringdal, F. (2004). Travel-times and Attenuation Relations for Regional Phases in the Barents Sea Region, *Pure Appl. Geophys.*, **161**, 1-19.

Jenkins, G. M., and Watts, D. (1968). *Spectral Analysis and It's Applications*, Holden-Day, San Francisco.

Kværna, T. and Ringdal, F. (1986). Stability of various f-k estimation techniques, *NORSAR Scientific Report: Semiannual Technical Summary No. 1 - 1986/1987*. NORSAR, Kjeller, Norway. pp. 29-40.

Kværna, T., and Ringdal, F. (1989). A multichannel processing approach to real time network detection, phase association and threshold monitoring, *Bull. Seism. Soc. Am.*, **79**, pp. 1927-1940.

Kværna, T., and Ringdal, F. (1994): Intelligent post-processing of seismic events. *Annali di Geofisica*, **37** (3), pp. 309-322.

Kværna, T., and Doornbos, D. J. (1991). Scattering of Regional Pn by Moho Topography, *Geophys. Res. Lett.*, **18**, pp. 1273-1276.

Leonard, M. and Kennett, B. L. N. (1999). Multi-component autoregressive techniques for the analysis of seismograms. *Phys. Earth Planet. Inter.*, **113**, pp. 247-263.

McLaughlin, K. L., Bonner, J. L., and Barker, T. (2004). Seismic source mechanisms for quarry blasts: modelling observed Rayleigh and Love wave patterns from a Texas quarry. *Geophys. J. Int.*, **156**, pp. 79-93.

Ringdal, F., and Husebye E. S. (1982). Application of seismic arrays for detection, location and identification of seismic events, *Bull. Seism. Soc. Am.*, **72**, pp. S201-S224.

Rivière-Barbier, F. and Grant, L. T. (1993). Identification and Location of Closely Spaced Mining Events, *Bull. Seism. Soc. Am.*, **83**, pp. 1527-1546.

Schweitzer, J. (2001a). HYPOSAT - An enhanced routine to locate seismic events, *Pure appl. geophys.*, **158**, pp. 277-289.

Schweitzer, J. (2001b). Slowness Corrections - One Way to Improve IDC Products, *Pure appl. geophys.*, **158**, pp. 375-396.

Thomson, D. J. (1982). Spectrum Estimation and Harmonic Analysis, *Proc. IEEE*, **70**, pp. 1055-1096.

Appendix 1. Ground Truth Mining Events from the Kola Peninsula Used for Calibration of Processing Parameters

The processing parameters for optimal phase estimation for seismic arrivals from events at the sites of interest were calibrated using confirmed events occurring during a 12-month period between October 1, 2001, and September 30, 2002. Subsequent confirmed events were used to evaluate the quality of location estimates made using the optimized site-specific processing algorithms. For sites in the Zapoljarni, Olenegorsk, Khibiny, and Kovdor regions of north-west Russia, colleagues at the Kola Regional Seismological Center (KRSC) compiled lists of Ground-Truth events from logs provided by the mining companies. These lists provided an estimated origin time to the closest second. Tables A1.1 through A1.13 provide lists of all the events during this period, specified by a manually verified P-arrival time estimate at the ARCES array. The second column of each table contains the estimated travel time from the listed origin time. Given the precision to which the origin time is specified, this number is provided primarily as a confidence measure that the phase studied is a likely candidate for the first arrival from the indicated event. It has to be remembered that many of these events are multiple ripple-fired shots which complicates both the estimation of the arrival time at ARCES and the determination of a meaningful event origin time from stations at short distances. The azimuth and apparent velocity (specified in km/s) are evaluated using broadband f-k analysis in the fixed frequency band 2.0 - 5.0 hz in a data window of length 3.0 seconds following the estimated arrival time. The SNR is measured on the theoretical P-beam filtered between 2.0 and 5.0 hz. The yield is specified in tons by the mining companies, but this may be of secondary importance since this number is indicates the total yield and it is not known how this yield is distributed over the firing sequence.

Table A1.1 Confirmed mining blasts at the Kirovsk mine (KH1: Khibiny Massif) between October 1, 2001, and September 30, 2002. See description on page 71 for details.

ARCES arrival time	Est. t.t.	SNR	Azi.	Vel.	Yield
2001-278:03.10.08.038	56.038	8.2	122.01	7.70	4
2001-280:05.10.24.663	55.663	17.0	122.16	7.42	8
2001-281:19.22.50.713	54.713	17.2	122.99	7.47	3
2001-282:20.14.05.213	55.213	4.7	122.13	7.46	4
2001-286:17.21.04.663	55.663	71.4	122.74	7.58	4
2001-287:02.44.13.338	56.338	120.4	123.29	7.52	77
2001-289:13.12.23.163	56.163	14.8	122.03	7.62	5
2001-290:13.00.02.888	55.888	5.1	121.64	7.57	1
2001-293:02.02.35.538	55.538	6.5	122.50	7.46	1
2001-293:08.09.20.813	55.813	4.4	125.00	7.29	1
2001-293:08.13.21.538	56.538	77.1	122.16	7.60	1
2001-293:20.21.15.488	55.488	19.3	123.26	7.52	7
2001-297:03.34.41.113	56.113	33.9	122.70	7.57	5
2001-299:12.27.03.963	55.963	4.6	122.58	7.51	218
2001-299:03.14.12.488	55.488	10.3	123.42	7.64	4
2001-300:02.09.06.113	56.113	6.1	122.69	7.40	1
2001-303:16.00.46.713	56.713	14.9	123.24	7.38	1

Table A1.1 Confirmed mining blasts at the Kirovsk mine (KH1: Khibiny Massif) between October 1, 2001, and September 30, 2002. See description on page 71 for details.

ARCES arrival time	Est. t.t.	SNR	Azi.	Vel.	Yield
2001-305:19.15.15.288	55.288	5.3	123.33	7.55	5
2001-307:04.51.05.188	56.188	8.9	122.47	7.45	6
2001-309:19.40.23.713	54.713	16.3	122.68	7.49	2
2001-310:11.31.20.113	56.113	4.6	121.79	7.47	1
2001-313:14.35.53.488	55.488	28.4	121.71	7.62	4
2001-314:03.49.17.613	55.613	14.1	122.21	7.49	3
2001-315:06.38.00.963	55.963	11.3	124.08	7.46	7
2001-317:04.08.37.888	55.888	9.3	122.34	7.50	2
2001-319:04.31.01.613	55.613	5.8	122.87	7.49	2
2001-320:00.58.08.113	56.113	4.6	119.90	7.75	2
2001-321:04.47.08.188	56.188	9.5	121.96	7.63	1
2001-322:03.17.21.313	55.313	143.0	121.61	7.67	123
2001-324:18.23.51.638	55.638	7.4	123.37	7.64	2
2001-325:21.16.22.788	55.788	10.0	121.53	7.64	2
2001-328:04.04.40.788	55.788	30.7	121.81	7.52	2
2001-328:16.41.19.088	56.088	47.3	122.30	7.55	5
2001-329:04.30.55.338	56.338	167.1	122.50	7.53	112
2001-335:18.56.55.063	56.063	6.9	119.76	7.33	3
2001-338:04.19.31.863	55.863	5.9	122.71	7.40	1
2001-340:03.50.22.488	55.488	17.2	121.82	7.46	5
2001-341:04.09.32.388	56.388	4.1	122.24	7.60	1
2001-343:04.39.02.288	56.288	152.0	123.30	7.50	77
2001-352:14.42.48.538	55.538	19.0	122.62	7.52	4
2001-353:14.19.53.463	55.463	10.6	122.73	7.52	1
2001-354:14.03.28.588	55.588	5.4	120.75	7.41	1
2001-355:14.17.39.388	55.388	7.5	122.51	7.56	2
2001-357:07.47.59.813	55.813	8.8	123.61	7.33	7
2001-359:04.10.00.413	56.413	9.5	121.82	7.55	2
2001-363:01.17.13.488	56.488	23.6	122.70	7.49	3
2001-365:05.18.04.788	55.788	256.8	122.41	7.59	140
2002-005:11.02.07.763	56.763	15.2	123.33	7.47	4
2002-005:17.00.50.663	55.663	38.2	122.23	7.59	5
2002-010:14.04.36.813	55.813	18.6	122.39	7.56	1
2002-011:14.22.26.638	55.638	4.3	120.15	7.09	2
2002-012:08.48.56.238	56.238	9.9	124.04	7.49	4
2002-013:08.03.43.763	55.763	16.2	123.18	7.43	10
2002-017:04.10.39.388	56.388	30.4	122.29	7.46	3
2002-018:04.26.37.188	56.188	8.7	122.12	7.43	2
2002-019:02.53.11.338	56.338	6.5	122.04	7.61	1
2002-020:03.45.49.788	55.788	141.6	122.39	7.55	36
2002-025:20.49.15.613	54.613	8.7	121.60	7.60	3
2002-025:21.07.48.438	56.438	20.8	122.80	7.53	2
2002-026:18.59.45.513	55.513	28.5	122.77	7.56	4
2002-031:14.16.52.163	56.163	10.7	123.55	7.42	3
2002-033:03.58.43.488	55.488	16.9	123.12	7.51	4
2002-036:04.17.44.738	55.738	8.3	123.23	7.54	2

Table A1.1 Confirmed mining blasts at the Kirovsk mine (KH1: Khibiny Massif) between October 1, 2001, and September 30, 2002. See description on page 71 for details.

ARCES arrival time	Est. t.t.	SNR	Azi.	Vel.	Yield
2002-038:03.04.11.438	56.438	8.2	123.62	7.62	1
2002-039:04.01.33.463	55.463	11.9	122.02	7.34	1
2002-040:04.41.35.113	56.113	12.4	122.50	7.55	2
2002-040:04.49.06.538	55.538	26.9	122.11	7.50	5
2002-040:05.18.20.938	55.938	8.3	122.34	7.90	1
2002-046:21.36.09.538	56.538	13.0	121.98	7.52	6
2002-047:16.09.14.088	56.088	18.6	123.58	7.59	7
2002-047:17.27.26.613	55.613	28.0	123.13	7.46	2
2002-048:07.31.44.563	56.563	23.6	122.79	7.54	10
2002-052:14.21.02.838	55.838	14.0	122.84	7.50	1
2002-054:04.01.33.238	56.238	110.0	122.68	7.54	76
2002-061:06.59.12.838	55.838	14.8	123.03	7.46	4
2002-061:15.20.41.788	55.788	21.8	122.48	7.54	4
2002-062:05.46.49.738	55.738	23.4	122.90	7.56	3
2002-066:19.17.51.063	56.063	3.9	123.70	7.43	2
2002-066:20.43.02.763	56.763	9.0	121.41	7.67	2
2002-066:21.13.08.788	55.788	30.2	122.85	7.49	3
2002-073:14.31.30.813	55.813	12.9	122.32	7.52	3
2002-076:03.32.32.213	56.213	65.9	122.53	7.56	30
2002-078:05.05.41.588	55.588	16.3	122.84	7.43	3
2002-083:04.14.18.288	56.288	429.9	122.63	7.57	202
2002-083:05.28.13.263	56.263	26.8	123.52	7.46	5
2002-086:18.56.14.363	56.363	13.3	122.83	7.48	2
2002-090:05.24.33.813	55.813	11.7	121.49	7.68	122
2002-093:13.41.56.413	56.413	17.5	122.36	7.54	4
2002-095:12.24.09.088	56.088	7.2	122.49	7.62	2
2002-096:02.58.00.388	56.388	6.9	121.07	7.55	3
2002-096:16.46.41.863	55.863	15.7	123.48	7.43	3
2002-101:03.37.58.188	56.188	25.7	122.82	7.51	2
2002-102:02.59.15.163	56.163	10.8	122.67	7.52	2
2002-102:03.27.36.163	56.163	29.2	122.60	7.47	3
2002-103:15.46.37.938	55.938	43.7	122.77	7.61	2
2002-104:04.38.27.788	55.788	23.0	123.59	7.48	5
2002-106:18.20.23.713	55.713	17.9	122.61	7.56	4
2002-107:20.17.12.513	55.513	39.1	122.60	7.47	1
2002-109:20.29.08.288	56.288	7.0	122.62	7.71	2
2002-114:13.35.46.088	56.088	4.8	122.13	7.61	2
2002-114:13.41.33.988	55.988	14.5	123.56	7.43	1
2002-115:13.23.27.613	55.613	32.1	122.46	7.46	4
2002-115:14.24.52.138	56.138	22.8	122.18	7.56	1
2002-115:14.42.26.588	55.588	15.4	122.28	7.56	2
2002-117:06.37.48.888	55.888	16.6	122.78	7.51	1
2002-118:02.23.44.963	55.963	177.6	121.98	7.69	59
2002-120:07.54.13.988	54.988	9.9	122.28	7.37	1
2002-126:01.28.18.513	57.513	3.0	122.79	7.56	3
2002-126:20.00.39.988	55.988	15.0	122.77	7.55	2

Table A1.1 Confirmed mining blasts at the Kirovsk mine (KH1: Khibiny Massif) between October 1, 2001, and September 30, 2002. See description on page 71 for details.

ARCES arrival time	Est. t.t.	SNR	Azi.	Vel.	Yield
2002-126:21.55.35.813	55.813	8.7	121.85	7.76	1
2002-134:13.07.53.088	56.088	10.3	122.33	7.52	1
2002-135:13.26.10.588	56.588	4.0	122.24	7.45	1
2002-137:09.58.58.413	55.413	25.7	123.25	7.41	2
2002-137:13.24.59.463	55.463	15.2	123.30	7.37	2
2002-141:03.19.54.113	56.113	15.0	123.19	7.50	1
2002-142:03.01.13.263	56.263	21.6	122.79	7.46	2
2002-142:03.08.53.288	56.288	24.7	122.30	7.55	2
2002-143:03.04.30.988	55.988	23.4	121.90	7.59	2
2002-144:03.04.53.363	56.363	11.6	122.13	7.48	2
2002-144:03.09.01.088	56.088	15.3	122.46	7.55	2
2002-147:18.53.37.138	56.138	53.7	121.53	7.66	5
2002-149:03.53.53.263	56.263	55.0	123.78	7.46	1
2002-150:00.41.37.138	57.138	14.3	122.42	7.53	2
2002-150:20.13.25.338	56.338	10.4	123.24	7.57	1
2002-152:00.09.18.088	56.088	16.6	121.10	7.62	2
2002-153:04.01.37.763	55.763	18.3	124.35	7.44	7
2002-156:10.24.20.538	54.538	13.1	122.18	7.42	2
2002-156:13.32.04.688	55.688	12.9	123.80	7.41	2
2002-157:13.10.33.763	55.763	19.1	122.65	7.47	3
2002-158:13.13.29.313	56.313	5.2	120.18	8.05	2
2002-159:12.15.45.688	55.688	32.3	121.66	7.57	7
2002-159:15.14.54.263	56.263	47.8	122.67	7.64	4
2002-162:01.29.08.438	56.438	22.4	122.65	7.59	2
2002-162:01.51.42.188	56.188	13.8	122.86	7.63	3
2002-166:05.20.04.063	56.063	69.0	122.06	7.65	10
2002-167:02.05.11.888	55.888	82.5	122.60	7.51	28
2002-169:18.51.58.813	55.813	8.7	123.46	7.45	1
2002-170:20.24.27.738	55.738	18.3	123.80	7.49	3
2002-174:11.02.42.713	56.713	97.3	122.16	7.63	146
2002-176:13.27.09.913	55.913	11.0	123.69	7.58	4
2002-176:13.35.57.163	56.163	4.9	122.29	7.52	2
2002-178:12.56.14.313	56.313	5.5	122.93	7.54	3
2002-179:13.39.44.863	56.863	9.2	122.25	7.58	3
2002-180:09.44.57.013	56.013	3.4	121.12	7.37	1
2002-180:15.55.11.013	56.013	6.2	122.47	7.16	2
2002-181:09.07.01.738	54.738	144.8	123.78	7.45	93
2002-185:03.25.41.963	55.963	17.6	122.16	7.51	2
2002-186:03.36.13.113	56.113	7.8	123.69	7.45	1
2002-187:03.12.54.138	56.138	31.5	122.02	7.46	2
2002-187:03.13.39.238	56.238	5.1	123.20	7.49	4
2002-188:05.05.06.713	55.713	20.6	123.24	7.69	3
2002-189:19.56.13.338	56.338	5.0	121.54	7.50	1
2002-194:15.09.55.513	56.513	19.2	121.57	7.68	3
2002-194:15.10.52.188	56.188	8.6	120.63	7.40	2
2002-194:16.43.01.513	55.513	25.0	124.37	7.39	5

Table A1.1 Confirmed mining blasts at the Kirovsk mine (KH1: Khibiny Massif) between October 1, 2001, and September 30, 2002. See description on page 71 for details.

ARCES arrival time	Est. t.t.	SNR	Azi.	Vel.	Yield
2002-195:05.28.26.813	55.813	32.9	122.94	7.50	5
2002-198:13.11.50.213	56.213	6.5	121.88	7.55	1
2002-200:13.11.29.613	56.613	17.5	122.62	7.55	3
2002-202:04.26.44.063	56.063	132.2	122.58	7.56	78
2002-202:05.10.57.163	56.163	110.2	122.79	7.56	9
2002-205:03.00.03.113	56.113	8.0	122.77	7.55	1
2002-207:00.29.15.663	56.663	15.7	122.72	7.57	1
2002-208:00.29.45.363	56.363	2.2	120.79	7.25	2
2002-209:09.25.42.288	56.288	19.5	122.69	7.68	2
2002-210:16.50.09.513	56.513	3.9	122.53	7.63	1
2002-213:20.09.43.788	55.788	10.3	121.79	7.69	4
2002-213:22.13.31.263	56.263	19.8	122.36	7.55	2
2002-217:13.11.54.188	56.188	11.9	123.01	7.47	6
2002-219:13.10.25.463	56.463	9.8	122.12	7.47	4
2002-220:11.58.04.588	55.588	6.6	122.85	7.65	3
2002-221:13.06.36.413	56.413	9.4	121.52	7.69	2
2002-221:13.11.04.563	56.563	17.3	122.73	7.50	4
2002-222:00.44.34.513	55.513	5.2	123.29	7.50	2
2002-222:17.58.38.363	56.363	26.5	122.75	7.58	4
2002-223:05.12.00.488	56.488	7.4	122.79	7.60	6
2002-225:03.11.22.463	56.463	19.9	122.14	7.64	5
2002-228:03.06.38.938	55.938	3.1	123.20	7.47	2
2002-244:04.17.35.063	56.063	286.7	122.69	7.55	127
2002-247:01.41.03.213	56.213	6.6	122.75	7.42	3
2002-247:03.13.08.038	56.038	13.2	121.77	7.56	4
2002-248:03.01.30.163	56.163	4.9	123.09	7.51	2
2002-248:03.25.57.988	55.988	14.7	122.85	7.64	3
2002-249:03.11.30.563	55.563	27.8	123.98	7.44	3
2002-249:03.18.48.963	55.963	9.2	122.59	7.36	4
2002-250:03.28.44.463	56.463	4.2	121.58	7.61	5
2002-250:18.05.54.713	55.713	24.5	122.18	7.68	5
2002-251:22.53.49.813	55.813	7.0	121.97	7.46	4
2002-252:20.12.26.388	56.388	5.5	121.95	7.49	2
2002-253:20.16.40.063	56.063	12.2	122.50	7.42	3
2002-254:20.05.21.088	56.088	10.4	122.05	7.59	2
2002-256:20.18.08.038	56.038	4.7	120.81	7.73	2
2002-257:15.19.40.688	55.688	50.3	121.53	7.71	2
2002-258:02.46.30.763	55.763	43.2	121.97	7.65	55
2002-258:04.49.20.513	55.513	22.9	123.20	7.48	10
2002-259:12.47.42.788	55.788	4.1	121.68	7.82	2
2002-260:13.32.26.313	56.313	6.1	123.17	7.37	1
2002-261:13.16.36.288	56.288	14.2	121.51	7.57	3
2002-261:13.47.17.188	56.188	12.7	123.32	7.42	3
2002-263:13.40.20.188	56.188	34.6	122.09	7.64	2
2002-264:09.50.54.713	56.713	56.4	122.38	7.60	5
2002-267:03.03.53.063	56.063	4.5	122.30	7.60	2

Table A1.1 Confirmed mining blasts at the Kirovsk mine (KH1: Khibiny Massif) between October 1, 2001, and September 30, 2002. See description on page 71 for details.

ARCES arrival time	Est. t.t.	SNR	Azi.	Vel.	Yield
2002-267:01.23.55.638	56.638	12.9	122.24	7.38	2
2002-269:03.32.03.938	55.938	19.9	123.34	7.51	2
2002-270:03.08.05.413	56.413	13.4	121.62	7.61	2
2002-272:05.12.53.563	55.563	158.8	123.04	7.53	117

Table A1.2 Confirmed mining blasts at the Rasvumchorr mine (KH3: Khibiny Massif) between October 1, 2001, and September 30, 2002. See description on page 71 for details.

ARCES arrival time	Est. t.t.	SNR	Azi.	Vel.	Yield
2001-276:16.13.14.888	56.888	3.3	123.55	7.56	2
2001-277:03.50.57.288	56.288	8.2	122.17	7.40	3
2001-279:03.38.43.163	56.163	46.1	123.52	7.41	2
2001-282:04.39.36.938	55.938	6.2	121.67	7.58	4
2001-285:03.31.54.963	55.963	9.0	122.14	7.40	1
2001-286:02.55.04.888	56.888	14.4	122.82	7.45	4
2001-290:03.55.57.613	56.613	3.2	123.27	7.39	1
2001-292:20.59.12.288	56.288	14.3	123.22	7.37	1
2001-299:03.36.51.488	57.488	10.4	123.12	7.44	3
2001-304:03.35.54.213	56.213	8.5	123.37	7.47	1
2001-306:20.56.44.838	56.838	9.3	122.97	7.15	1
2001-310:20.52.02.463	56.463	38.0	123.70	7.45	7
2001-314:03.50.07.938	56.938	7.6	122.88	7.43	4
2001-314:04.13.47.963	56.963	36.5	123.53	7.36	3
2001-319:05.02.39.163	56.163	16.8	122.80	7.36	3
2001-320:21.22.20.038	56.038	18.1	123.75	7.42	2
2001-334:04.28.37.963	56.963	24.3	123.27	7.47	4
2001-340:04.48.42.788	56.788	10.8	123.22	7.44	1
2001-341:04.30.42.938	55.938	5.2	125.19	7.22	2
2001-348:21.54.12.263	56.263	23.4	123.32	7.39	4
2001-351:22.07.24.188	56.188	20.2	123.25	7.43	3
2001-353:04.31.13.713	56.713	8.7	123.92	7.49	4
2001-355:12.33.20.988	55.988	10.2	121.27	7.62	2
2001-356:03.36.32.938	56.938	43.2	123.27	7.42	52
2001-360:04.55.17.463	56.463	35.4	122.96	7.40	3
2002-004:22.44.06.813	56.813	14.7	122.04	7.44	1
2002-008:21.42.20.013	57.013	7.0	122.16	7.25	3
2002-009:04.32.36.763	56.763	17.9	123.12	7.36	5
2002-010:04.31.56.163	57.163	15.5	124.10	7.43	2
2002-011:21.43.01.613	56.613	18.8	123.41	7.46	2
2002-012:04.31.37.063	57.063	39.3	123.09	7.43	5
2002-016:04.34.21.813	56.813	9.4	122.66	7.39	5

Table A1.2 Confirmed mining blasts at the Rasvumchorr mine (KH3: Khibiny Massif) between October 1, 2001, and September 30, 2002. See description on page 71 for details.

ARCES arrival time	Est. t.t.	SNR	Azi.	Vel.	Yield
2002-019:12.24.06.638	56.638	16.2	122.39	7.45	4
2002-025:04.45.01.738	56.738	12.1	122.06	7.46	1
2002-026:03.06.01.613	56.613	35.5	122.98	7.45	5
2002-031:13.34.20.963	55.963	6.2	121.54	7.67	1
2002-032:03.57.04.988	55.988	11.5	121.52	7.59	2
2002-039:04.27.58.813	56.813	51.4	123.68	7.45	5
2002-043:21.46.37.313	56.313	8.1	122.52	7.35	1
2002-046:05.00.57.413	56.413	11.9	122.55	7.42	4
2002-051:04.28.25.263	56.263	14.4	122.21	7.47	1
2002-053:21.56.27.438	56.438	8.4	123.05	7.42	6
2002-058:23.16.42.638	57.638	13.3	123.07	7.45	2
2002-060:21.24.39.438	56.438	21.6	123.88	7.42	7
2002-060:21.33.36.938	55.938	5.4	123.89	7.52	3
2002-064:04.37.06.563	56.563	59.8	122.09	7.43	3
2002-065:04.33.48.513	56.513	17.5	123.85	7.38	1
2002-066:21.05.47.163	57.163	18.0	123.33	7.39	3
2002-066:23.35.27.038	56.038	12.1	123.02	7.46	6
2002-074:04.45.05.888	56.888	56.7	123.51	7.48	7
2002-075:12.44.05.713	56.713	8.9	123.23	7.43	4
2002-081:21.37.06.488	56.488	57.0	123.37	7.42	3
2002-082:10.40.05.138	57.138	13.8	122.62	7.44	2
2002-087:04.32.59.263	56.263	32.4	123.60	7.43	2
2002-088:04.32.17.888	56.888	5.6	122.70	7.11	2
2002-093:03.46.21.563	56.563	89.0	122.41	7.40	7
2002-094:04.33.51.363	55.363	45.2	123.74	7.42	5
2002-095:04.25.09.688	56.688	10.6	121.42	7.50	1
2002-095:14.04.05.513	55.513	8.0	121.72	7.63	1
2002-095:21.00.06.488	56.488	38.8	122.83	7.39	2
2002-096:06.17.59.313	56.313	29.2	123.21	7.46	4
2002-101:03.30.02.763	56.763	16.1	123.35	7.47	3
2002-104:00.22.13.588	58.588	2.8	123.34	7.44	3
2002-109:03.30.04.063	57.063	57.2	122.01	7.47	2
2002-110:05.03.47.188	56.188	351.5	122.48	7.45	145
2002-120:11.33.08.588	56.588	13.1	122.98	7.43	3
2002-128:20.51.09.988	56.988	14.7	120.97	7.65	3
2002-136:03.01.53.613	56.613	18.3	123.77	7.50	3
2002-137:02.18.42.763	56.763	5.3	122.55	7.49	2
2002-138:03.49.01.788	56.788	41.7	123.36	7.43	5
2002-145:03.45.59.763	56.763	19.6	123.07	7.45	2
2002-148:20.38.11.963	55.963	9.3	122.25	7.35	5
2002-151:03.45.16.288	56.288	14.0	123.48	7.43	2
2002-157:04.12.25.838	56.838	41.7	123.33	7.45	5
2002-158:20.46.06.588	56.588	14.8	123.70	7.38	2
2002-166:03.20.05.038	56.038	26.7	122.25	7.58	4
2002-166:03.41.55.838	56.838	59.3	123.22	7.49	2
2002-171:04.02.50.488	56.488	20.4	123.03	7.42	2

Table A1.2 Confirmed mining blasts at the Rasvumchorr mine (KH3: Khibiny Massif) between October 1, 2001, and September 30, 2002. See description on page 71 for details.

ARCES arrival time	Est. t.t.	SNR	Azi.	Vel.	Yield
2002-172:03.38.16.763	56.763	16.1	123.97	7.36	1
2002-172:19.57.25.888	56.888	23.2	122.48	7.43	1
2002-179:03.54.39.138	56.138	81.0	123.41	7.43	2
2002-184:03.26.52.263	57.263	45.6	123.61	7.45	2
2002-187:03.05.31.688	56.688	15.2	123.46	7.43	2
2002-192:03.12.11.063	57.063	13.2	123.23	7.47	2
2002-199:03.57.46.513	56.513	8.5	122.09	7.61	1
2002-200:08.38.57.238	56.238	35.2	122.70	7.44	3
2002-206:03.53.01.513	56.513	20.2	122.36	7.40	2
2002-207:03.22.14.988	56.988	9.5	122.61	7.48	3
2002-208:02.51.27.063	57.063	17.1	123.78	7.31	3
2002-219:03.55.26.313	56.313	10.6	121.70	7.41	1
2002-220:03.08.59.038	57.038	5.7	123.54	7.55	1
2002-221:03.47.24.388	56.388	4.3	122.19	7.46	6
2002-225:03.38.09.038	57.038	30.1	123.54	7.43	3
2002-226:03.47.26.638	56.638	13.5	123.44	7.42	2
2002-248:03.55.37.888	56.888	21.6	122.09	7.48	1
2002-249:03.26.52.938	56.938	16.3	123.85	7.43	1
2002-254:03.20.46.013	57.013	37.1	123.72	7.40	2
2002-255:03.34.19.713	56.713	26.1	123.21	7.41	2
2002-256:07.21.09.463	56.463	82.6	121.94	7.62	1
2002-257:06.16.51.488	56.488	26.4	124.12	7.40	7
2002-262:04.40.08.538	56.538	35.4	123.28	7.45	3
2002-268:03.46.39.688	56.688	11.3	122.25	7.49	1
2002-269:03.38.33.963	56.963	52.5	122.24	7.47	3
2002-271:03.14.54.813	55.813	25.0	122.15	7.53	5

Table A1.3 Confirmed mining blasts at the Central mine (KH4: Khibiny Massif) between October 1, 2001, and September 30, 2002. The shaded entry is the event which resulted in the coda phases displayed in Figure 13). See description on page 71 for details.

ARCES arrival time	Est. t.t.	SNR	Azi.	Vel.	Yield
2001-278:11.31.13.463	56.463	70.9	123.60	7.45	133
2001-285:11.27.17.688	56.688	66.5	121.89	7.35	391
2001-289:15.07.49.438	57.438	90.7	122.87	7.36	123
2001-292:11.28.58.388	57.388	27.5	122.75	7.38	203
2001-306:12.34.26.163	56.163	55.8	122.42	7.42	90
2001-310:12.26.02.263	57.263	2.2	122.74	7.20	69
2001-314:12.06.39.288	57.288	32.0	122.93	7.43	68
2001-317:12.19.01.538	55.538	13.6	122.23	7.41	11
2001-320:12.35.08.488	56.488	40.0	122.44	7.42	29

Table A1.3 Confirmed mining blasts at the Central mine (KH4: Khibiny Massif) between October 1, 2001, and September 30, 2002. The shaded entry is the event which resulted in the coda phases displayed in Figure 13). See description on page 71 for details.

ARCES arrival time	Est. t.t.	SNR	Azi.	Vel.	Yield
2001-324:12.21.45.988	55.988	10.1	121.38	7.30	47
2001-327:12.03.20.238	56.238	42.1	122.46	7.51	164
2001-331:10.01.04.263	56.263	31.1	122.13	7.60	27
2001-334:10.54.53.288	56.288	116.2	122.63	7.40	69
2001-341:12.33.01.413	56.413	86.4	122.47	7.45	223
2001-345:11.55.05.913	56.913	71.9	123.80	7.42	113
2001-349:12.07.05.263	56.263	9.9	125.27	7.11	135
2001-355:10.53.53.238	56.238	53.4	122.17	7.38	122
2001-363:11.24.54.413	56.413	172.1	122.22	7.51	214
2002-005:11.01.27.613	57.613	55.9	122.15	7.42	104
2002-012:12.02.45.838	56.838	71.2	122.91	7.49	256
2002-015:12.23.52.263	56.263	85.6	122.03	7.39	14
2002-018:12.01.16.813	56.813	46.3	123.57	7.47	71
2002-025:12.29.34.563	56.563	152.1	122.70	7.41	308
2002-031:12.30.50.963	56.963	58.4	122.04	7.45	185
2002-032:12.12.08.213	57.213	59.7	122.04	7.46	13
2002-037:12.27.16.838	55.838	41.4	121.93	7.40	16
2002-039:12.30.36.788	56.788	49.1	122.89	7.35	202
2002-046:12.28.05.188	57.188	88.4	122.37	7.44	216
2002-053:12.33.34.763	56.763	46.5	121.97	7.43	281
2002-060:12.29.42.688	56.688	79.1	122.53	7.45	105
2002-081:12.36.52.988	56.988	36.1	122.20	7.37	1
2002-088:09.40.44.388	57.388	20.0	123.81	7.42	83
2002-095:11.28.20.613	56.613	36.5	123.30	7.39	155
2002-102:11.35.27.113	56.113	156.5	121.98	7.38	294
2002-109:11.31.11.188	56.188	119.4	121.97	7.51	185
2002-116:11.41.03.463	57.463	88.4	123.08	7.38	272
2002-128:12.06.07.513	57.513	85.8	122.49	7.40	277
2002-134:11.55.49.788	56.788	48.9	122.18	7.38	103
2002-137:11.30.14.963	56.963	59.6	122.76	7.38	215
2002-144:11.43.59.713	56.713	174.8	123.16	7.37	342
2002-151:11.54.51.388	56.388	104.1	122.89	7.37	350
2002-158:12.23.45.463	56.463	245.6	122.41	7.40	312
2002-166:11.43.44.838	55.838	123.1	122.57	7.46	254
2002-172:11.35.16.363	56.363	7.4	121.03	7.76	284
2002-179:11.33.13.413	56.413	146.8	122.22	7.47	271
2002-186:11.43.55.488	56.488	87.9	124.30	7.46	266
2002-194:11.34.05.313	56.313	155.5	124.01	7.43	128
2002-200:11.52.22.088	56.088	52.7	122.68	7.38	236
2002-207:11.38.37.138	57.138	37.7	123.21	7.49	332
2002-249:11.36.29.063	57.063	68.9	123.01	7.42	333
2002-254:11.41.13.438	56.438	28.5	123.81	7.47	49
2002-256:11.42.50.238	58.238	40.4	123.44	7.36	197
2002-263:11.53.24.088	57.088	82.2	122.80	7.43	386

Table A1.3 Confirmed mining blasts at the Central mine (KH4: Khibiny Massif) between October 1, 2001, and September 30, 2002. The shaded entry is the event which resulted in the coda phases displayed in Figure 13). See description on page 71 for details.

ARCES arrival time	Est. t.t.	SNR	Azi.	Vel.	Yield
2002-270:11.13.52.613	56.613	117.5	123.42	7.37	38
2002-274:11.18.53.388	56.388	30.5	123.18	7.42	89

Table A1.4 Confirmed mining blasts at the Koashva mine (KH5: Khibiny Massif) between October 1, 2001, and September 30, 2002. See description on page 71 for details.

ARCES arrival time	Est. t.t.	SNR	Azi.	Vel.	Yield
2001-278:06.11.19.513	56.513	55.3	122.60	7.55	127
2001-285:07.41.32.538	56.538	74.5	122.06	7.68	106
2001-299:08.42.07.738	56.738	96.6	121.76	7.55	147
2001-306:07.53.36.263	56.263	80.3	122.36	7.60	111
2001-320:08.03.06.588	56.588	60.4	120.97	7.61	190
2001-327:08.10.53.388	56.388	47.9	121.93	7.52	93
2001-334:09.35.04.513	56.513	26.0	122.09	7.59	70
2001-339:09.18.08.263	56.263	12.7	119.61	7.64	202
2001-352:08.12.45.388	56.388	16.8	121.76	7.54	73
2001-362:07.24.38.563	56.563	41.5	121.08	7.56	86
2002-011:09.31.19.163	57.163	38.5	121.83	7.68	140
2002-018:09.16.02.438	56.438	100.8	122.21	7.59	131
2002-023:09.41.47.488	57.488	31.4	120.11	7.80	145
2002-025:09.16.13.238	57.238	54.7	122.01	7.62	173
2002-030:09.06.43.288	57.288	61.0	120.38	7.66	203
2002-032:08.45.45.788	56.788	47.2	122.15	7.58	172
2002-039:06.58.05.788	57.788	60.8	122.47	7.65	106
2002-046:08.02.34.488	56.488	39.4	121.79	7.60	73
2002-053:08.09.35.688	56.688	66.2	122.56	7.56	167
2002-060:08.44.38.488	56.488	57.5	121.63	7.64	92
2002-081:08.34.07.163	57.163	20.5	122.78	7.63	189
2002-088:06.15.51.413	57.413	11.3	121.62	7.64	13
2002-102:07.09.11.563	56.563	33.6	122.15	7.54	236
2002-106:14.36.20.988	57.988	6.7	122.35	7.67	1
2002-109:07.18.01.138	57.138	71.7	121.84	7.63	135
2002-116:07.27.20.638	56.638	18.9	122.59	7.55	119
2002-128:07.20.14.388	57.388	55.1	121.33	7.66	162
2002-137:06.16.25.838	56.838	55.7	121.07	7.64	125
2002-144:07.07.58.563	57.563	35.4	122.05	7.59	107
2002-150:05.02.45.388	57.388	68.8	121.72	7.60	153
2002-150:06.23.42.988	57.988	5.3	121.52	7.82	50
2002-158:06.37.37.138	56.138	184.4	121.78	7.65	154
2002-162:05.36.33.363	57.363	12.8	121.99	7.62	25

Table A1.4 Confirmed mining blasts at the Koashva mine (KH5: Khibiny Massif) between October 1, 2001, and September 30, 2002. See description on page 71 for details.

ARCES arrival time	Est. t.t.	SNR	Azi.	Vel.	Yield
2002-172:06.50.25.313	56.313	48.3	121.65	7.60	92
2002-179:06.47.12.163	57.163	90.8	122.29	7.57	159
2002-186:07.19.25.238	57.238	128.9	121.61	7.59	141
2002-192:07.46.40.388	57.388	114.9	122.43	7.59	187
2002-200:06.49.18.438	57.438	36.9	121.82	7.63	121
2002-207:07.33.38.413	57.413	60.5	122.30	7.67	99
2002-226:08.13.22.188	56.188	52.4	119.78	7.76	31
2002-228:07.32.17.263	57.263	65.0	121.25	7.71	80
2002-249:08.01.24.838	56.838	104.7	121.12	7.68	192

Table A1.5 Confirmed mining blasts at the Norpakh mine (KH6: Khibiny Massif) between October 1, 2001, and September 30, 2002. See description on page 71 for details.

ARCES arrival time	Est. t.t.	SNR	Azi.	Vel.	Yield
2001-290:06.28.49.088	57.088	56.2	120.70	7.68	150
2001-304:07.59.54.163	57.163	72.7	119.74	7.78	189
2001-316:09.41.21.738	56.738	59.0	119.91	7.62	177
2001-341:08.33.26.138	58.138	15.9	121.76	7.62	190
2001-355:08.43.50.988	56.988	139.4	120.45	7.82	198
2001-360:07.20.34.838	56.838	27.1	119.96	7.75	14
2002-004:09.05.20.813	57.813	27.1	120.50	7.84	164
2002-051:08.24.57.488	56.488	234.0	120.20	7.75	262
2002-066:07.23.04.613	57.613	96.2	119.93	7.72	428
2002-074:10.03.03.363	57.363	8.3	120.32	7.61	322
2002-095:07.12.06.688	57.688	113.7	119.71	7.76	274
2002-107:07.14.18.713	57.713	186.6	120.10	7.82	171
2002-126:05.55.26.813	57.813	23.8	119.90	7.82	80
2002-135:06.23.38.588	58.588	42.7	120.07	7.83	152
2002-177:06.57.12.763	57.763	29.7	120.32	7.89	313
2002-194:11.17.26.388	57.388	77.5	117.78	7.48	192
2002-198:05.39.18.563	58.563	26.5	119.19	7.72	58
2002-212:07.55.35.463	58.463	22.5	119.70	7.78	152
2002-235:04.31.05.713	57.713	25.6	121.82	7.51	91
2002-254:09.08.19.588	57.588	77.1	121.53	7.65	332

Table A1.6 Confirmed mining blasts at the Kovdor mine (KV1: Kovdor) between October 1, 2001, and September 30, 2002. See description on page 71 for details.

ARCES arrival time	Est. t.t.	SNR	Azi.	Vel.	Yield
2001-279:10.28.58.113	43.113	75.7	136.64	7.35	307
2001-286:10.29.33.713	42.713	33.0	135.80	7.19	284
2001-293:10.36.32.738	42.738	81.0	133.46	7.15	255
2001-300:10.25.28.063	43.063	39.6	134.45	7.16	293
2001-307:11.27.57.288	42.288	109.7	136.77	6.99	281
2001-314:11.21.22.188	43.188	39.3	134.85	7.06	213
2001-321:11.45.16.863	42.863	92.8	134.24	7.03	304
2001-328:11.21.24.463	42.463	47.0	134.26	7.11	148
2001-332:12.05.31.513	43.513	63.4	135.61	7.19	112
2001-335:11.21.01.088	43.088	32.5	133.34	6.96	155
2001-342:11.39.58.188	43.188	45.4	134.44	6.85	308
2001-349:11.18.05.738	42.738	50.2	133.46	6.92	220
2001-356:11.21.54.613	42.613	91.1	135.77	7.44	244
2001-363:10.56.01.638	42.638	66.1	134.99	7.43	293
2002-005:11.16.30.163	42.163	72.3	134.36	7.12	185
2002-012:11.13.37.738	42.738	59.2	134.55	7.15	181
2002-019:11.34.07.613	42.613	77.3	134.81	7.23	368
2002-026:11.21.40.413	46.413	15.5	135.42	7.21	291
2002-040:11.32.10.138	43.138	64.5	135.52	7.17	198
2002-047:11.48.01.538	44.538	15.5	136.32	7.20	406
2002-053:11.25.29.238	44.238	9.1	135.73	7.22	292
2002-061:11.16.52.513	44.513	16.2	135.45	7.31	216
2002-082:11.30.04.888	43.888	20.0	135.11	7.05	226
2002-089:11.11.26.788	43.788	41.1	134.59	7.17	196
2002-096:10.14.11.263	44.263	13.8	134.49	7.17	244
2002-103:10.24.35.188	43.188	39.8	133.34	7.28	195
2002-110:10.23.33.138	43.138	69.4	135.56	7.09	315
2002-118:10.13.32.188	43.188	63.0	134.72	7.11	365
2002-124:10.14.02.363	43.363	63.7	134.80	7.08	108
2002-128:10.20.37.538	43.538	21.1	136.54	7.17	98
2002-138:10.30.31.088	44.088	14.6	135.05	7.11	221
2002-145:10.17.28.288	43.288	33.1	134.23	7.22	185
2002-152:10.17.28.838	43.838	20.4	135.92	7.17	203
2002-159:10.23.14.013	45.013	14.7	135.15	7.28	405
2002-166:10.17.01.038	44.038	16.8	135.33	7.22	240
2002-173:10.22.21.488	44.488	23.9	135.11	7.10	312
2002-180:10.21.01.863	43.863	27.8	134.66	7.10	247
2002-187:10.31.45.363	44.363	15.5	132.80	6.82	256
2002-201:10.18.58.163	43.163	42.6	135.75	7.10	276
2002-208:10.23.25.488	44.488	13.9	134.49	7.13	221
2002-215:10.50.16.413	45.413	10.3	134.69	7.38	241
2002-222:10.37.05.588	43.588	15.9	133.94	6.95	42
2002-229:10.20.08.613	44.613	15.5	135.24	7.21	306
2002-233:11.07.34.488	43.488	24.1	135.26	7.13	72
2002-236:10.25.29.663	43.663	38.9	133.23	6.91	278

Table A1.6 Confirmed mining blasts at the Kovdor mine (KV1: Kovdor) between October 1, 2001, and September 30, 2002. See description on page 71 for details.

ARCES arrival time	Est. t.t.	SNR	Azi.	Vel.	Yield
2002-250:10.20.07.788	43.788	18.1	134.65	7.32	273
2002-257:10.55.18.938	44.938	6.4	134.84	6.97	197
2002-264:10.23.40.538	44.538	15.4	134.99	7.08	246
2002-271:10.52.23.088	45.088	9.8	135.44	7.05	452

Table A1.7 Confirmed mining blasts at the Olenegorsk mine (OL1: Olenegorsk) between October 1, 2001, and September 30, 2002. See description on page 71 for details.

ARCES arrival time	Est. t.t	SNR	Azi.	Vel.	Yield
2001-285:12.10.24.188	48.188	63.0	118.70	7.94	95
2001-298:08.58.13.663	49.663	25.0	118.10	7.99	137
2001-306:13.13.50.613	49.613	6.7	106.77	5.66	90
2001-310:10.24.21.763	48.763	85.2	113.29	7.99	60
2001-318:12.15.56.813	47.813	34.1	112.85	7.92	77
2001-327:12.13.27.213	48.213	137.9	118.53	7.95	204
2001-335:08.00.35.863	48.863	24.3	114.26	8.12	114
2001-341:10.41.01.888	49.888	13.9	114.89	7.47	49
2001-355:12.35.29.663	47.663	73.5	116.20	7.91	183
2002-010:12.35.07.888	48.888	31.9	113.39	8.35	66
2002-024:11.37.59.738	48.738	57.4	115.88	8.02	117
2002-045:13.11.58.188	48.188	74.8	114.55	7.84	368
2002-057:10.23.08.438	49.438	86.2	119.13	7.97	134
2002-066:11.48.36.638	48.638	57.0	116.64	7.71	77
2002-074:11.31.01.563	49.563	13.7	116.75	7.52	21
2002-087:13.26.41.963	48.963	67.1	118.34	7.84	227
2002-099:12.16.24.088	49.088	25.2	116.46	7.82	57
2002-109:11.47.35.888	49.888	45.3	115.99	7.72	205
2002-126:11.12.38.263	50.263	7.1	117.49	7.93	219
2002-136:11.26.07.563	49.563	15.6	117.46	7.82	141
2002-149:09.36.31.613	49.613	19.9	114.23	7.95	220
2002-172:12.50.51.388	50.388	6.9	117.04	8.04	289
2002-185:12.06.08.088	49.088	36.8	115.44	7.81	49
2002-192:12.31.07.713	49.713	29.1	113.63	8.15	243
2002-212:12.15.19.963	49.963	8.8	114.73	7.87	25
2002-218:12.57.09.988	50.988	4.8	118.48	7.92	151
2002-224:11.10.01.988	49.988	10.3	116.89	7.92	90
2002-228:12.40.38.188	49.188	27.0	114.99	7.39	33
2002-235:11.52.01.163	49.163	55.0	115.71	8.08	255
2002-247:09.43.50.788	48.788	45.2	115.03	7.87	119
2002-255:08.26.42.788	49.788	23.2	116.00	8.06	115
2002-270:10.17.52.663	49.663	21.4	117.76	7.91	139

Table A1.8 Confirmed mining blasts at the Kirovogorsk mine (OL2: Olenegorsk) between October 1, 2001, and September 30, 2002. See description on page 71 for details.

ARCES arrival time	Est. t.t.	SNR	Azi.	Vel.	Yield
2001-276:09.49.27.213	53.213	6.5	118.92	7.76	164
2001-293:11.01.03.263	48.263	60.3	115.34	7.61	122
2001-304:11.22.22.313	49.313	54.1	116.40	7.67	221
2001-313:12.56.00.638	48.638	43.7	117.59	7.65	66
2001-321:10.34.29.113	48.113	83.9	118.07	7.66	216
2001-333:13.18.22.138	48.138	46.8	114.06	7.90	2
2001-348:12.23.04.713	48.713	98.9	121.29	7.50	226
2001-356:11.00.06.738	47.738	106.2	120.18	7.50	175
2001-360:11.20.38.688	47.688	66.9	115.92	7.67	80
2002-004:10.15.54.713	48.713	23.3	120.23	7.79	37
2002-018:12.07.53.088	50.088	67.4	121.17	7.56	87
2002-025:11.46.20.363	48.363	59.7	116.88	7.58	85
2002-053:12.18.28.163	49.163	124.8	119.89	7.54	106
2002-060:12.02.16.838	49.838	28.3	121.83	7.49	4
2002-075:12.10.39.413	49.413	39.9	117.33	7.47	124
2002-085:12.26.58.188	49.188	44.6	120.39	7.57	297
2002-095:12.59.17.538	48.538	30.3	118.68	7.60	223
2002-116:12.16.48.738	49.738	26.6	118.93	7.46	196
2002-127:10.38.55.963	49.963	23.9	121.20	7.55	153
2002-143:09.14.54.338	49.338	39.2	118.35	7.73	112
2002-151:09.02.42.288	49.288	13.9	116.86	7.75	105
2002-157:11.18.21.513	48.513	125.1	124.01	7.42	74
2002-176:11.14.54.163	49.163	74.9	121.51	7.46	172
2002-186:11.21.25.013	50.013	28.3	120.90	7.40	122
2002-199:12.57.32.563	49.563	46.6	122.15	7.61	259
2002-225:11.38.04.588	49.588	44.2	119.23	7.63	146
2002-234:12.17.07.638	48.638	72.9	123.20	7.45	225
2002-248:11.42.19.563	48.563	28.1	113.35	7.85	49
2002-256:12.29.05.788	48.788	62.1	121.98	7.40	152
2002-274:13.00.33.538	48.538	52.6	121.87	7.31	128

Table A1.9 Confirmed mining blasts at the Bauman mine (OL3: Olenegorsk) between October 1, 2001, and September 30, 2002. The shaded event (2002-032) is unable to be identified from the Pn phase at ARCES in the 2-5 hz frequency band due to an interfering signal (see Figure 13). See description on page 71 for details.

ARCES arrival time	Est. t.t.	SNR	Azi.	Vel.	Yield
2001-277:12.08.27.563	49.563	31.1	118.43	7.83	78

Table A1.9 Confirmed mining blasts at the Bauman mine (OL3: Olenegorsk) between October 1, 2001, and September 30, 2002. The shaded event (2002-032) is unable to be identified from the Pn phase at ARCES in the 2-5 hz frequency band due to an interfering signal (see Figure 13). See description on page 71 for details.

ARCES arrival time	Est. t.t.	SNR	Azi.	Vel.	Yield
2001-291:08.50.56.663	49.663	15.6	117.74	7.53	41
2001-305:09.39.41.688	49.688	36.2	115.12	7.66	48
2001-320:10.19.53.238	50.238	43.9	115.34	7.87	55
2001-331:12.49.10.613	49.613	71.8	118.41	7.55	252
2001-352:10.27.51.963	49.963	9.3	116.04	7.32	70
2001-362:11.39.20.963	49.963	37.3	115.67	8.22	170
2002-011:10.31.27.313	50.313	9.7	116.83	7.88	74
2002-032:12.13.00.013	51.013	1.33	119.52	3.20	253
2002-052:13.28.00.338	51.338	24.6	115.44	8.03	231
2002-066:11.44.12.888	49.888	23.8	116.69	7.78	36
2002-093:12.25.56.463	50.463	37.3	114.93	7.86	324
2002-110:07.21.08.588	49.588	50.4	115.64	8.09	76
2002-128:11.20.30.213	50.213	11.1	114.56	8.11	144
2002-141:13.38.13.863	51.863	14.5	116.48	7.64	276
2002-150:07.57.45.488	49.488	70.1	116.05	8.08	3
2002-158:11.50.41.888	50.888	28.9	117.47	7.63	216
2002-162:11.20.14.313	50.313	13.0	115.23	8.02	137
2002-193:11.04.24.188	50.188	16.8	114.52	7.99	102
2002-200:15.23.29.613	49.613	94.8	114.28	7.81	152
2002-213:11.30.26.913	49.913	33.1	119.75	7.53	144
2002-220:12.59.29.613	51.613	11.1	114.35	8.20	84
2002-227:14.01.21.188	51.188	9.4	115.44	8.20	48
2002-233:13.19.34.863	49.863	24.6	115.94	8.20	35
2002-249:09.40.03.288	50.288	31.7	116.96	8.10	61
2002-259:14.07.55.688	50.688	9.9	115.49	7.86	144
2002-267:09.49.30.138	50.138	17.4	115.90	7.66	32

Table A1.10 Confirmed mining blasts at the Oktjabirsk mine (OL4: Olenegorsk) between October 1, 2001, and September 30, 2002. See description on page 71 for details.

ARCES arrival time	Est. t.t.	SNR	Azi.	Vel.	Yield
2001-284:09.33.17.463	50.463	21.2	118.14	7.82	108
2001-299:09.16.26.063	49.063	23.0	114.33	8.58	64
2001-306:13.43.19.488	48.488	20.1	114.42	7.30	61
2001-332:09.38.08.513	49.513	21.2	116.55	7.85	64
2001-340:10.03.18.013	49.013	41.6	114.25	7.86	114
2001-363:10.00.46.813	48.813	6.5	118.12	7.82	2
2002-039:13.25.03.213	51.213	8.4	115.98	7.94	33
2002-064:10.47.30.963	49.963	102.7	115.37	8.07	86
2002-102:11.12.18.638	48.638	25.3	117.02	7.49	139

Table A1.10 Confirmed mining blasts at the Oktjabirsk mine (OL4: Olenegorsk) between October 1, 2001, and September 30, 2002. See description on page 71 for details.

ARCES arrival time	Est. t.t.	SNR	Azi.	Vel.	Yield
2002-137:10.37.03.063	50.063	25.3	114.68	8.13	152
2002-144:08.15.23.338	49.338	44.0	113.88	8.17	60
2002-179:11.01.43.138	50.138	37.7	116.90	8.25	221
2002-206:09.06.46.288	49.288	50.0	113.80	8.25	55
2002-211:11.17.00.513	50.513	15.7	118.13	8.23	72
2002-234:08.03.03.163	50.163	16.3	114.93	8.13	8
2002-263:09.50.35.913	49.913	69.2	115.52	8.17	15

Table A1.11 Confirmed mining blasts at the Komsomolsk mine (OL5: Olenegorsk) between October 1, 2001, and September 30, 2002. See description on page 71 for details.

ARCES arrival time	Est. t.t.	SNR	Azi.	Vel.	Yield
2001-277:09.06.37.488	50.488	22.3	113.47	8.23	100
2001-290:08.22.18.063	51.063	48.1	118.23	7.96	60
2001-345:10.12.53.463	49.463	9.8	117.91	6.99	3
2001-353:13.08.53.463	50.463	89.3	118.10	7.92	201
2002-022:10.37.32.638	50.638	56.5	117.99	7.91	74
2002-038:11.57.31.788	51.788	35.1	118.77	7.95	70
2002-079:12.24.12.388	50.388	45.8	117.72	7.98	114
2002-108:11.08.10.738	50.738	25.4	119.42	7.88	184
2002-135:09.23.13.013	50.013	32.4	117.56	8.00	66
2002-156:09.46.05.038	51.038	20.0	118.43	7.91	51
2002-171:07.53.54.288	50.288	25.4	118.99	7.80	123
2002-177:08.43.18.188	50.188	41.6	116.71	7.81	34
2002-198:08.45.23.313	50.313	29.4	118.71	8.04	23
2002-221:10.43.32.538	50.538	24.3	117.55	8.03	47
2002-240:10.57.48.113	51.113	13.0	120.57	7.43	43
2002-254:09.25.44.813	50.813	21.0	118.22	7.50	34
2002-268:09.48.51.263	51.263	28.2	118.85	7.95	90

Table A1.12 Confirmed mining blasts at the Zapadny mine (ZP1: Zapoljarni) between October 1, 2001, and September 30, 2002. See description on page 71 for details.

ARCES arrival time	Est. t.t.	SNR	Azi.	Vel.	Yield
2001-283:11.26.24.613	30.613	470.1	93.98	7.98	97
2001-292:11.05.03.913	29.913	205.8	95.95	8.03	29
2001-299:11.01.24.363	30.363	449.1	95.01	7.81	109

Table A1.12 Confirmed mining blasts at the Zapadny mine (ZP1: Zapoljarni) between October 1, 2001, and September 30, 2002. See description on page 71 for details.

ARCES arrival time	Est. t.t.	SNR	Azi.	Vel.	Yield
2001-306:12.10.32.763	29.763	78.6	95.74	7.90	48
2001-313:12.11.51.738	29.738	108.7	95.04	8.04	35
2001-320:12.41.13.613	29.613	358.7	95.81	7.78	81
2001-327:12.49.57.413	29.413	298.9	93.39	8.03	63
2001-332:12.21.03.413	30.413	214.5	93.52	8.04	38
2001-341:12.02.11.963	28.963	120.6	94.90	7.86	16
2001-355:12.11.35.738	28.738	166.7	94.11	8.08	54
2001-362:12.05.53.763	30.763	335.1	94.58	7.93	102
2002-016:13.01.38.863	32.863	135.0	93.21	8.16	108
2002-023:12.39.22.238	31.238	320.0	94.13	7.98	68
2002-030:12.21.01.063	31.063	237.0	93.71	8.03	75
2002-037:12.03.32.913	31.913	140.8	94.65	7.93	44
2002-044:12.06.10.588	31.588	125.1	93.00	7.94	26
2002-053:13.02.38.988	31.988	133.8	94.20	8.16	76
2002-053:13.04.33.263	31.263	51.4	91.88	7.93	36
2002-058:11.54.57.513	31.513	414.1	92.93	8.08	56
2002-072:12.24.31.688	31.688	16.9	94.47	8.07	5
2002-074:12.19.32.613	31.613	57.9	92.28	7.94	24
2002-079:12.31.14.663	31.663	215.7	93.30	8.11	127
2002-088:12.15.10.188	31.188	95.7	94.40	8.05	63
2002-093:11.02.24.038	31.038	154.6	92.76	8.00	36
2002-096:06.09.18.463	30.463	142.3	86.78	6.85	24
2002-107:11.03.24.538	31.538	232.9	93.76	8.01	47
2002-114:11.35.10.438	32.438	89.2	93.38	7.97	25
2002-128:11.00.18.913	31.913	158.6	95.81	7.90	125
2002-137:11.05.15.613	31.613	412.2	93.40	8.14	115
2002-144:11.00.16.613	31.613	104.5	91.34	7.93	20
2002-165:11.15.03.613	31.613	380.7	94.71	8.03	89
2002-172:11.05.02.863	31.863	68.4	93.50	7.86	49
2002-179:11.05.12.238	32.238	73.1	95.72	7.87	67
2002-191:11.34.36.988	31.988	125.3	93.27	7.91	49
2002-198:11.06.13.338	31.338	170.8	95.32	7.93	71
2002-205:11.06.25.988	31.988	120.4	92.69	7.90	90
2002-219:11.18.00.788	31.788	275.9	93.71	8.12	129
2002-228:11.04.05.988	31.988	233.9	94.03	7.88	94
2002-233:11.00.41.738	31.738	305.7	93.14	8.10	52
2002-242:11.06.29.788	32.788	62.3	94.17	8.08	82
2002-263:11.12.23.913	31.913	177.4	91.54	7.82	94
2002-270:10.55.59.113	32.113	264.4	94.47	8.05	59

Table A1.13 Confirmed mining blasts at the Central mine (ZP2: Zapoljarni) between October 1, 2001, and September 30, 2002. See description on page 71 for details.

ARCES arrival time	Est. t.t.	SNR	Azi.	Vel.	Yield
2001-278:10.59.23.038	29.038	424.2	91.20	7.87	41
2001-290:11.12.26.038	32.038	174.0	94.03	7.61	80
2001-304:12.12.53.113	31.113	268.2	92.36	7.65	69
2001-318:12.05.25.213	30.213	87.0	90.90	7.76	20
2001-325:12.13.19.063	30.063	371.7	91.07	7.79	47
2001-339:12.15.09.838	29.838	218.6	92.84	7.84	44
2001-353:12.10.44.288	30.288	213.9	92.65	7.84	26
2001-360:12.39.22.038	30.038	267.7	93.19	7.97	63
2002-004:12.09.33.363	31.363	251.7	92.78	7.64	59
2002-011:12.01.54.638	32.638	106.7	91.86	7.89	37
2002-018:12.04.16.613	32.613	61.3	91.53	7.61	86
2002-025:11.51.54.313	31.313	119.2	91.67	7.81	59
2002-032:11.59.18.013	32.013	44.5	92.44	7.59	21
2002-039:12.14.13.288	31.288	129.2	92.59	7.88	44
2002-046:11.57.06.863	31.863	183.5	93.23	7.72	50
2002-051:12.02.41.088	31.088	194.7	93.27	7.62	28
2002-060:11.57.21.263	32.263	171.9	91.45	7.78	50
2002-072:12.23.43.963	30.963	203.5	92.48	7.67	43
2002-095:11.04.55.938	31.938	269.3	91.77	7.76	80
2002-102:10.59.48.513	32.513	124.1	94.75	8.00	92
2002-109:11.10.46.938	32.938	104.5	92.35	7.63	31
2002-114:11.28.15.113	32.113	149.9	96.20	7.97	51
2002-116:10.57.05.938	31.938	133.6	91.53	7.74	25
2002-135:11.17.46.963	32.963	104.0	96.44	7.96	71
2002-156:11.40.43.388	32.388	216.2	95.27	7.84	103
2002-158:11.03.51.788	31.788	131.9	90.50	7.83	68
2002-170:11.04.26.038	31.038	387.0	92.18	7.63	41
2002-177:11.07.34.838	31.838	162.2	93.98	8.07	67
2002-186:11.04.08.413	32.413	229.8	91.42	7.80	61
2002-193:11.08.48.988	32.988	51.9	93.42	8.23	39
2002-200:11.18.54.063	32.063	139.8	93.86	7.79	71
2002-207:11.03.41.463	33.463	44.3	96.66	7.97	70
2002-214:11.05.51.588	31.588	325.1	94.16	7.88	99
2002-226:10.52.19.563	32.563	82.4	94.25	7.89	33
2002-249:11.07.48.713	31.713	447.6	92.93	8.04	116
2002-254:11.02.30.963	32.963	45.3	95.40	7.95	77

Appendix 2. Catalog of Finnish military explosions

The signals from the Finnish military explosions showed remarkable waveform similarity from event to event and this made them amenable to detection using full waveform correlation using the procedure detailed in Gibbons and Ringdal (2006). This means that the error in the origin time estimate is essentially identical for each event. Estimated origin times are listed in Table A2.1.

Table A2.1 Origin times for Finnish explosions according to cross-correlation analysis. The master waveform template begins at a time 2005-244:10.30.27.075. Assuming the origin time of the master event to be 2005-244:10.29.59.068, we estimate the origin time of all other events to be 28.007 seconds prior to the time of maximum correlation.

2001-228:13.59.59.505	2002-251:13.29.59.938	2004-242:11.30.03.553
2001-229:12.29.58.991	2002-252:11.59.59.483	2004-243:11.00.03.839
2001-230:13.29.58.192	2002-253:11.59.59.947	2004-244:11.00.03.986
2001-231:12.59.59.023	2002-254:11.44.59.738	2004-245:11.30.03.556
2001-232:10.59.59.045	2002-255:10.44.59.803	2004-246:11.00.00.846
2001-233:14.29.58.501	2002-256:10.44.59.615	2004-247:10.30.00.039
2001-234:11.29.59.331	2002-257:10.00.00.387	2004-248:10.00.00.883
2001-235:11.59.59.649	2002-258:10.00.00.087	2004-249:10.59.59.905
2001-236:11.29.59.104	2002-259:11.00.00.112	2004-250:10.00.00.207
2001-237:12.59.56.807	2002-260:10.14.59.787	2004-251:10.00.00.301
2001-238:11.59.56.607	2003-233:12.00.01.685	2004-252:10.30.01.126
2001-239:15.59.56.761	2003-234:11.00.01.756	2004-253:09.00.01.088
2001-240:13.29.56.924	2003-235:11.00.00.283	2004-254:09.00.00.480
2001-241:13.29.56.093	2003-236:10.30.00.027	2004-255:10.00.00.684
2001-242:12.44.56.485	2003-237:10.30.00.185	2004-256:08.59.59.571
2001-243:12.44.56.390	2003-238:11.59.59.930	2004-257:09.29.58.714
2001-244:12.29.56.414	2003-239:09.30.00.915	2004-258:09.00.01.861
2001-245:12.14.56.175	2003-240:10.59.59.804	2005-236:12.00.03.287
2001-246:12.59.59.983	2003-241:10.29.59.778	2005-237:11.00.03.265
2001-247:12.44.59.496	2003-242:10.29.59.588	2005-238:11.00.01.462
2001-248:11.44.59.142	2003-243:09.59.59.906	2005-239:10.00.02.689
2001-249:11.45.00.103	2003-244:11.59.59.408	2005-240:10.59.59.776
2001-250:11.59.56.659	2003-245:11.29.59.139	2005-241:10.59.59.828
2001-251:11.59.57.022	2003-246:10.44.58.987	2005-242:10.59.59.449
2001-252:10.29.56.870	2003-247:09.59.58.642	2005-243:11.59.59.870
2001-254:12.44.55.638	2003-248:09.59.58.486	**2005-244:10.29.59.068 (fixed)**
2002-241:13.29.59.647	2003-249:10.29.58.397	2005-245:10.59.59.022
2002-242:13.29.59.542	2003-250:11.29.58.247	2005-246:10.59.59.647
2002-243:13.30.00.118	2003-251:09.59.58.067	2005-247:11.00.03.608
2002-244:12.30.00.072	2003-252:10.29.57.973	2005-248:09.00.00.681
2002-245:12.29.59.664	2003-253:10.00.00.555	2005-249:10.00.00.401
2002-246:12.29.59.481	2003-254:11.29.59.883	2005-250:09.45.00.083
2002-247:12.59.59.211	2004-238:13.30.03.333	2005-251:09.45.00.086
2002-248:13.29.58.978	2004-239:12.00.03.518	2005-252:11.30.00.289
2002-249:12.29.58.839	2004-240:11.29.03.564	2005-253:10.45.00.017
2002-250:12.59.58.477	2004-241:11.29.04.079	2005-254:09.59.59.828